Freie Universität Berlin

A Kinetic Model for the Anionic Ring-opening Polymerization of Glycidol

Dissertation zur Erlangung des Grades
eines Doktors der Naturwissenschaften (Dr. rer. nat.)
am Fachbereich für Mathematik und Informatik
der Freien Universität Berlin

von

Maximilian Ernst Richard Weiss

Berlin
August 2012

1. Gutachter: Prof. Dr. Christof Schütte
2. Gutachter: Prof. Dr. Piet Iedema
3. Gutachter: Dr. Michael Wulkow

Tag der Disputation: 29.11.2012

Ehrenwörtliche Erklärung

Hiermit erkläre ich, dass ich diese Arbeit selbstständig verfasst und keine anderen als die angegebenen Hilfsmittel und Quellen verwendet habe.

Maximilian Weiss
Berlin, August 2012

ACKNOWLEDGMENTS

I would like to start by thanking my supervisor Prof. Dr. Christof Schütte. Without his scientific guidance and support this project could not have been completed with such success. He provided me with a well-equipped workplace, helped to establish my collaborations, and introduced me to the Biocomputing group through which I met a lot of great people and gained many friends.

Big gratitude also goes to Dr. Michael Wulkow. I have been working with him since my Master studies and he was always available for discussions about the PREDICI software and general modeling concepts.

Furthermore, I thank Dr. Anatoly Nikitin for his endless support which was crowned by our publication. His many years of experience helped me immensely and gave new impulses for my research direction. I enjoyed working with him very much and I hope that we stay in contact for many more years.

My collaboration partners were just as important for this project as the people in my institute. I thank Prof. Dr. Rainer Haag and his work group for conducting the experiments and for many, many helpful discussions. Without their excellent chemical expertise, I could not have grasped all the elemental mechanisms that had to be considered in this study. I would like to especially thank Florian Paulus, Dirk Steinhilber and Haixia Zhou who put an enormous amount of work into this project. Furthermore, I'd like to thank Dr. Pamela Winchester for proofreading my thesis.

I thank the Dahlem Research School for the financial support as well as Bettina Felsner and Stephanie Auerbach for taking care of all the administrative issues.

Last but not least, I thank my entire family and all my friends for everything they did for me. My parents, my brother, and Pooja always believed in me and with the security they gave me, I always had a safe haven to fall back to. My friends were always there for me to provide alternatives to all the hard work and they comforted me in difficult situations. Thank you all, I could never have done this without you.

CONTENTS

1. INTRODUCTION

Polymer science is a well established subfield of materials science that concerns synthetic macromolecules. Over the past century this discipline provided techniques to synthesize a large variety of unique materials, such as polyethylene, neoprene, Teflon, nylon, Kevlar, and many more.[1] Although the synthesizing procedures have been constantly improved,[2] new modeling and engineering techniques have to be developed to control the polymers' architecture on a nanometer scale. Great research efforts have been undertaken to study dendritic polymers which constitute the most recently discovered class of macromolecules with complex architecture. These substances possess very potent properties, such as compactness, multi-valency, solubility, and very good biocompatibility.[3] Therefore, they are often used in biomedical applications, such as conjugation with peptides, drug encapsulation, and surface modifications.[4–8] The polymers can be categorized further by the degree of perfection of their molecular structure. Dendrimers are characterized by their perfectly symmetric, tree-like structure, and hyperbranched polymers exhibit an ill-defined branching topology. In addition, the common synthesizing strategies for dendrimers allow very good control over the molecular size, which is usually not the case for hyperbranched polymers.

The goal of this study was to develop a mathematical model that can be used to simulate the synthesis of hyperbranched polyglycerol. The process is categorized as a one-pot, one-step ring-opening polymerization and was developed more than ten years ago.[9] The produced polymers feature properties very similar to those of their dendrimer counterpart and present a cheap and efficient alternative. Performing simulations will speed up the advancements in the process' optimization. Theories can be tested through simulations rather than elaborate experiments, which benefits the process engineers.

Modeling the chemical kinetics for the reactions of hyperbranched polymers is very challenging because the molecules' reactivities depend on their exact nano-architecture. Therefore, calculating the reaction rate for a given molecule requires detailed knowledge about the type, amount, and the location of all functional groups it contains. Since hyperbranched molecules can form many different architectures, polymer species have to

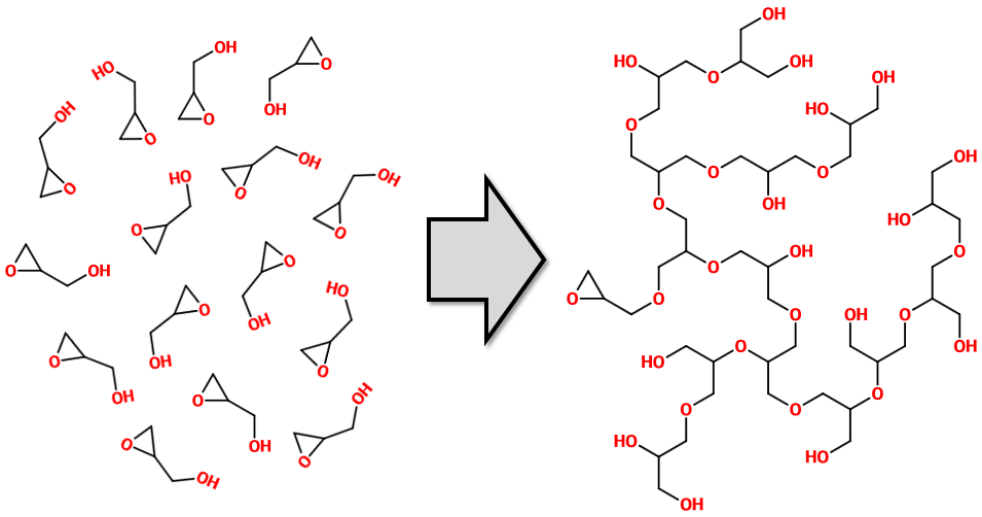

Figure 1.1. Illustration for the ring-opening polymerization of glycidol.

be modeled with multidimensional property indexes, and a large number of reaction rates has to be considered.

Since the model was designed to reproduce and predict the outcome of the synthesis, the simulations had to be comparable to the available experimental data. The performed measurements can only predict the polymers' structure to a certain degree. Average molecular weights and the polydispersity indexes were the most reliable source for structural information and the average degree of branching was determined to appraise the dendritic state. Although the polymers' most important properties could be assessed, these averaged values did not provide enough details to describe all reaction rates. This requires a compromise between the modeling detail and the robustness of the estimator for the kinetic reaction rates.

There are several ways to model chemical processes, but in order to model a polymerization process on a laboratory scale, only stochastic and deterministic approaches are actually feasible. To make a well-founded decision for any of these approaches, one has to consider the main advantages and disadvantages of both. As mentioned before, calculating exact reaction rates requires a multidimensional state space to describe the polymer species. This directly motivates the use of a stochastic model because the number of dimensions and the total size of the state space are unrestricted. However, by averaging the output of many randomly simulated trajectories, a sampling error is introduced which is very hard to quantify. Therefore, the quality of a stochastic simulation cannot easily be associated with the input parameters of the underlying model and optimizing the process

on the basis of experimental data is very complicated. Methodologies, such as maximum likelihood estimators, have to be applied which generally converge towards an optimum, but they are not guaranteed to reach a solution in a reasonable time. This major disadvantage can be associated directly with the biggest advantage of the deterministic approach. Due to the fact that every deterministic simulation is reproducible, the output can be formulated as a function of the input parameters of the kinetic model. Therefore, the difference between the simulated output and the measurement data can be minimized with well understood mathematical concepts, e.g., the gradient descent method.[10] It is still necessary to control the numerical errors, but random effects like the sampling error can be avoided completely. The main drawback of the deterministic approach is that calculating the derivatives for every chemical species can be computationally challenging. Additionally, the parameter estimation does not work well for systems with many degrees of freedom because the parameter space cannot be completely covered and the solution may not be the global optimum.

A strong emphasis on the comparability between simulations and experiments is placed for this kind of early stage research; therefore, a deterministic approach is appropriate. The ability to use robust parameter estimation methods to adjust the model to the rather uncertain measurement data is very important. However, in order to apply these methods effectively, the parameter space will have to be reduced drastically. Therefore, different simplification strategies have been analyzed to reduce the model's size, while still maintaining the needed level of detail to ensure realistic results that can be compared to the experiments. The software package PREDICI was used because it has been especially designed for the deterministic modeling of polymerization processes, and it provides sophisticated parameter estimation tools.

This manuscript describes the efforts to find a simplified, deterministic model that captures the essential reaction kinetics of the anionic ring-opening polymerization of glycidol. In the initial stage of this project, the involved mechanisms and reactions were collected from literature and a full-scale model was designed. This model was much too complex to be simulated in the given software framework due to the large sizes of the state space and the high number of kinetic parameters. Therefore, the number of chemical species was lumped and the reaction rates for the individual molecules were approximated by functions depending on the polymer size and some additional factors. The remaining kinetic parameters were optimized to achieve the best possible agreement between the simulations and the available experimental data. The results of this analysis proved to be

unsatisfactory because the parameter space still remained too big to provide a conclusive optimum based on the less detailed measurement data. However, the general direction for further investigations became evident and additional experiments were requested where crucial, anionic reactions were prevented by the experiments' design. On the basis of the additional data, a subset of parameters could be estimated very accurately and the results could be incorporated into the more complex model. After a final adjustment of the model based on the new findings, the previously excluded parameters could be satisfactorily estimated to reproduce all the experiments. The model presents a powerful tool for testing different experimental set-ups and postulating new hypotheses that can be used to improve the synthesis further.

This thesis is divided into five chapters. Chapter 2 gives historical background about the synthesized material. The classical categorization of polymers by their structure and the development of dendritic polymers are summarized. Chapter 3 highlights the use of glycidol in ring-opening polymerizations. This includes a general description of epoxides, their properties, and different polymerization techniques based on glycidol. The modeling technique is the topic of Chapter 4. The principle of classical chemical reaction kinetics and how the concept can be used for numerical simulations are explained. The chapter also summarizes preceding studies of similar processes which contributed to the knowledge base for this study. Furthermore, the newly developed modeling concepts for the anionic ring-opening polymerization of glycidol are presented and alternative modeling approaches are discussed. Chapter 5 describes the design of the experiments and the processing procedure for the measurement data. The results of the parameter estimation analysis are reported in Chapter 6. Details about the simplification strategy and the chronological development of the model are discussed as well. Chapter 7 closes this thesis with a brief summary and the conclusions of the study. The insight gained through this study and the model's relevance for the design of new synthesizing strategies are discussed.

2. BACKGROUND

Polymers with complex molecular structures have proven to be particularly useful and exhibit many different properties. This has fascinated many researchers ever since Staudinger formulated his "macromolecular hypothesis" in the 1930s.[11] Thanks to the constant improvement in mathematics and computer science, it is feasible to analyze the synthesizing processes that produce these materials.[5,7]

Traditionally, polymers were categorized according to their structure into three major groups: linear, crosslinked, and branched polymers.[12,13] In the 1930s, engineers were merely able to control the synthesis of linear polymer chains, but by the end of the 50s, scientist were already analyzing the potential of more complex molecules.[14,15]

In the 1980s a new type of polymer was introduced, the dendritic polymers, which are now widely recognized to constitute the fourth major class of polymers.[16,17] These polymers show very promising properties that can vary depending on the type of monomer used.[18]

The class of dendritic polymers can be further divided into different subclasses depending on the degree of structural perfection and symmetry. Dendrimers are the best studied and the most widely used of the dendritic polymers.[19] They are composed of core, branching, and terminal units as can be seen in Figure 2.1. A very important fact is that the common synthesizing procedures lead to perfectly controlled, monodisperse polymer mixtures and the produced polymers are nearly identical in size and structure.

2.1 Perfect Dendrimers

Dendrimers are usually synthesized in multiple steps that lead to a generation-wise growth by adding additional layers to the polymer iteratively. In every generation, an exponential number of end groups is added onto the polymers, while the molecule's diameter increases linearly. Therefore, the properties of the final material are mostly defined by the nature of the functional end groups at the surface of the molecules. This multivalency permits many surface modifications that allows one to define multiple interactions with surrounding

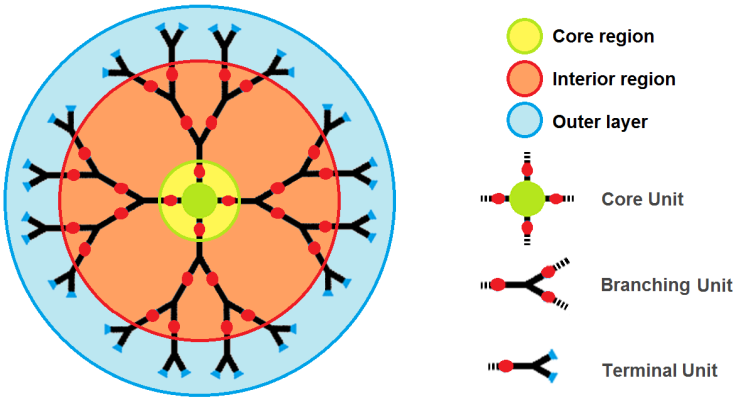

Figure 2.1. Molecular structure of a dendrimer. It is composed of 3 different structural units: core, branching and terminal units. The diversity of the polymer properties arises from the many combinations of structural units.

molecules, i.e., solvent or other chemical/biological species.[20–23] The core unit may also contain different types of functional groups making the product even more universal in its use. Choosing different or even opposing functionalities for the end and core groups creates a microenvironment around the core unit that can be exploited, e.g., to form micelles through incorporation of hydrophobic and hydrophilic functional groups.[24,25] The branching units define the flexibility, strength, and density of the molecules,[18] but they are usually not in contact with the surrounding environment (at least in comparison to the terminal groups) so that their interactions with solvents are often irrelevant. The difference between dendrimers and dendrons is that the core unit of dendrimers is located in the center of the molecule, so that it is isolated from molecules in the vicinity of the polymer, whereas dendrons have an exposed core unit that adds more functionalities to the material. Therefore, dendrimers typically take spheroidal or ellipsoidal shapes and dendrons tend to form hemispheroids and cones.

The most important properties of dendrimers and dendrons arises from the synthesizing techniques. Because the polymers are assembled in a step-wise manner and every end group is extended in every step, the polymer size and structure can be controlled perfectly. This is very crucial for delicate biological and medical applications which are highly sensitive to small impurities. Dendrimers have already been applied to many different biomedical fields.[26–39]

Two popular synthesizing strategies exist to obtain well-defined dendrimers, the divergent and the convergent strategy. Figure 2.2 summarizes both approaches and how they result in similar molecule structures.

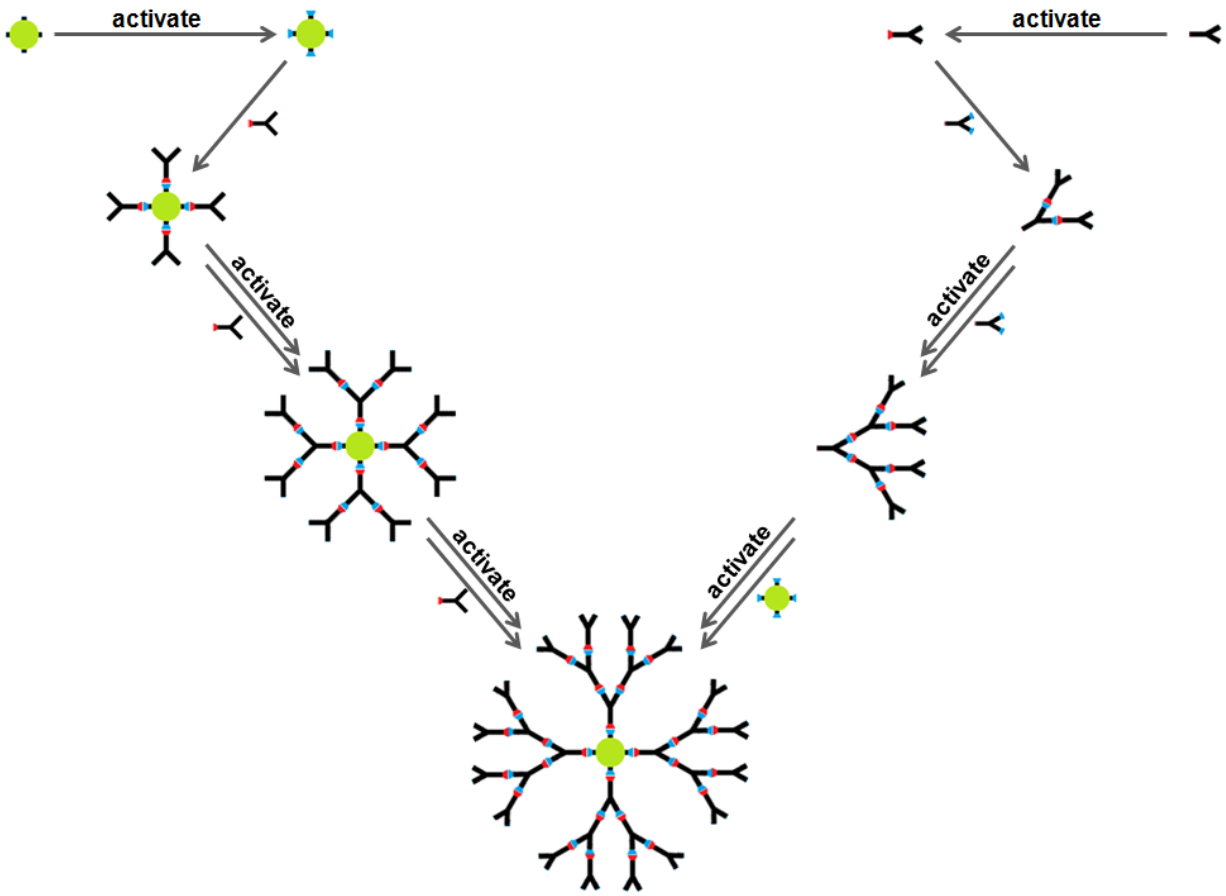

Figure 2.2. Comparison of the divergent (left) to convergent (right) approach that lead to polymers of similar structure (middle). Both approaches are multi-step procedures that build up the polymers in a generation-wise manner, but the order in which the generations are assembled differs.

In both cases, the polymers are built up in multiple, sequential steps. In the divergent strategy one starts by activating the end groups of the core molecule and then adds monomers that form the first "layer" of the macromolecule. Iterating these two steps at high conversion leads to the formation of nearly identical dendrimers. In the convergent strategy, on the other hand, the system is initialized with singly activated monomers that will later form the "outer layer" of the macromolecule. Further monomers that are added to the system will automatically form branching units which can again be activated at the "focal" unit to bind more monomers in the subsequent steps. This way tree like molecules are formed which can be considered dendrons. In a final step of the convergent strategy the dendrons are activated as the previous generations, but instead of adding more monomers, core units are used to combine the dendrons into symmetrical dendrimers.

The advantages of these strategies are the perfect control over the polymer's size and structure and the fact that the number of end groups added in every synthesizing iteration grows exponentially, making the procedure more efficient with every consecutive step. A disadvantage, on the other hand, is the iterative nature of the process. In each step, every end group needs to be activated and consecutively propagated by binding a monomer. This procedure is very time consuming and chemically tedious.

There exists a variation of this approach, where relatively small dendrons are created as in the convergent approach, but instead of adding core units in the final step, the dendrons are either attached onto linear polymers (Graft-Onto) or they are further modified so that they can be used as macromonomers (Graft-Through). In both cases, the product shows slight imperfections in the molecular structure, but the average size can be easily increased and the new material can be used in a more versatile manner.[19]

2.2 Random Hyperbranched Polymers

Compared to dendrimers, hyperbranched polymers can form a much bigger variety of structures because the interior backbone of the molecules may not exclusively consist of branching units but also contains unused functional end groups. Therefore, the backbone is composed of linear and dendritic segments, as illustrated in Figure 2.3.

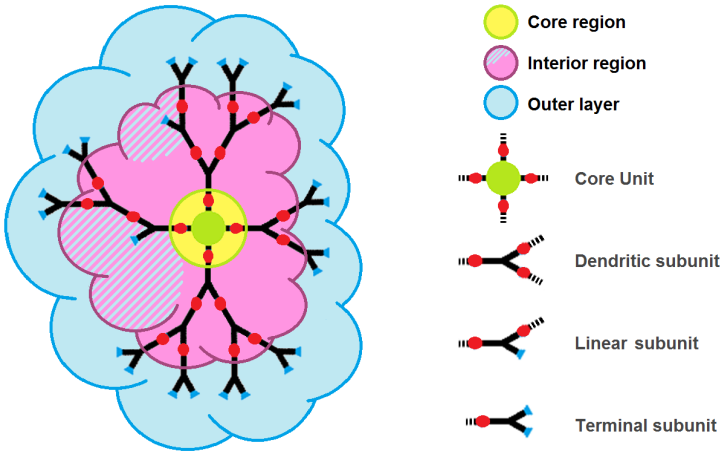

Figure 2.3. Molecular structure of a hyperbranched polymer. It is composed of 4 different structural units: core, branching (dendritic), linear, and terminal units. In contrast to dendrimers, the interior region is ill-defined because the functional end groups do not only have to be located on the molecule's surface.

Hyperbranched polymers have often been regarded as the "dendrimer's poor cousin"

due to their structural imperfection. However, if high degrees of branching can be achieved in a controlled manner, hyperbranched polymers offer a cheap and easily available alternative to dendrimers because they exhibit very similar properties. Additionally, unreacted functional groups on the backbone and the more loose structure can be exploited for various purposes, such as encapsulation of small molecules or better solubility.

There are various different synthesizing strategies for obtaining hyperbranched polymers. These can be broadly categorized into single molecule methodology (SMM) and double molecule methodology (DMM).[7] The SMM can be further categorized by the underlying reaction mechanics. One can distinguish further among (a) polycondensation of AB_n or latent AB_n-type monomers, (b) self-condensing vinyl polymerization (SCVP), (c) self-condensing ring-opening polymerization (SCROP) (d) proton-transfer polymerization (PTP), and some others.

Polycondensation reactions of AB_n-type monomers are the best studied of the SSM category and were successfully applied to produce hyperbranched polyphenylenes,[40] polyethers,[41,42] polyesters,[43–46] polyamides,[47,48] polycarbonates,[49] and poly(ether ketone)s.[50–52] Polyaddition reactions of AB_n monomers have also proven useful for the synthesis of hyperbranched polyurethanes,[53] polycarbosilanes,[54,55] polyamides,[56] and poly(acetophenone)s.[57]

In 1995, Frechet et al. developed the concept of SCVP.[58] This technique is very interesting because one starts out with AB-type monomers which have to be activated by an external source first to provide an AB^* molecule. Two monomers can then combine through the reaction of an A group (vinyl) with the B^* group (initiating group) to form a dimer (AbA^*B^*) that comprises a vinyl group (A), a propagating group (A^*), and an initiating group (B^*) as active sites. Because both the propagating and initiating groups can undergo further reactions, this dimer behaves like an AB_2 monomer. This way, the number of reactive centers increases proportionally to the degree of polymerization. However, the different reactivities for growth and initiating sites result in a lower degree of branching in comparison to the polycondensation approach. Additional disadvantages arise due to side reactions leading to a broad molecular mass distribution. In order to overcome these side effects, SCVP is often coupled with "living polymerizations" such as group transfer polymerization (GTP)[59,60] or atom transfer radical polymerization (ATRP).[61,62]

SCROP can be used to prepare hyperbranched polyamines,[63] polyethers[64–68] and polyesters.[69] This is a very convenient mechanism, but the high reactivity of the ring structures constraints control over the process and introduces side reactions. One approach

to control the reactivity of the growing polymers is to introduce a proton-transfer dynamic which catalyzes anionic or cationic polymerizations.[70,71]

A variety of very well written and illustrative reviews have been produced by some of the most influential researchers in this field. People interested in a more detailed overview about the SMM are advised to read the reviews by renowned researchers.[6,72–76] For more information about the DMM, see the work of Kakimoto,[77] Fréchet,[78] and Gao.[7]

3. SYNTHESIS OF HYPERBRANCHED POLYGLYCEROL

The main focus of this work is to improve the synthesis of hyperbranched polyglycerol. It has been shown that the use of glycidol as a "latent cyclic AB_2-type monomer" omits control of the molecular mass and the degree of branching of the product.[66,68] Therefore, the ring-opening mechanism will be analyzed carefully in this chapter.

Details about the elemental, chemical mechanisms that are relevant to the reaction of glycidol are discussed. The mechanics will be described from a purely chemical point of view and not from a mathematical one. It is important to know the chemical details while attempting to formulate abstract interpretations of such reactions. The aim of this chapter is to develop the right mind set which is necessary in order to derive a mathematical model that is capable to mimic and interpret the essence of a dynamical change introduced by a chemical reaction. For that purpose it is necessary not to focus only on the mechanics for the process at hand, but also on other possible reactions that could theoretically be exploited to form dendritic polyglycerol. The reasoning for using the specific synthesizing procedure and possible alternatives are explained.

3.1 The Use of Epoxides and Ring-opening Reactions for Polymer Science

Epoxide derivatives are very reactive end groups. This cyclic ether approximately forms an equilateral triangle with bond angles of around 60°. That is very different to the tetrahedral angle of approximately 109°, so that the ring is considered to be highly strained and has a high tendency to open. In addition, the carbon-oxygen bonds are slightly polar due to the differences in electronegativity. This makes the ring prone to nucleophilic attacks. The ring-opening reaction can be catalyzed in various ways that will be discussed in detail in the following sections.

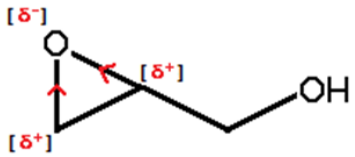

Figure 3.1. Structure of glycidol

3.2 The Use of Glycidol as Monomer for Ring-opening Polymerization Processes

2,3-Epoxy-1-propanol, also called glycidol, contains one epoxide derivative and one hydroxyl group as functional end groups. Its properties are very promising for the synthesis of polyglycerol because both end groups can react with each other to form glycerol derivatives. The resulting macromolecules continue to react without much external force to form polyglycerol. The ring-opening reaction is catalyzed under basic or acidic conditions.

Before going into the details of the catalyzed variations of this ring-opening polymerization, the various products that can be formed by the ring-opening reaction of glycidol have to be analyzed. This is best illustrated by the thermally induced ring-opening reaction of glycidol. At high enough temperatures, an epoxide derivative can be attacked by any weak nucleophile, e.g., the hydroxyl group of another monomer or polymer.

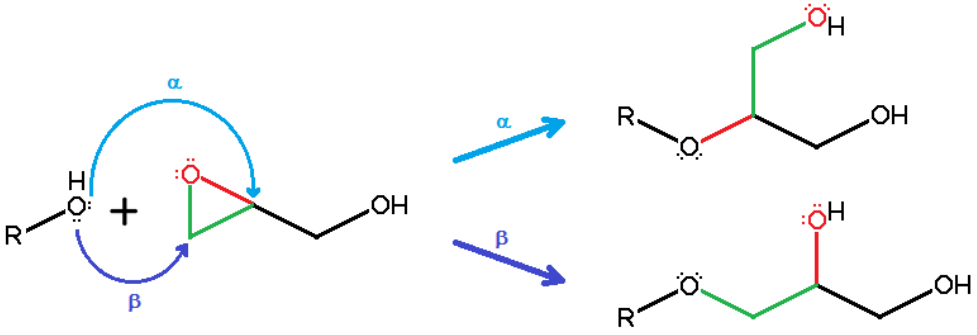

Scheme 3.1. Thermal ring-opening reaction induced by a weak nucleophile, i.e., a hydroxyl group of an alcohol *ROH*.

Scheme 3.1 shows the general ring-opening reaction of glycidol with a weak nucleophile that contains at least one lone pair of electrons, e.g., a hydroxyl group of an arbitrary alcohol *ROH*. The scheme depicts the two possible directions the ring can open, depending on which carbon atom is subject to the nucleophilic attack. This denotes which bond is broken and either two primary (α) groups or a primary and a secondary (β) hydroxyl group

arise. Regarding only the thermal ring-opening reaction, one can assume that the C_1 atom of the epoxide ring will be more likely to be attacked by the nucleophile because there is less sterical hindrance for the less substituted carbon atom. The partial positive charge on the two carbon atoms should be similar enough to play only a minor role in this reaction. However, the steric hindrance at the C_2 carbon atom is not big enough to suppress the secondary ring-opening direction (α) completely.

The thermally induced ring-opening reaction of glycidol can be exploited to derive a synthesizing process for polyglycerol. This has not been reported in detail so far, even though the reaction has been known as a side effect from storing glycidol at room temperature for a long time.[79] This is not surprising because the reaction rate for the thermal ring-opening reaction is so slow that in a time frame of around 5 months the percentage of dimers and trimers formed rose from around 2% to 14%. This is not a very promising stating point for the design of a polymerization process that aims at high levels of monomer conversion. However, testing the behavior of glydicol reacting in batch and semi-batch modes at elevated temperatures helps one to understand the role of thermal ring-opening reactions in terms of unavoidable side reactions.

3.3 Cationic Ring-opening Polymerization of Glycidol

In the presence of an acid, the oxygen gets protonated and thereby positively charged. This enhances the probability of a nucleophilic attack on the carbon atoms of the epoxide ring. Scheme 3.2 shows the basic mechanism.

The reaction starts with an intermediate step (I) where the glycidol molecule reacts with the acid. The oxygen of the epoxide ring is protonated and receives a positive charge while the acid catalyst gets deprotonated. Due to the electron donating nature of the substituent, the positive charge is delocalized between the oxygen and the more highly substituted carbon atom. Therefore, the carbon atom bares a partial positive charge and can be subject to a nucleophilic attack by a weak nucleophile (II), e.g., a hydroxyl group. The carbon-oxygen bond breaks and a protonated ring-opened species is formed as a result. This new intermediate will be deprotonated by the conjugate base of the original acid (III) to yield the ultimate ring-opening product and regenerate the acid catalyst.

It should be noted that the nuleophilic attack may also occur at the less substituted carbon atom, but this reaction should be much less prominent than the other variant. However, following the literature examples,[67] all possible outcomes of the ring-opening

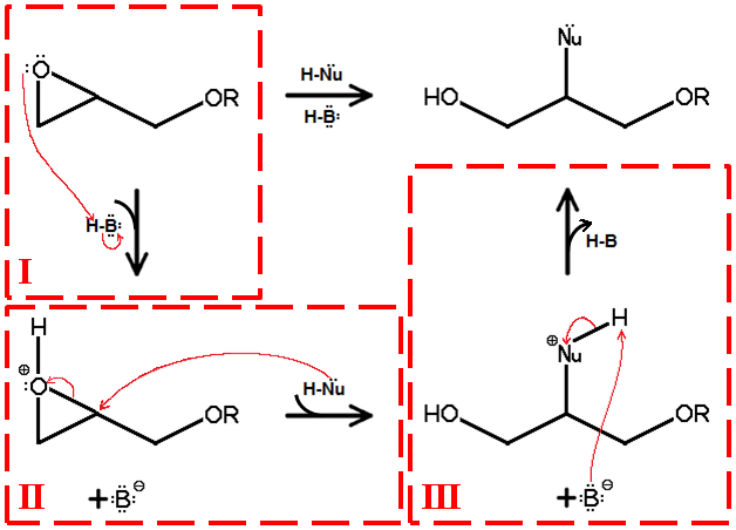

Scheme 3.2. General Scheme for an acid-catalyzed ring-opening reaction of glycidol. The red boxed indicate intermediate steps.

reactions must be considered. The justification for this stems from the sterical hindrance that makes a nucleophilic attack on the CH part of the expoxide less likely whereas the above-mentioned partial positive charge compensates for it. After all, there are arguments for both ring-opening directions which must be considered.

In the context of the synthesis of polyglycerol, this means that glycidol gets protonated by the catalyzing acid and then binds to any hydroxyl group in the system. Therefore, it can bind to another monomer or a polymer, resulting either in an initiation or a propagation reaction.

The first cationic ring-opening polymerization of glycidol was reported by Goethals in 1991 and the product was described as a branched polyol.[80] Acid-catalyzed polymerization of trimethylsilyl glycidyl ether (TMSGE) and *tert*-butyl glycidyl ether (TBGE) was briefly discussed by Vandenberg in 1985.[66]

In 1994, Tokar et al. described the cationic ring-opening polymerization of glycidol to study the effect of two competing mechanisms, the active chain end (ACE) and the activated monomer (AM) mechanism.[67] Schemes 3.3-3.5 summarize both mechanisms.

In Scheme 3.3 a positively charged epoxide forms the ACE of a polymer that can bind to the oxygen atom of the epoxide derivative of a free monomer. This reaction can result in two different substructures that are indistinguishable for measurements, but they can nonetheless arise. In both cases a linear 1,3-glycerol repeating unit ($-CH_2-CH(CH_2OH)-O-$) is created, meaning that the first to the third atoms of the monomer

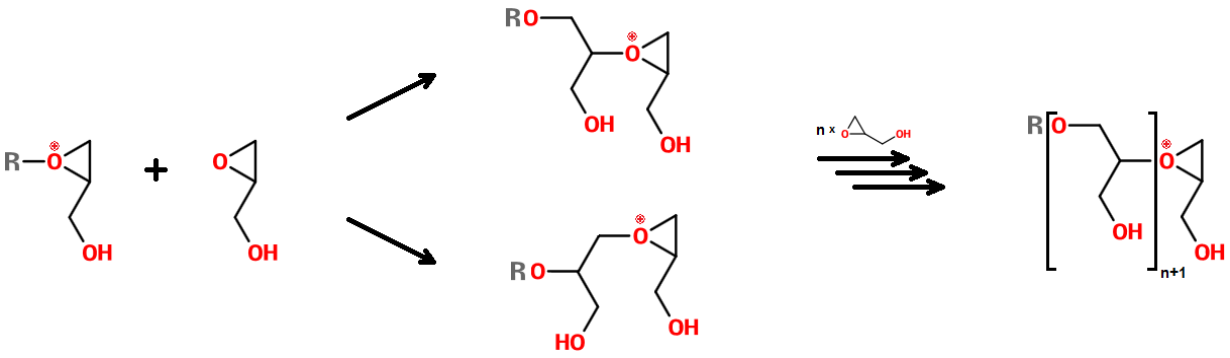

Scheme 3.3. Simple reaction scheme for a cationic ring-opening polymerization through the Active Chain End mechanism. A linear polyether is formed with exclusively primary hydroxyl groups as side chains.

form the linear polymer chain. This also means that there are only primary hydroxyl groups ($-CH_2OH$) attached to the polyether backbone.

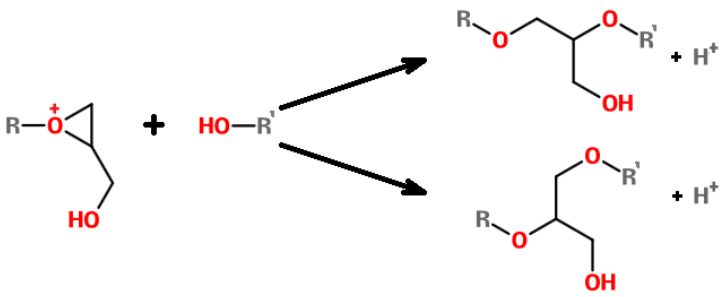

Scheme 3.4. Reaction between an Active Chain End with an arbitrary hydroxyl group. Independent of the direction in which the ring breaks, a new primary hydroxyl group is added to the backbone and a proton is released which can react with another nearby molecule.

Scheme 3.4 illustrates a reaction of the ACE with an arbitrary hydroxyl group. This forms a protonated intermediate that is likely to donate its surplus proton, i.e., the conjugate acid catalyst or a free monomer, where the latter case directly facilitates the AM mechanism. This reaction can lead to the formation of a branching unit if the reacting hydroxyl group was part of another linear polymer chain, but it can neither produce 1,4-linear subunits ($-CH_2 - CH(OH) - CH_2 - O-$) nor secondary hydroxyl groups ($-CH(OH)-$) as side arms. Such a structure can only arise through the AM mechanism.

Scheme 3.5 shows the reaction of an active (protonated) monomer with an arbitrary hydroxyl group that can be located either on another monomer or polymer. The AM mechanism gives rise to more complex structures than the ACE one because 1,3-linear,

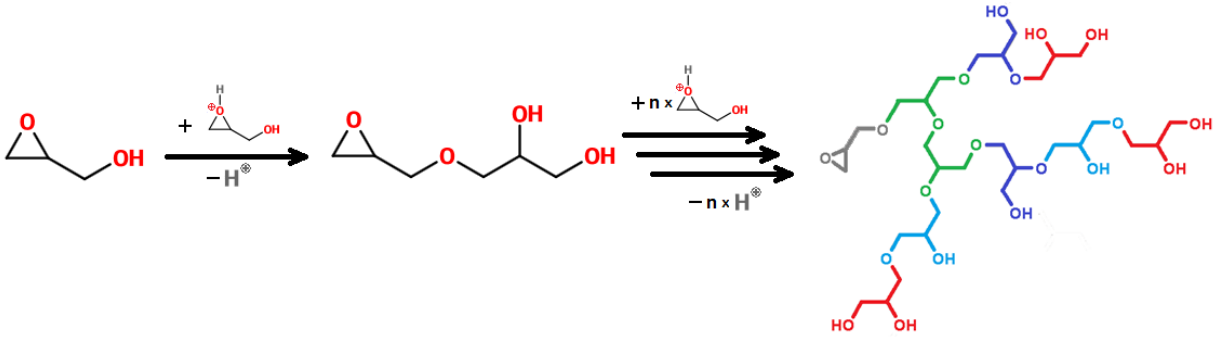

Scheme 3.5. Reaction scheme for the cationic ring-opening polymerization of glycidol through the Active Monomer mechanism. Since the activated monomer can bind at any hydroxyl group, a hyperbranched structure is produced. In the illustrated example polymer, dendritic subunits are colored green, 1,3-linear subunits dark blue, 1,4-linear subunits light blue, and terminal subunits are colored red.

1,4-linear and branching units can be created. The example polymer illustrated in the scheme includes all possible substructures which are visualized with different colors.

3.4 Anionic Ring-opening Polymerization of Glycidol

In 1966, Sandler and Berg described the polymerization of glycidol at room temperature in the presence of various bases.[81] Before that, Rider and Hill reported in 1930 that pyridine polymerized glycidol to a water-solvable black tar, whereas calcium chloride caused an exothermal reaction that produced a water-solvable red tar.[79]

Sandler and Berg reported the possible reaction mechanisms that lead to the polymerization of glycidol. They elaborated the ring-opening reaction of a free monomer with a base and the proton exchange reaction between bases and monomers leading to deprotonated and therefore activated monomers that can bind other free monomers, just like the base-catalyzed mechanism. Both schemes are depicted in Scheme 3.6. By this method only oligomers of size smaller or equal to four repeat units were achieved and they were assumed to exhibit a purely linear structure.

In 1985, Vandenberg[66] picked up on this topic and extended the reaction scheme by intramolecular proton exchange reactions between the primary and secondary hydroxyl group of the terminal units as illustrated in Scheme 3.7. Because of that, the polymer's backbone can have primary and secondary hydroxyl groups attached to it and branching units can be formed. The results were verified by extensive analysis with nuclear magnetic resonance (NMR) measurements, but the size of the polymers was not determined.

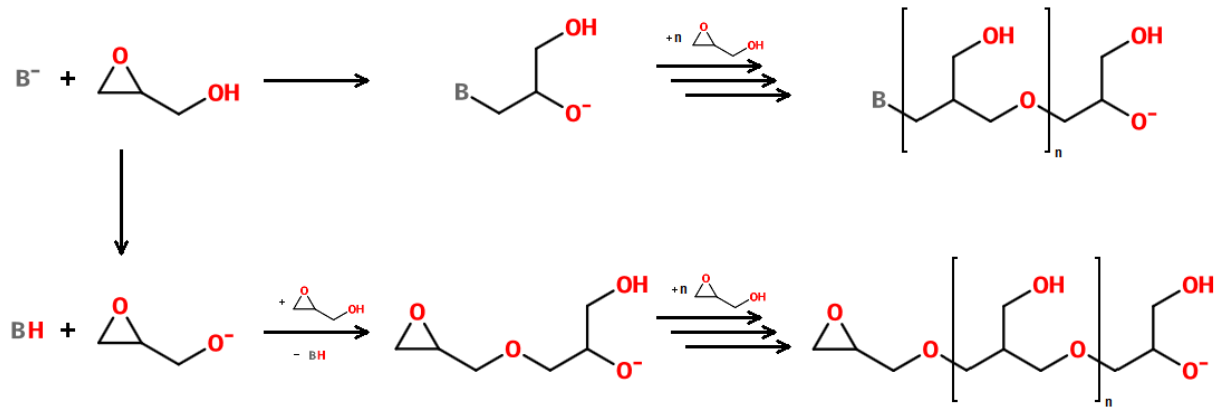

Scheme 3.6. Basic scheme for the anionic ring-opening polymerization reported by Sandler and Berg.

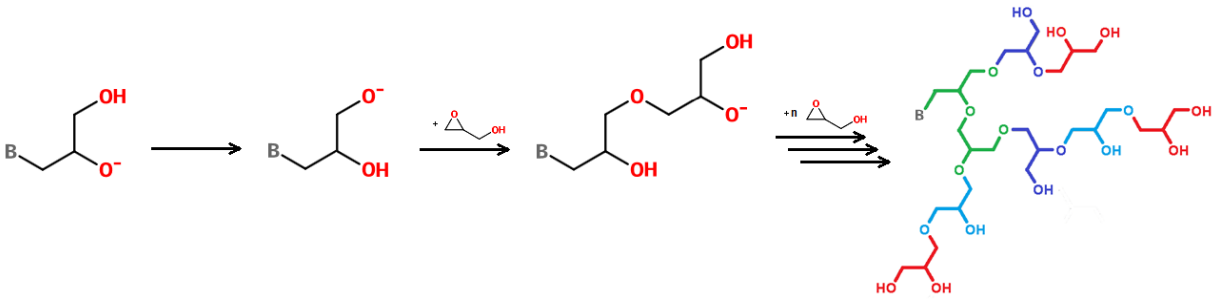

Scheme 3.7. Additional side reactions discovered by Vandenberg.

According to the literature at hand, the basic mechanism and the underlying polymerization process will be discussed in detail. The basic mechanism for the propagation reaction is a base-catalyzed ring-opening reaction of the epoxide derivative of glycidol.

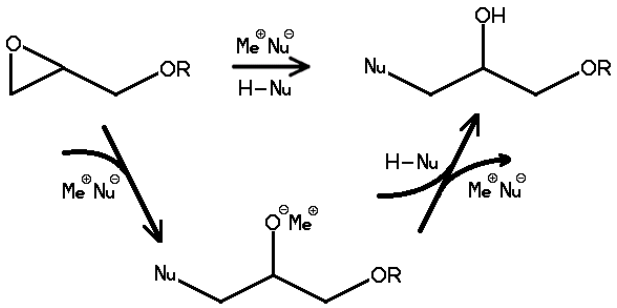

Scheme 3.8. General reaction scheme for the base-catalyzed ring-opening reaction of glycidol. The red frames indicate intermediate steps.

Scheme 3.8 shows a typical ring-opening reaction of glycidol with a weak nucleophile under basic conditions. An epoxide itself is a weak electrophile due to its electron deficient

carbon atoms which can be attacked by an activated, negatively charged nucleophile (anion), e.g., a deprotonated hydroxyl group. The nucleophile is most likely to attack the less substituted carbon atom because there is less steric hindrance, but both ring-opening directions are possible. The respective carbon-oxygen bond is broken and the ring-opened alcoxide intermediate is produced. The intermediate acts as a strong base that can absorb the proton of another molecule, such as the conjugate acid of the anionic nucleophile. This forms the ultimate ring-opening product and regenerates the anionic catalyst.

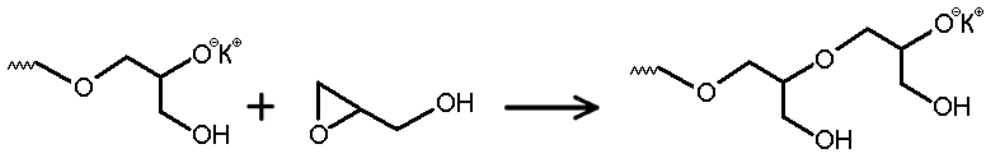

Scheme 3.9. Reaction scheme for the anionic ring-opening reaction of glycidol. The reacting polymer itself functions as the catalyst.

Scheme 3.9 is a special variant of the general base-catalyzed ring-opening mechanism. Here the growing polymer chains form the negatively charged nucleophiles directly. This is possible by using a cation exchanger to replace some of protons of the initially present hydroxyl groups by counter ions, e.g., potassium $K^{\oplus}$ as illustrated in the scheme. The alcoxides form ionic bonds with the counter cations typifying active sites. When an active end group meets an epoxide in space, the ring opens as described above and the product again contains a negatively charged end group that forms an ionic bond to the counter ion. Furthermore, the counter ion can be exchanged with the proton of a nearby hydroxyl group, so that the active sites become delocalized and the polymer may grow in random directions which results in the formation of a hyperbranched molecular structure. A proton exchange reaction may also occur intermolecularly, in which case the active site is transferred to another molecule. This leads to a (partial) deactivation and permits multiple activation of polymers.

3.5 Characterization of Hyperbranched Polyglycerol

The procedure to synthesize hyperbranched polyglycerol described above leads to a nonuniform mixture of polymers of different sizes and different structures. It is desirable to have a final product that is as homogeneous as possible. Therefore, it is necessary to characterize the mixture of the different polymers. Besides the homogeneity, the molecules should be as big and as branched as possible in order to compete with perfect dendrimers.

These are the desired qualities of the produced material and optimizing the synthesis in this context requires the ability to measure these properties in the most accurate way.

In this study, three types of measurements were used to assess the quality of the product, i.e., size exclusion chromatography (SEC) to obtain the average molecular mass, matrix assisted laser desorption/ionization (MALDI) for high resolution molecular mass distributions, and nuclear magnetic resonance (NMR) spectroscopy which allows the quantification of various substructures composing the polymers. All three methods have advantages and disadvantages, but before going into the details about the measurement techniques, some general nomenclature needs to be introduced to evaluate the quality of a polymer samples.

The molecular mass distribution (MMD) of a sample contains information about the number of present molecules with a certain molecular mass.[82] Traditionally, this is often referred to as molecular weight distribution (MWD) which is essentially the same, but since the actual mass is important and the weight is just a manifestation of external forces, the more general term MMD is used in ongoing research studies. In the context of polymer science this concept can be directly translated to the polymer size distribution (PSD) since every incorporated monomer adds to the overall mass of the polymer together with some additional compounds, such as initiators, counter ions, transfer agents, etc. The most crucial difference between an MMD and a PSD is that the former is defined on a continuous scale whereas the latter is a series of discrete values, i.e., the amount of polymers of different sizes.

The fact that different polymer species may have different masses, even though they incorporate the same amount of monomers, makes it even more useful since, in theory, one can derive separate PSDs for different polymer species. However, it is also possible that different polymers add up to the same mass, in which case, the PSDs cannot be distinguished easily from the combined MMD. For example, it is easy to separate self-initiated polymers from polymers that were initiated by a core-forming molecule because a core forming molecule has a different mass than a monomer. On the other hand, in a copolymerization the molecular masses may overlap for polymers of different sizes and the PSDs cannot be separated.

In many cases, the detailed information about the whole MMD or the individual PSDs is not required and especially for the purpose of estimating kinetic parameters, it is often more useful to describe the distribution solely by its moments. Let N_i denote the number

of polymers of size i, then the k^{th} moment is defined as follows.[83,84]

$$\mu_k = \sum_{i=1}^{\infty} i^k \cdot N_i$$

In the case of a MMD the sum is replaced by an integral over all possible masses and for $N(w)$ representing the density of molecules with a mass equal to w the k^{th} moment is defined as:

$$\mu'_k = \int_0^{\infty} w^k \cdot N(w) dw$$

Obviously, the zeroth moment corresponds to the total amount and the first moment to the total mass of all considered molecules. Moments of higher order are more complicated to explain in words, but together the moments can be used to describe the general shape of the distribution. It is very common to use the zeroth, first, and second moment to calculate the number- and weight-average degree of polymerization ($\overline{P}_n$ and $\overline{P}_w$) or the equivalent for the average molecular weight ($\overline{M}_n$ and $\overline{M}_w$) as follows.

$$\overline{M}_n = \mu'_1/\mu'_0 \tag{3.1}$$

$$\overline{M}_w = \mu'_2/\mu'_1 \tag{3.2}$$

$$\overline{P}_n = \mu_1/\mu_0 \tag{3.3}$$

$$\overline{P}_w = \mu_2/\mu_1 \tag{3.4}$$

For simple polymerization schemes regarding a polymer that is composed of exclusively s many monomeric subunits, P_s, the molecular mass can be calculated exactly when the molecular mass of a monomer, w_M, is known.

$$W_s = s \cdot w_M \tag{3.5}$$

In this case, the average molecular weight is correlated to the average degree of polymerization and can be expressed in terms of the moments of the PSD.

$$\overline{M}_n = \frac{\sum_i W_i \cdot N_i}{\sum_i N_i} = \overline{P}_n \cdot w_M = \frac{\mu_1}{\mu_0} \cdot w_M \tag{3.6}$$

$$\overline{M}_w = \frac{\sum_i W_i^2 \cdot N_i}{\sum_i W_i \cdot N_i} = \overline{P}_w \cdot w_M = \frac{\mu_2}{\mu_1} \cdot w_M \tag{3.7}$$

Another important example for the process at hand is the case where polymers contain not

only one type of monomer with mass w_M, but also a fixed number of additional derivatives, such as initiators or counter ions. This induces an offset for the mass of a polymer which can be calculated through the summed mass of the additional derivatives, w_X, and the new mass formula is:

$$W_s = s \cdot w_M + w_X \tag{3.8}$$

After inserting this formula, the average molecular weights can be expressed as follows.

$$\overline{M}_n = \frac{\sum_i (i w_M + w_X) N_i}{\sum_i N_i} = \frac{w_M \mu_1 + w_X \mu_0}{\mu_0} = \overline{P}_n \cdot w_M + w_X \tag{3.9}$$

$$\overline{M}_w = \frac{\sum_i (i w_M + w_X)^2 N_i}{\sum_i (i w_M + w_X) N_i} = \frac{w_M^2 \mu_2 + 2 w_M w_X \mu_1 + w_X^2 \mu_0}{w_M \mu_1 + w_X \mu_0} \tag{3.10}$$

One can see that the weight-average molecular weight cannot be expressed exactly in terms of the degree of polymerization, but for samples containing mostly large polymers, i.e., $\mu_2 > \mu_1 >> \mu_0$ one can see that $\overline{M}_w$ approaches $\overline{P}_w \cdot w_M + 2 \cdot w_X$.

By definition, if the polymer sample is monodisperse in the sense that all molecules have similar molecular weights, the number- and weight-average molecular weights are nearly identical. Furthermore, broader distribution exhibit higher ratios of $\overline{M}_w$ to $\overline{M}_n$. Therefore, this ratio has become a popular indicator for the inhomogeneity (or the dispersity) of the MMD. The so-called polydispersity index (PDI) is defined as follows.

$$PDI = \frac{\overline{M}_w}{\overline{M}_n} = \frac{\mu_2' \mu_0'}{{\mu_1'}^2} \tag{3.11}$$

These are the most common properties that describe the PSDs and MMDs of a polymer sample. In general, the molecular structure is not solely described by the size of polymers and there can be a big variety of different structures for polymers of the same size. Other important properties of the polymers include the diameter, volume, and the gyration as a measure for symmetry. Such properties can be measured by light scattering or electron microscopy, but such techniques require high effort and are very sensitive to conceptual errors. Instead, the composition of the polymers in terms of its categorized derivatives is analyzed. In the case of hyperbranched polymers, the structural compounds are core units, various monomeric subunits, and possible extra modifications to the reactive end groups. The monomeric subunits can be categorized into dendritic, subdendritic, linear, and terminal units, depending on the type of monomers used. The most commonly used monomers result in tri-functional branching points, in which case no subdendritic units

have to be regarded. In the less common case of tetra-functional branching points there is exactly one type of subdendritic units and additional types of subdendritic units have to be introduced for systems with even more growth directions. In the case of hyperbranched polyglycerol, one can only observe trifunctional branching points, so that no subdendritic units have to be considered. Figure 3.2 illustrates the different monomeric subunits that can be formed by polymerizing glycidol. It should noted though, that not all subunits are distinguishable by the measurements, e.g., the dendritic subunits (left column).

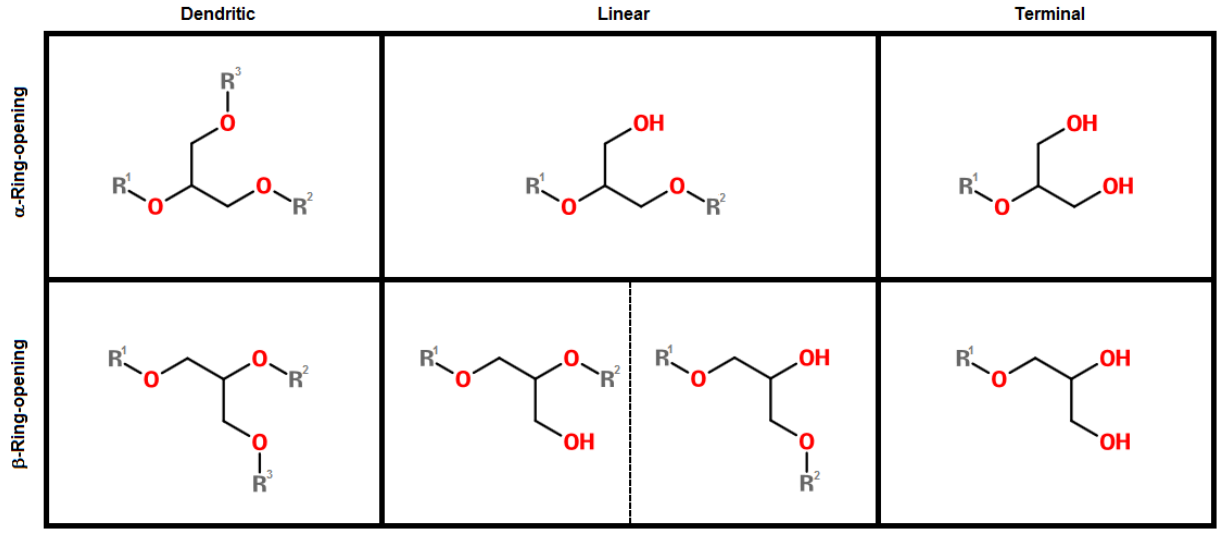

Figure 3.2. Possible monomeric subunits of Polyglycerol. Depending on which C-O bond of the epoxide is broken, either α- or β-ring-opening products are formed. R^1, R^2, and R^3 represent the continuation of the polymer chain.

Since the basic idea behind the synthesizing strategy is to produce polymers with a structure as close to that of its dendrimer counterpart, a new property called degree of branching (DB) was introduced. It is a measure of the structural relatedness to a dendrimer. The term was firstly introduced by Hawker et al.[43] and a similar terminology was derived by Kim et al.[40] In the 1990s, the following formula was widely used to assess structure of polymers with tri-functional branching points.

$$DB_{Fréchet} = \frac{D+T}{D+L+T} \tag{3.12}$$

Here D, L, and T stand for the amounts of the dendritic, linear, and terminal subunits, respectively. One can determine the degree of branching for a single molecule, but also for a mixture of molecules by summing all the amounts of subunits across all polymers, i.e., the

average degree of branching $\overline{DB}$. Obviously, the DB of a perfect dendrimer is 1 because it only consists of dendritic and terminal subunits. Linear polymers, however, do not exhibit a DB of zero as one might expect. This fact motivated Hölter and Frey to introduced a modified definition for the degree of branching which considers the ratio of dendritic subunits present in a molecule to the maximum number of branch points that would be contained by the "closest related dendrimer."[85] In order to convert a hyperbranched polymer into a dendrimer, one could rearrange the chains so that two linear units form one terminal and one dendritic subunit. Therefore, the maximal amount of dendritic units can be assumed to be $D + 0.5L$ and the modified degree of branching, as it was defined by Hölter and Frey, reads as follows.

$$DB_{Frey} = \frac{D}{D_{max}} = \frac{2D}{2D + L} \tag{3.13}$$

For the polymerization of AB_2-type monomers, it is well known that the number of terminal units is always one plus the number of dendritic units. Therefore, if N is the number of polymers, then the total number of dendrimers must be $D = T - N$ and Frey's definition can be written as

$$\overline{DB}_{Frey} = \frac{2T - 2N}{2T - 2N + L} = \frac{D + T - N}{D + L + T - N} \tag{3.14}$$

While inspecting this formulation the difference between the two definitions becomes obvious. Since every polymer has at least one terminal group, ignoring the core unit as an end group, 1 has to be subtracted for every molecule from the numerator and the denominator. The same conclusion was also drawn by Yan and Müller.[86]

In addition, the modified formula is more convenient for the determination by measurements since it is no longer necessary to evaluate the amounts of dendritic and terminal subunits at the same time. Also, when considering large molecules D and T become much bigger than N and one can use either the signals for terminal and/or dendritic subunits since, the following approximation holds.

$$DB = \frac{2D}{2D + L} \approx \frac{D + T}{D + T + L} \approx \frac{2T}{2T + L} \tag{3.15}$$

The last two properties of the polymer sample discussed here are the amount of residual monomers and the total number of polymers. The latter is of utter importance when determining the average molecular weight of a sample. In the ideal case, monomers bind exclusively to the initiators, so that the total number of molecules at the end of the

reaction is equal to the initial amount of initiators. Knowing the total number of molecules allows to calculate the number of polymers created by the spontaneous combination of two monomers. The converse argument might be helpful as well. By definition, self-initiated polymers lack the initiator derivative, so that the molecular mass is different to a primary polymer that incorporates the same number of monomeric subunits. This can be exploited to determine the ratio between normal and self-initiated polymers. Another noteworthy fact is that self-initiated polymers still contain an unreacted epoxide ring at first and unless they get combined with other polymers, this will most likely lead to an intramolecular ring-opening reaction and a macromolecular cycle is formed. Measuring the amount of cycles in a sample would help to determine the total number of molecules as well, but up to now it has not been possible to differentiate the cyclic polymers because their physical properties are too close to the normal polymers.

4. MODELING THE ANIONIC RING-OPENING POLYMERIZATION OF GLYCIDOL

There are several ways to model the dynamic behavior of a chemical system to depict various levels of detail. Probably the most exact methods utilize a molecular dynamics (MD) approach where reactions between molecules depend on force potentials that can be calculated with the knowledge about the positions and velocities of every atom in the system.[87,88] Such simulations can capture the dynamics between a very small number of molecules, but are obviously not suitable for the simulation of molecules in the amount of mol. Therefore, in that respect harsh simplification assumptions have to be made.

Firstly, the reaction rates are not calculated through the positions and velocities of the molecules, but rather from the amount or concentration alone. The underlying assumption is that molecules can travel throughout the system very quickly and collide so many times that the overall number of reactions can be estimated by the statistical average number of collisions per time unit. Secondly, not the interactions between atoms themselves, but between the molecules as entities are regarded. The molecular conformation and structure will be regarded implicitly by modifying the reaction rate per molecule in dependence on general properties such as molecule size or averaged composition of functional groups.

4.1 Classical Chemical Reaction Kinetics

The modeling concept is based on the law of mass action and the rate of a reaction depends mainly on the physical state of the reactants, their concentration, and the temperature of the system.[89] A process can be modeled as an initial value problem where the state space captures the concentrations of every molecular species including initiators and monomers as well as every type of polymer, i.e., of different sizes. For every entry in the state vector an ordinary differential equation (ODE) is formulated and the system is treated with well-established solvers. In simple cases the solution can be derived analytically, but for systems as complicated as the one at hand, numerical solutions are necessary.

4.1.1 Reaction Equations and Ordinary Differential Equations

To illustrate the concept of general mass action kinetics,[89] one has to understand the concept of reaction equations and how they can be used to simulate the dynamical changes of the concentrations of all chemical species. Firstly, one has to define the chemical species, e.g. A, B, and C, and their concentration at time t. A concentration is traditionally denoted by square brackets, e.g., $[A]_t$. However, these brackets will only be written in this section and will be omitted later for the sake of clarity as long as the context clearly indicates a reference to the concentration, e.g., A or $A(t)$ with time dependency. The interactions between the chemical species are defined through reaction equations of zeroth, first or second order.[90] Reactions of higher order can be realized as sequential combination of lower-order reactions,[91] but because such reactions were not considered in this study, this issue will not be elaborated further. All reactions are regarded to be irreversible, so that a possible backward reaction has to be formulated as a separate equation.

The elemental reactions can be formulated as follows. Every example contain only one product, C, but in general a reaction may produce an arbitrary number of chemical species. One can even consider reactions that have no product which could be used to model the extraction of some species from the system. The absence of any molecules is denoted by the empty set, $\emptyset$.

$$\begin{aligned}
R_0&: & \emptyset &\xrightarrow{k_0} C\\
R_1&: & A &\xrightarrow{k_1} C\\
R_{2a}&: & A + B &\xrightarrow{k_{2a}} C\\
R_{2b}&: & 2\,A &\xrightarrow{k_{2b}} C
\end{aligned}$$

Scheme 4.1. Basic reaction equations for reactions of zeroth, first, and second order.

The reaction rate coefficients in Scheme 4.1, k_0, k_1, k_{2a}, and k_{2b}, can be used to calculate the reaction rates for each reaction. These rates provide information about the number of molecules that react or are produced per time unit. For the above-mentioned reactions,

the rates can be calculated as follows.

$$\mathrm{Rate}_t(R_0) = k_0 \tag{4.1}$$

$$\mathrm{Rate}_t(R_1) = k_1 \cdot [A]_t \tag{4.2}$$

$$\mathrm{Rate}_t(R_{2a}) = k_{2a} \cdot [A]_t \cdot [B]_t \tag{4.3}$$

$$\mathrm{Rate}_t(R_{2b}) = k_{2b} \cdot \frac{[A]_t \cdot ([A]_t - 1)}{2} \approx k_{2b} \cdot \frac{[A]_t^2}{2} \tag{4.4}$$

One can see that the zeroth-order reaction, R_0, only depends on the constant reaction coefficient whereas the first-order reaction, R_1, depends of the concentration of the reacting species at a specific time, t. The second-order reactions, R_{2a} and R_{2b}, show a non-linear dependency on the concentrations of the reacting species. The approximation in Equation 4.4 is justified because this study regards large quantities of molecules at the same time.

Knowing these reaction rates and the concentrations of every chemical species at a specific time, t, one can approximate the concentrations after a reasonable period of time, Δt. Considering the fact that the species C is produced by every reaction in Scheme 4.1, it is clear that its concentration has to change as follows.

$$[C]_{t+\Delta t} = [C]_t + \Delta t \cdot [\mathrm{Rate}_t(R_0) + \mathrm{Rate}_t(R_1) + \mathrm{Rate}_t(R_{2a}) + \mathrm{Rate}_t(R_{2b})] \tag{4.5}$$

This equation can be rearranged to form a differential quotient for the time-dependent concentration of the chemical species C. Regarding infinitesimally small time periods, the differential equation can be written as follows.

$$\frac{d[C]_t}{dt} = \lim_{\Delta t \to 0} \frac{[C]_{t+\Delta t} - [C]_t}{\Delta t} = \mathrm{Rate}_t(R_0) + \mathrm{Rate}_t(R_1) + \mathrm{Rate}_t(R_{2a}) + \mathrm{Rate}_t(R_{2b}) \tag{4.6}$$

This concept can be applied to the reacting species as well. Reactant A is used up in reactions R_1, R_{2a}, and R_{2b}, whereas reactant B is only involved in reaction R_{2a}. Additionally, reaction R_{2b} depends on the squared concentration of species A and a single reaction event consumes two molecules of A. All these factors are reflected in the following differential equations.

$$\frac{d[A]_t}{dt} = -\mathrm{Rate}_t(R_1) - \mathrm{Rate}_t(R_{2a}) - 2\,\mathrm{Rate}_t(R_{2b}) \tag{4.7}$$

$$\frac{d[B]_t}{dt} = -\mathrm{Rate}_t(R_{2a}) \tag{4.8}$$

Inserting Equations 4.1-4.4 into Equations 4.6-4.7 results in the following set of ordinary differential equations.

$$\frac{d[A]_t}{dt} = -k_1[A]_t - k_{2a}[A]_t[B]_t - k_{2b}[A]_t^2 \tag{4.9}$$

$$\frac{d[B]_t}{dt} = -k_{2a}[A]_t[B]_t \tag{4.10}$$

$$\frac{d[C]_t}{dt} = k_0 + k_1[A]_t + k_{2a}[A]_t[B]_t + k_{2b}\frac{[A]_t^2}{2} \tag{4.11}$$

For the mathematical representation, all concentrations are usually written in a state vector, e.g.

$$x(t) = \{[A]_t, [B]_t, [C]_t\}^\mathsf{T} , \tag{4.12}$$

and the time derivative for this vector is written as follows.

$$\frac{dx(t)}{dt} = f(t, x, p) \tag{4.13}$$

The function f was defined earlier in Equations 4.9-4.11 and depends on the time, t, the current state, x, and a parameter vector, p. In the above-mentioned example the parameter vector only contains the fixed reaction coefficients, but additional factors, such as temperature, pressure, and volume, may be specified individually.

Finally, with the knowledge about the starting concentration of all chemical species, i.e., the initial state

$$x(0) = x_0 \tag{4.14}$$

one can simulate the process by solving the associated initial value problem. Such systems are very common and there exist sophisticated methods to solve them, e.g., Euler or Runge-Kutta methods.[92,93]

Due to the deterministic nature of this approach, the parameter vector can be optimized with well-understood and robust methods in order to accurately reproduce an expected output.[10] This aspect is very important for the comparison of simulated to experimental data and this study relied heavily on parameter estimation methods to validate the derived models on the basis of measurement data.

4.1.2 Special Characteristics of Polymerization Kinetics

The concept of general mass action kinetics can also be applied to polymerization processes, but some specific aspects have to be considered. Due to the nature of polymerization processes, the molecules in the system can have a broad range of molecular masses which can affect the dynamics drastically. Furthermore, the average molecular weight is usually the most important property of a polymer mixture and analyzing the MMD requires to model polymers of different sizes as individual chemical species. Therefore, even for very simple polymerization processes the state space becomes very high-dimensional. On the contrary, polymers of similar sizes often show similar quantities, i.e., if one imagines the PSD as a continuous function, it could be considered as smooth. This property motivates the approximation of the PSD by a known functional and if the shape of a PSD is already known, e.g., experiments indicate a Schulz-Flory or a Poisson distribution, then only a few parameters (e.g., three or less) are needed to describe the whole PSD. In cases where the shape of the PSD is not known *a priori*, one can still utilize certain discretization methods to model the MMD and PSD of a polymer mixture.

The simulation software PREDICI that was employed in this study utilizes a so-called "Galerkin h-p-method" to approximate the PSD. In order to approximate the smooth parts of the distribution as cost-efficient as possible without introducing too big of an error for the non-smooth regions, a mixture of a global and local approximation strategy was proposed by Wulkow.[94] The basic idea is to subdivide the polymer size domain into various intervals and locally approximate the PSD on each interval by a polynomial of a certain order. In the literature on the numerical solution of partial differential equations the approach where the intervals and the orders of the local expansions can be adapted individually is referred to as "h-p-method". Given a grid that is defined as a set of interval-order-pairs, $\Delta = \{(I_1, p_1), ..., (I_M, p_M)\}$, a given PSD, P_s, can be locally expressed as follows.

$$P_s \Big|_{I_m} \approx \widetilde{P}_{m,p_m}(s) := \sum_{k=0}^{p_m} a_{m,k} t_{m,k}(s) \tag{4.15}$$

Here, $a_{m,k}$ are the local expansion coefficients and $t_{m,k}(s)$ denote the discrete Chebyshev polynomials of k-th order which are defined as zero for s outside on the interval I_m. These polynomials are orthogonal with respect to the scalar product

$$\langle t_{m,k}, t_{m,j} \rangle := \sum_{s \in I_m} t_{m,k}(s) t_{m,j}(s) = \gamma_{m,k} \delta_{k,j} \tag{4.16}$$

where $\delta_{k,j}$ denotes the Kronecker symbol and $\gamma_{m,k}$ is a normalizing factor on I_m. On the respective intervals the polynomials can easily be calculated through the well-known three-term recurrence.[95] It is important to note that by increasing the degree of the local polynomial, the non-smooth parts of the PSD can be approximated nearly exactly if necessary. After defining an appropriate metric for each interval, e.g., between two PSDs, P and Q,

$$\|P - Q\|_m^2 = \sum_{s \in I_m} (P_s - Q_s)^2 \tag{4.17}$$

the orthogonality of the Chebyshev polynomials can be used to evaluate the local approximation error as follows.

$$\epsilon_m^2 = \left\| \widetilde{P}_{m,p_m} - P \right\|_m^2 = \sum_{s \in I_m} \left(\widetilde{P}_{m,p_m}(s) - P_s \right)^2 \tag{4.18}$$

The thus resulting error estimate

$$\widetilde{\epsilon}_m = \left\| \widetilde{P}_{m,p_m+1} - P_{m,p_m} \right\|_m^2 = a_{m,p_m+1}^2 \gamma_{m,p_m+1} < \epsilon_m \tag{4.19}$$

can then be used in a heuristic multilevel grid refinement strategy. The grid can be improved by changing the intervals, i.e., through subdivision, or by increasing the degree of the local polynomials, which gives the reasoning behind the name "h-p-method". Without going into the details of the algorithm, it suffices to say that the possible refinement steps can be evaluated on the basis of the local approximation error estimates, $\widetilde{\epsilon}_m$. After all, the optimal choice for one interval is given by maximizing the "accuracy per normalized work" and by improving only the "most erroneous" intervals, an equilibrium of the local errors is reached.[96] This ensures a good convergence rate towards a fixed approximation error tolerance Tol_S and an efficient implementation. Cases where it is better to use a more coarse grid in subsequent time steps are also considered by initiating a refinement step with a coarsened grid and with polynomials of lower orders. For more information about the grid propagation the reader is referred to the original work by Wulkow.[83]

Traditionally, when the state space needs to be approximated, the time evolution equations have to be reformulated in terms of the applied approximation scheme. Therefore, instead of propagating the state vector in time, the degrees of freedom of the approximated representation, e.g., the expansion coefficients, have to be updated in every time step. Such methods have become known as methods of lines,[97] but in most cases this approach cannot be combined with an adaptive approximation scheme as it was described

above. Therefore, the PREDICI software was designed to implement Rothe's method which was introduced by Bornemann in 1990.[98] The basic idea is to discretize in time first and then solve the resulting stationary problem subsequently.[96,99]

Considering the original problem formulated in Equations 4.12-4.14, the task is to approximate $x_1 \approx x(t+\tau)$ on the basis of the current state at time t, $\phi = x(t)$, for a reasonable time step length τ. This can be done with a linear-implicit Euler scheme

$$(\mathcal{I} - \tau\mathcal{A})\Delta x_0 = \tau f(\phi) \tag{4.20}$$

$$x_1 = x_0 + \Delta x_0 \tag{4.21}$$

where $\mathcal{I}$ denotes the identity matrix and $\mathcal{A} = \frac{df}{dx}(\phi)$ is the total derivative of all right hand sides with respect to all variables.

The approximation can be improved by Bornemann's multiplicative error correction (MEC) which allows to estimate the time error by solving the following correction equation with the same left-hand size matrix as in Equation 4.20.

$$(\mathcal{I} - \tau\mathcal{A})\Delta x_1 = -\frac{\tau}{2}\mathcal{A}\Delta x_0 \tag{4.22}$$

$$x_2 = x_1 + \Delta x_1 \tag{4.23}$$

Because the approximation x_2 is one order higher than x_1 the time error is easily computed with an appropriate norm, $\|\cdots\|$.

$$\epsilon_T = \|\Delta x_1\| \tag{4.24}$$

After performing a time step with the original time step length, τ, a new step size τ_{new} can be calculated as follows.

$$\tau_{new} = \tau\sqrt{\rho\frac{Tol}{\epsilon_T}} \tag{4.25}$$

Here, $\rho < 1$ is a safety factor and Tol is a user-defined error tolerance.

This method is straightforward for normal ODEs, but it can also be applied if the state space cannot be calculated exactly. It is a special feature of Rothe's method that the approximation scheme for the state space can be chosen independent from the time integrator, as long as the stationary error of the approximations for x_1 and x_2 stays below Tol_S.[96] By matching the temporal and the stationary errors to keep the total error below a predefined tolerance the time integration can be combined with an adaptive state space

approximation scheme as it was presented above. That means that a time step is computed for the grid of the previous one and if the resulting stationary error is not below the stationary tolerance, the grid refinement procedure is executed. Only after an "optimal grid" was obtained, the new time step size can be computed and the state vector can be updated.

In order to compute one time step as it is defined in Equation 4.20 for a given grid that is composed of M interval-order-pairs (I_m, p_m), a so-called Galerkin matrix $G = (g_{jk})$ has to be constructed. This is essentially the product of the total derivative $\mathcal{A} = \frac{df}{dx}(\phi)$ and the solution Δx_0 expressed in terms of the chosen basis functions $t_{m,k}(s)$.[83] Calculating the matrix' entries requires summations of the following form.

$$g_{jk} = \sum_{s=1}^{\infty} \mathcal{A}t_k(s)t_j(s) \tag{4.26}$$

Here, the interval index was omitted, so that j and k count all base base functions for all intervals in the grid ($\sum_{i=1}^{M} p_m$ many). The final Galerkin equations can be derived on the basis of Equation 4.20:

$$G\alpha = \left(\sum_{s=1}^{\infty} b_s t_j(s) \right)_j \tag{4.27}$$

Here, b_s corresponds to the right hand side of Equation 4.20 expressed in terms of the chosen basis functions and α is the solution vector with which all expansion coefficients can be updated within a time step.

Evaluating the depicted summations is potentially very demanding to the algorithm and it is crucial to do this efficiently. Therefore, the simulation software is based on Gauß-Christoffel-summations which are directly induced by the orthogonal Chebyshev polynomials. This leads to the following approximation of an arbitrary function f defined on an interval I.

$$\sum_{s \in I} f(s) \approx \sum_{i=1}^{n} w_i f(s_i) \tag{4.28}$$

The nodes, s_i, and weights, w_i, are chosen so that the approximation is exact as long as $f(s)$ is a polynomial of order $2n-1$. In that case, the nodes are simply the zeros of the discrete Chebyshev polynomials and can easily be computed from a triangular eigenvalue problem along with the weights.[10] The matrix entries are given by the factors of the three-term recursion of the polynomials.

As it will be shown later in this chapter, there are cases in which one property index

does not suffice to correctly model the state space and the according reaction rates. Such systems cannot be treated easily by the simulation software and this issue is part of the ongoing research to improve the algorithm. The above-sketched concept cannot be simply extended to multidimensional polynomials. For the same reasons orthogonal polynomials were chosen for approximating of the polymer size domain, it was attempted to use tensor products for the approximation of two-dimensional polymer species. This would permit simple calculations of summations over the individual property indexes, but since the number of parameters needed for the state space approximation rises quadratically, this approach is not useful for a high throughput of simulations. Therefore, applications that require many trials, such as parameter estimation procedures, cannot be used for such models. Increasing the number of dimensions even higher has not been attempted because the algorithm can be expected to become so inefficient that only a very few problems could be solved and for these cases there exist other more efficient methods, e.g., Monte-Carlo methods.

There are some alternative approaches to treat systems that require additional information about the polymer species and their PSDs. Recently, the trend is to couple the highly optimized algorithm with Monte-Carlo methods.[100] The idea is to divide the dynamics into parts that can be described either by the deterministic Galerkin methodology or by a stochastic simulation. These dynamics are treated separately for the most part and can influence each other in between time steps. However, there are also concepts that can be directly applied to the PREDICI software as it is available at the moment. In cases where the additional dimensions are very small, one can attempt to formulate separate polymer species (represented by separate PSDs) for every additional value. This would introduce a pseudo-two-dimensionality where the additional dimension is not approximated at all. Obviously, the state space can become large very quickly, which is why the number of additional species has to be strictly limited, but in some cases the additional information is already enough to clearly improve the simulation. It should also be noted that many and fast interactions between these separate polymer species can introduce inefficiencies in each others h-p-approximation schemes, but this is hard to predict. Another option to alter the polymer species without adding an extra property index is to use global variables to approximate polymer properties that are averaged over all polymers in the system. This can often be done easily by introducing artificial low molecular species that do not effect the reaction kinetics, i.e., they have no mass, no volume, and do not react with other molecular species in the system. However, they do have a concentration which can be

used to "count" how often a specific reaction has occurred in total ever since the reaction has started. This information can, for instance, be used to update kinetic parameters for reactions that depend on the history of the process.

Later in this chapter, the concepts that do not involve an algorithmic change of the simulation software will be used to model the anionic ring-opening polymerization of glycidol.

4.2 Proceeding Studies of Hyperbranched Polymers

There are a couple of proceeding studies that are very important for the system at hand. Even though nobody has performed a detailed mathematical analysis of the exact process, some very similar conditions have already been studied.

This section summarizes three publications that had a great impact on this study's approach to model the ring-opening polymerization of glycidol. Firstly, the fundamental work of Flory from the middle of the last century formed the basis for the analytical analysis of random polycondensation processes.[101–105] He derived mathematical expressions for the MMD of randomly hyperbranched polymers and formulated their time evolution equations. His work is still cited by many researchers nowadays which shows the importance of his findings for this scientific field. The second publication was written by Müller and Yan who extended the concept to the SCVP and compared the two processes.[84,86] They derived time- and conversion-dependent expressions for the whole MMD, the average molecular weight, the polydispersity index and the average degree of branching. Furthermore, they analyzed the impact of different reactivities of the functional groups. The last paper to be presented here is from Radke et al. who used the same formalism to test alternative polymerization strategies to improve the final product of SCVP.[106] They tested two modified reaction schemes which utilize core-forming molecules and a slow monomer addition technique to prevent self-initiation reactions between free monomers. They could show that the average molecular weight becomes controllable through the ratio of the amounts of monomers to that of the core-forming molecules and that the polydispersity index could be improved drastically.

4.2.1 Flory's Fundamental work on Random Polycondensation Reactions

In the 1940s Flory already derived the mathematical foundation for predicting the MMD of randomly hyperbranched polymers with a special focus on random AB_2 polycondensation

and $A_2 + B_3$ polycondensation reactions.[102,103] He also developed hypotheses about the structures formed and the critical conditions that lead to the formation of "structurally insoluble gels."[101] Most interesting for this study is his comprehensive work from 1952 though.[105]

Flory defined the randomly branched polymer as a graph where every edge represents a molecular chain and the nodes describe the branching points. The nodes have an outgoing degree of 3, which is the case for tri-functional monomers. Figure 4.1 shows an illustration of such a graph. One can see that the number of branching points, n, is correlated to the number of chains, z, by $z = 2n + 1$.

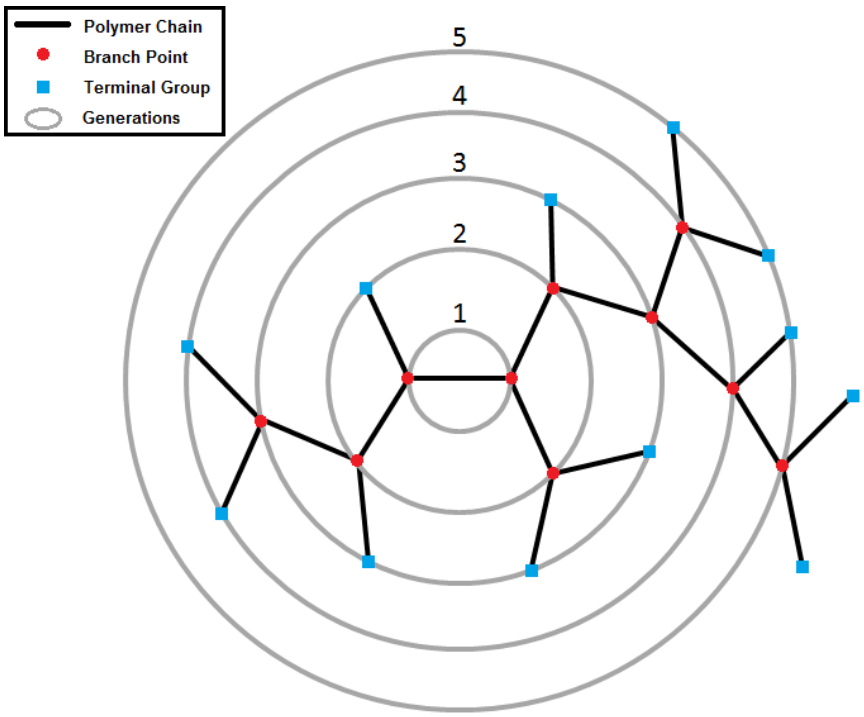

Figure 4.1. Schematic structure of a randomly branched polymer. After fixing a core, the rest of the polymer's chains can be assigned to a generation, indicated by the numbers. A branching point is defined as a point on a cycle that is connected to more than one other cycle by an edge.

The figure also shows how the graph can be clustered into generations (indicated as cycles in the figure) by defining a "core" chain and regarding its distance to every node in the graph. The structure can be analyzed on the basis of the probability, α, of any chain to end in a branch point, i.e., the probability that an edge starting on one of the cycles is connected to another branching point on the next bigger cycle. If the number of branch points on the i-th cycle is Y_i, then the expected number of branch points on cycle $i + 1$ is $Y_{i+1} = 2\alpha Y_i$. This expectation value becomes nearly exact for very large

graphs. An infinite series of Y_i will converge to zero if $\alpha \leq 1/2$ and will approach infinity if $\alpha > 1/2$. To illustrate this, one can compare this series to the path of a random walker who takes one step forward with probability α and one step backwards with the complementary probability. The probability for the walker to reach the origin in infinite time is known to be unity for all values $\alpha \leq 1/2$ and zero otherwise. This can be generalized to systems with f-functional branching points and Flory formulated the critical condition, α_c, for the gel formation for polycondensation reactions of f-functional monomers.

$$\alpha_c = 1/(f-1) \tag{4.29}$$

Flory calculated theoretical values of α_c for various processes, including for A_3-, A_3+B_2- and also $A-R-B_{f-1}$-polycondensation reactions. The latter will be described in more detail because the system at hand behaves in a similar manner.

Using monomers of type $A-R-B_{f-1}$ produces f-functional branching points and it is assumed that reactions can only occur between A and B groups and only intermolecularly. This results in the formation of polymers with one unreacted A group and the number of unreacted B groups is $(f-2)x+1$, where x denotes the number of monomeric subunits. The branching probability, α, is simply expressed as the conversion of B groups, p_B. Since A and B groups are consumed in equal amounts, the conversion of A groups is given as $p_A = (f-1)p_B$. Therefore, the branching probability can be written as follows.

$$\alpha = p_A/(f-1) \tag{4.30}$$

As the A group conversion goes to unity, α approaches but never reaches the critical value of $\alpha_c = 1/(f-1)$, so the process will not produce a gel as it was defined earlier. Interestingly, copolymerizing AB_2- and AB-type monomers will not change the branching structure and the only effect it has is that the molecular chains connecting the branch points will vary in length. However, introducing A_2- or B_2-type monomers will directly permit gelation.

Flory also derived the molecular size distribution as the probability of an unreacted A group to be connected to an x-mer through any series of reactions where $x-1$ B groups reacted while the other $fx-2x+1$ did not. As a result, the molecular size distribution, N_x, can be calculated as follows.

$$N_x = \frac{1-\alpha}{\alpha}\omega_x\beta^x \tag{4.31}$$

where the number of configurations is given as

$$\omega_x = \frac{(fx - x)!}{(fx - 2x + 1)!x!} \tag{4.32}$$

and for clarity

$$\beta = \alpha(1 - \alpha)^{f-2} \tag{4.33}$$

In order to evaluate the number- and weight-average degrees of polymerization, Flory defined the following generating function.

$$S_m = \frac{\alpha}{1 - \alpha} \sum_{x=1}^{\infty} x^m N_x \tag{4.34}$$

This function has the property that

$$S_1 = \beta \frac{dS_0}{d\beta} \tag{4.35}$$

$$S_2 = \beta \frac{dS_1}{d\beta} \tag{4.36}$$

Substitution of $d\beta$ with $d\alpha$ (through Equation 4.33) and considering that $\sum N_x = 1$ results in

$$S_0 = \frac{\alpha}{1 - \alpha} \tag{4.37}$$

$$S_1 = \frac{\alpha}{1 - \alpha} \times \frac{1}{1 - \alpha(f - 1)} \tag{4.38}$$

$$S_2 = \frac{\alpha}{1 - \alpha} \times \frac{1 - \alpha^2(f - 1))}{[1 - \alpha(f - 1)]^3} \tag{4.39}$$

From this, one can easily calculate the weight fraction distribution of x-mers as $W_x = xN_x / \sum xN_x$. Furthermore, the number- and weight-average degree of polymerization as

well as the polydispersity index become evident.

$$\overline{P}_n = S_1/S_0 = \frac{1}{1-\alpha(f-1)} \tag{4.40}$$

$$\overline{P}_w = S_2/S_1 = \frac{1-\alpha^2(f-1))}{[1-\alpha(f-1)]^2} \tag{4.41}$$

$$PDI = \overline{P}_w/\overline{P}_n = \frac{1-\alpha^2(f-1))}{[1-\alpha(f-1)]} \tag{4.42}$$

Flory's conclusions were that the number and weight fraction distribution is monotonically decreasing with increasing A group conversion for all values of α below the critical value $\alpha_c = 1/(f-1)$ which is never reached. This means that small polymers make up a big portion of the mixture even at high conversion of A groups. Additionally, one can see that the molecular size distribution merges with the x-axis as the conversion approaches unity. This concludes that in the limiting case $\alpha = \alpha_c$ the distribution is infinitely broad and infinitesimally high. This can also be seen in the expressions for $\overline{P}_n$ and $\overline{P}_w$, which both go to infinity, but $\overline{P}_w$ does so faster, so that the PDI as well goes to infinity.

4.2.2 Analytical expressions for MMD and $\overline{DB}$ in SCVP and AB_2 Polycondensation Reactions

In 1997, Müller et al.[84] derived analytical expressions for the MMD for the SCVP and the polycondensation of AB_2-type monomers at the same time. These two processes will be referred to as AB^*-process and AB_2-process throughout this section. The processes were compared by the dynamical change in number- and weight-average degree of polymerization, $\overline{P}_n$ and $\overline{P}_n$, as well as the polydispersity index $PDI = \overline{P}_w/\overline{P}_n$. These quantifiers for the MMD were regarded with respect to the reaction time, t, and to the conversion of vinyl groups, x, which is not equivalent to the monomer conversion.

The chemical mechanisms involved in the processes are very different, but the rough structure of the products can be compared. Figure 4.2 shows a few reaction steps for both processes. It can be seen, that the monomers of SCVP contain only two functional groups (A is the vinyl group and B an initiating group). Despite this fact, branching units can still be formed because upon the reaction of a vinyl group a new propagating group, A^*, is formed which is also capable of reacting with other vinyl groups. Every functional group that is capable of reacting with a vinyl group is shown with an asterisk and unreactive derivatives that resulted form a previous reaction are shown as small letters. However, it

is questionable whether all functional groups have the same reactivity. This was one of the main focuses of the Müller's work.

For clarity, the monomers are highlighted to distinguish the subunits better and the first monomer which can be found in every reaction step is marked in blue. The final product is merely an example to illustrate the different types of subunits which can be summarized into branching points, linear and terminal units. For the SCVP one can specify the linear units further in dependence on whether it contains an unreacted initiating or propagating group.

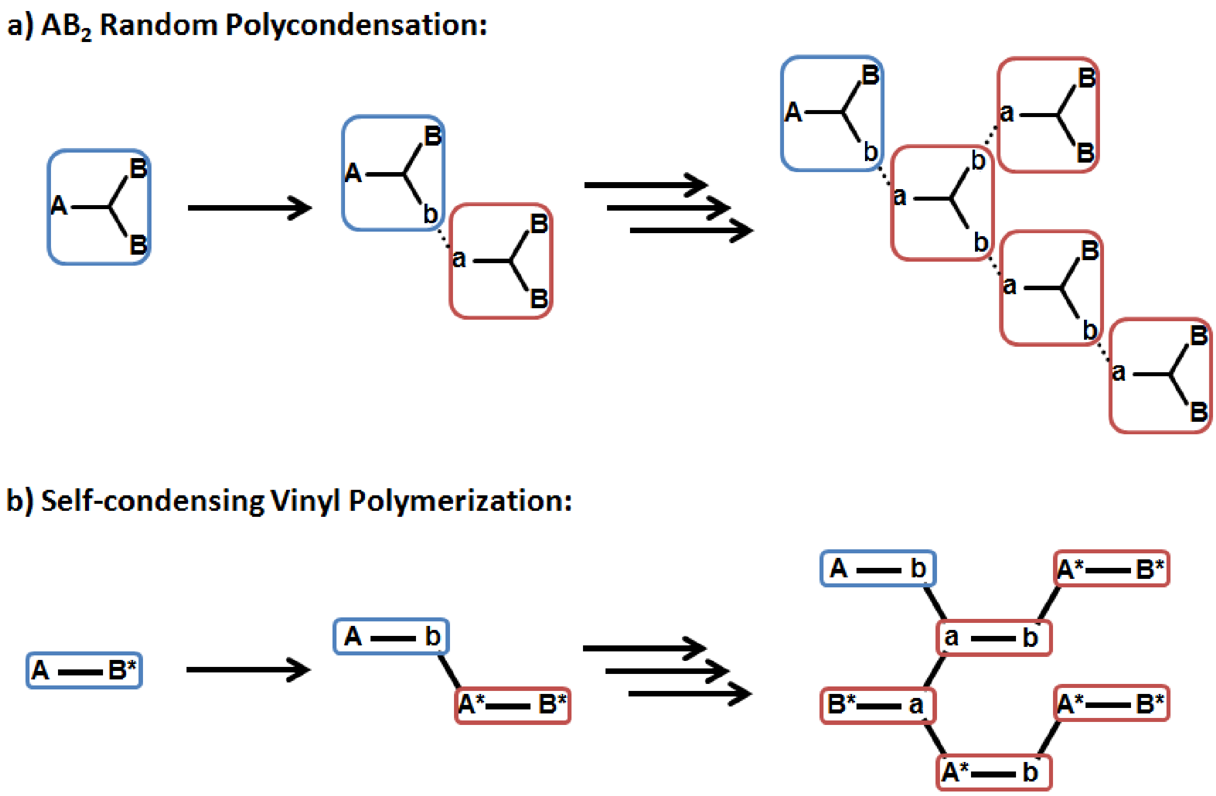

Figure 4.2. Schematic illustration of the initial steps of the compared polymerization processes. Random polycondensation of AB_2-type monomers is shown on top and SCVP at the bottom.

Most importantly, both processes produce hyperbranched structures and growing polymers accumulate more functional groups and thereby the reactivity increases proportionally to the polymer size. To analyze the PSD and its moments, Schemes 4.2 and 4.3 were formulated.

The difference of the reaction rate coefficient arises from the definition of the polymers. In both cases the subscript denotes the degree of polymerization, i.e., the number of

$$P_i + P_j \xrightarrow{k\cdot(i+j)} P_{i+j}$$

Scheme 4.2. Reaction scheme for the self-condensing vinyl polymerization (AB^*-process).

$$P_i + P_j \xrightarrow{k\cdot(i+j+2)} P_{i+j}$$

Scheme 4.3. Reaction scheme for the polycondensation of AB_2-type monomers (AB_2-process).

monomeric subunits composing the polymer. In the SCVP the total number of active sites, i.e., initiating groups B^* and propagating groups A^* is equal to the degree of polymerization, whereas in the case of AB_2 random polycondensation, the number of active sites, i.e., the number of B groups, is equal to the degree of polymerization plus one. In other words, an AB_2-type monomer has two active sites and an AB^*-type one only one.

The ODEs describing the change of concentration for each molecule species differ for the two processes slightly and can be formulated as follows. It should be noted that the concentration of a chemical species within a differential equation is always denoted by the identifier of that species, e.g., P_i represents the concentration of a polymer with a degree of polymerization of i.

For the AB^*-process:

$$\frac{dP_i}{dt} = \frac{k}{2} \sum_{0<j<i} iP_jP_{i-j} - kP_i \left[i \sum_j P_j + \sum_j jP_j \right] \tag{4.43}$$

And for the AB_2-process:

$$\frac{dP_i}{dt} = \frac{k}{2} \sum_{0<j<i} (i+2)P_jP_{i-j} - kP_i \left[(i+2) \sum_j P_j + \sum_j jP_j \right] \tag{4.44}$$

The initial condition is the same for both processes, since at time $t = 0$ there are only monomers which are modeled as P_1 in both cases.

$$P_i(t=0) = \delta_{i,1} M_0 \tag{4.45}$$

M_0 is the initial concentration of monomers and $\delta_{i,j}$ is the Kronecker delta which is defined as:

$$\delta_{i,j} = \begin{cases} 1, \text{ if } i = j \\ 0, \text{ if } i \neq j \end{cases} \tag{4.46}$$

The k-th moment of a polymer size distribution is defined as usual:

$$\mu_k = \sum_{i=1}^{\infty} i^k P_i \tag{4.47}$$

The first two moments, μ_0 and μ_1, can be calculated with the same formula for both processes if the number of unreacted A groups and the initial amount of monomer is known. It is clear from the nature of both processes that the zeroth moment must be equal to the number of unreacted A groups, which are defined as the time dependent variable A. The first moment stays the same throughout both polymerizations due to the material balance condition and is defined solely by the initial amount of monomers, M_0.

$$\mu_0 = \sum_i P_i \ = A \tag{4.48}$$

$$\mu_1 = \sum_i i P_i = M_0 \tag{4.49}$$

For both processes, the conversion of A groups, x, is defined as

$$x = \frac{M_0 - A}{M_0} \tag{4.50}$$

Let B^* and A^* denote the concentration of initiating and propagating groups in the polymers of the SCVP, respectively. The overall number of active sites is equal to the initial number of monomers.

$$A^* + B^* = \sum_i i P_i = M_0 = \mu_1 \tag{4.51}$$

Furthermore, let B denote the total concentration of B groups in the AB_2-process. From the composition of the AB_2-type monomer, the following relation is known.

$$B = \sum_i (i+1) P_i = M_0 + A = \mu_1 + \mu_0 \tag{4.52}$$

For both processes, the conversion of functional groups that may react with the A groups is defined as α. For the SCVP, $\alpha = 1$ remains unchanged over the course of the polymerization because for every reacting group, a new A^* group arises by the addition to the vinyl group. For the AB_2 polycondensation, on the other hand, one B and one A

groups are converted into unreactive derivatives. Therefore, α decreases over the course of the polymerization and because initially there are twice as many B groups than A groups, $\alpha = x/2$ must hold.

For both processes, the concentration of A groups at a specific time, t, can be calculated analytically, by summation of both sides of the respective ODEs (eqs. 4.43 and 4.44) over the index i.

For the AB^*-process:

$$\frac{d}{dt}\sum_i P_i = \dot{\mu}_0 = -k\mu_1\mu_0 = -kM_0A \tag{4.53}$$

For the AB_2-process:

$$\frac{d}{dt}\sum_i P_i = \dot{\mu}_0 = -k\left[\mu_1\mu_0 + \mu_1^2\right] = -kM_0A - kM_0^2 \tag{4.54}$$

Knowing the time derivative for A, it is easy to assess the dynamical change of the A group conversion, dx/dt.

For the AB^*-process:

$$\frac{dx}{dt} = kM_0(1-x) \tag{4.55}$$

For the AB_2-process:

$$\frac{dx}{dt} = kM_0(1-x) + kM_0 \tag{4.56}$$

Examining the A group conversion for the AB^*-process, one finds

$$x = 1 - e^{\tau} \tag{4.57}$$

where τ is a reduced time which is defined as

$$\tau = kM_0t \tag{4.58}$$

This is different for the AB_2-process:

$$x = 2\frac{1-e^{\tau}}{2-e^{\tau}} \tag{4.59}$$

As mentioned before, α differs as well. While it is unity at all time for the SCVP, it

varies for the AB_2 polycondensation in the following way.

$$\alpha = \frac{1 - e^{\tau}}{2 - e^{\tau}} \tag{4.60}$$

The ODEs for the polymer species can be reformulated and solved with respect to x by dividing equations 4.43 and 4.44 by 4.55 and 4.56, respectively. The initial condition has to be adjusted as well, so that $P_i(x = 0) = M_0\delta_{i,1}$. With this, the system can be solved analytically to obtain the conversion-dependent PSDs.

For the AB^*-process:

$$P_i = M_0(1 - x)\frac{(ix)^{i-1}e^{-ix}}{i!} \tag{4.61}$$

For the AB_2-process:

$$P_i = M_0(1 - x)\frac{(2i)!}{i!(i + 1)!}\left(\frac{x}{2}\right)^{i-1}\left(1 - \frac{x}{2}\right)^{i+1} \tag{4.62}$$

In the same manner, one can derive ODEs for the polymer distribution's moments. This is trivial for the zeroth and first moment. Deriving the second moment is more complicated, but can be done analytically.

For the AB^*-process:

$$\frac{d\mu_2}{dt} = \frac{2\mu_2}{1 - x} \tag{4.63}$$

Integration with initial condition $\mu_2(x = 0) = M_0$ results in:

$$\mu_2 = \frac{M_0}{(1 - x)^2} \tag{4.64}$$

The second moment for the PSD resulting from the AB_2 polycondensation can be formulated in dependence on the A group conversion as well.

$$\mu_2 = M_0\frac{1 - x^2/2}{(1 - x)^2} \tag{4.65}$$

Knowing the first three moments of a PSD allows one to calculate the well known number- and weight-average degree of polymerization, $\overline{P}_n$ and $\overline{P}_w$, which can be compared to measurements data, such as size exclusion chromatography.

For the SCVP the theoretical profiles of these properties are as follows.

$$\overline{P}_n = \frac{\mu_1}{\mu_0} = \frac{1}{1-x} \tag{4.66}$$

$$\overline{P}_w = \frac{\mu_2}{\mu_1} = \frac{1}{(1-x)^2} \tag{4.67}$$

These are different for the polycondensation of AB_2-type monomers for which the profiles are given by:

$$\overline{P}_n = \frac{\mu_1}{\mu_0} = \frac{1}{1-x} \tag{4.68}$$

$$\overline{P}_w = \frac{\mu_2}{\mu_1} = \frac{1-x^2/2}{(1-x)^2} \tag{4.69}$$

Finally, one can compare the polydispersity index which is defined as the quotient of $\overline{P}_w$ and $\overline{P}_n$:

$$PDI = \frac{1}{1-x} \qquad = \overline{P}_n \quad \text{, for SCVP} \tag{4.70}$$

$$PDI = \frac{1-x^2/2}{1-x} = \frac{\overline{P}_n^2 + 2\overline{P}_n - 1}{2\overline{P}_n} \qquad \approx \frac{\overline{P}_n}{2} \quad \text{, for } AB_2 \text{ polycondensation} \tag{4.71}$$

The work of Müller et al. is complemented by considering different reactivities of A^*- and B^* groups as well as the filtration of low molecular species such as residual monomers. They also compare experimental data to their theoretical results, but the conclusions are cautiously formulated because there are many other factors contributing to the system that are not described by the Schemes 4.2 and 4.3. These other factors were also discussed in detail by the authors. After all, the theoretical analysis was very interesting and helpful for the process described by this manuscript.

Summarizing the conclusions of Müller et al., one was able to see that the dynamics of SCVP differ to that of the well-known AB_2 random polycondensation processes due to the slightly varying number of functional groups. This is manifested mainly in the polydispersity index which is two times higher for SCVP. For both processes the PSDs become very broad as was already concluded by Flory in 1952.[105] The polydispersity index is proportional to the degree of polymerization. On the other hand, it was shown by experimental assessment that the PDI takes lower values for SCVP, which can be explained by a higher reactivity of the initiating site (B^*) in comparison to the propagating

site (A^*). However, further NMR measurements indicate that this is unlikely for some SCVP processes and other side effects may have to be considered. The deviations from the ideal behavior discussed in the publication include steric hindrance in larger molecules, intramolecular loop formation, termination by recombination or disproportion, which may also lead to molecules with more than one vinyl group, and backbiting reactions that may remove whole branches from the polymers lowering their molecular mass considerably.

4.2.3 Analysis of the Slow Monomer Addition Technique in the Presence of Core-forming Molecules

In the last paper to be summarized here which was published by Radke et al. in 1998 the same methodology was used.[106] The authors studied the beneficial effect of using core-forming molecules (CFM) in combination with the slow monomer addition technique (SMA) on the PSD and the degree of branching in SCVP. For this they considered two different systems and derived the PSD, its moments, and the degree of branching in a similar manner as described above.

The first system (Scheme 4.4) incorporates core-forming molecules containing f many initiating groups, G_f. Upon binding monomers, these molecules form polymers that differ from the SCVP product by not having any vinyl groups. Other than that, they are assumed to be indistinguishable from the main polymer species. The reaction scheme can be easily formulated in the same manner as above. However, the reactivities for initiating and propagating centers are assumed to be equal and will be denoted with a single reaction coefficient, k.

$$\begin{aligned} P_i + P_j &\xrightarrow{k(i+j)} P_{i+j} \\ G_{f+i} + P_j &\xrightarrow{k(f+i)} G_{f+i+j} \end{aligned}$$

Scheme 4.4. Reaction scheme for the bulk polymerization in the presence of core-forming molecules.

The first reaction equation is obviously the same as it was used for the standard SCVP. The scheme is extended by the introduction of the CFM which can react with the vinyl groups of the main polymers. This includes the residual monomers which are modeled here as P_1.

Combining the proceeding results for the SCVP and formulating the moment equations in terms of the number of monomers incorporated in the polymers, one can derive analytical

expressions for the average molecular weight of the system as follows.

$$\overline{P}_n = \frac{M_0}{M_0(1-x) + G_f^0} \tag{4.72}$$

$$\overline{P}_w = \frac{(\gamma + f)z^2 - 2fz + f}{\gamma} \tag{4.73}$$

Here, x again stands for the conversion of vinyl groups, M_0 is the initial concentration of monomers, G_f^0 the initial concentration of CMFs, and $\gamma = M_0/(fG_f^0)$ is the initial fraction of initiating groups located on monomers, and z is an auxiliary function

$$z(x) = \frac{1+\gamma}{1+\gamma(1-x)} = \overline{P}_n \frac{\gamma+1}{\gamma} \tag{4.74}$$

The important result of this analysis is that the average degree of polymerization stays finite for full conversion of vinyl groups.

$$\overline{P}_n\big|_{x\to 1} = f\gamma = \frac{M_0}{G_f^0} \tag{4.75}$$

$$\overline{P}_w\big|_{x\to 1} = f\gamma + (\gamma+1)^2 \tag{4.76}$$

The polydispersity index can be calculated as well.

$$\left.\frac{\overline{P}_w}{\overline{P}_n}\right|_{x\to 1} = 1 + \frac{\left[(\overline{P}_n/f) + 1\right]^2}{\overline{P}_n} \tag{4.77}$$

For high degrees of polymerization, this means that

$$PDI \approx 1 + \frac{\overline{P}_n}{f^2} \tag{4.78}$$

The second system analyzed by Radke et al. is based on the assumption that slow addition of highly diluted monomers prevents the combination of monomers and instead only the CFMs propagate. This way, no polymer in the system contains any vinyl groups and combination reactions between polymers do not occur either. Such an idealized system can simply be modeled with the following Scheme 4.5.

Since this system does not account for polymers with vinyl groups, monomers are modeled explicitly as M. The second reaction equation is an artificial construct where products are created from nothing with a specific, possibly time dependent rate. This

$$\begin{aligned} G_{f+i} + M &\xrightarrow{k(f+i)} G_{f+i+1} \\ \emptyset &\xrightarrow{\psi(t)} M \end{aligned}$$

Scheme 4.5. Reaction scheme for the semi-batch SCVP in the presence of core-forming molecules. Highly diluted monomers are added to the system with a predefined rate. This prevents self-initiation reactions and monomers bind exclusively to the growing polymers that arise from the core-forming molecules.

mimics the effect of adding monomers to the system and in the case regarded in the mentioned publication the rate coefficient is a fixed constant. As concluded by the authors, the definition of ψ does not have a big impact on the polydispersity of the final product as long as $M << G_f^0$ holds true at all time. After deriving the reduced time $\tau = \int_0^t kMdt$ and the generating function for the polymer distribution, one can derive time profiles for the moments of the MMD and the resulting average degrees of polymerization are

$$\overline{P}_n = f(e^\tau - 1) \tag{4.79}$$

$$\overline{P}_w = 1 + (f+1)(e^\tau - 1) \tag{4.80}$$

The polydispersity index is given as

$$\frac{\overline{P}_w}{\overline{P}_n} = \frac{1}{\overline{P}_n} + \frac{f+1}{f} \tag{4.81}$$

For high τ and high degrees of polymerization the PDI can be approximated as follows.

$$\frac{\overline{P}_w}{\overline{P}_n} \approx 1 + \frac{1}{f} \tag{4.82}$$

Contrary to the polydispersity index calculated for the batch polymerization described above, the semi-batch process produces MMDs with polydispersities independent from the degree of polymerization. This is a crucial improvement since polymers to be synthesized should be as big as possible.

Beside the considerations described here, the authors also derived analytical expressions for the whole MMD and the distribution of monomeric subunits across the different generations of the polymers. The term generations is defined in agreement with the divergence approach to synthesize dendrimers[17] in the sense that monomeric subunit are categorized by their distance to the core unit. By defining generating functions for the individual linear, branched, and terminal subunits, they were able to show that the average

degree of branching, $\overline{DB}$, could be improved to approximately 2/3 for the semi-batch process whereas the original batch process was limited to values of 0.5.

4.3 New Concept for this Study

In order to calculate the reaction rate between two functional groups as accurate as possible, in theory, one would need to know the exact structures of all reacting molecules in the system. A good way to describe the possible molecular structures in the system is to differentiate the molecules by the number and types of the functional groups they contain. A functional group considered here can be distinguished by whether or not it is

- an epoxide ring at the core of a molecule
- a primary or secondary hydroxyl group
- a normal or a deprotonated hydroxyl group
- attached to the surface or the backbone of a molecule

In order to consider molecules with an arbitrary number of each functional group, a polymer would have to be modeled as a 9-tuple and considering every possible structure is obviously impossible for the expected molecular sizes ($\overline{P}_n > 100$). Therefore, further simplification assumptions have to be employed. How this can be accomplished will be illustrated and discussed in the following sections together with the effects that arise from such simplifications.

4.4 M0: A Simplistic Model

The first model is the most simplified one and various ways will be presented in which this model can be extended. Every model needs to account for the amount of trifunctional initiators B_3, monomers AB and polymers of various sizes B_s. In this case every initiator is assumed to have the same reactivity. Monomers that are added to the system can bind to initiator or polymers with the same rate, but not to each other.

Such a system can easily be described with the following system of reaction equations (Scheme 4.6).

This system can easily be formulated as an initial value problem (IVP) by regarding the initial concentration of initiators $B_3(0) = I_0$ and adding one more reaction scheme (4.7) to model the addition of monomers to the system.

$$\text{Prop(s):} \quad B_s + AB \quad \xrightarrow{k_p} \quad B_{s+1}$$

Scheme 4.6. Reaction scheme for the most simplistic model.

$$\text{Mfeed:} \quad \emptyset \quad \xrightarrow{k_{feed}} \quad AB$$

Scheme 4.7. Reaction equation to model the monomer addition to the reactor.

The reaction equations are translated into a set of ODEs for the time-dependent concentration of monomers, AB, and polymers, B_s.

$$\frac{d}{dt}AB = k_{feed} - k_p \cdot AB \cdot \sum_{r=3}^{\infty} B_r \tag{4.83}$$

$$\frac{d}{dt}B_3 = -k_p \cdot AB \cdot B_3 \tag{4.84}$$

$$\forall\ s > 3: \quad \frac{d}{dt}B_s = k_p \cdot AB \cdot (B_{s-1} - B_s) \tag{4.85}$$

4.5 M1: Modeling the Active Sites

The simplistic model is unlikely to capture the actual dynamic of the system. As it will be discussed later, only 10 percent of all hydroxyl groups of the trifunctional initiators are deprotonated. Therefore, it becomes obvious that there will be some inactive molecules. In accordance to the mechanistic findings of Sander and Berg,[81] as well as by Vandenberg,[66] active molecules are capable of donating an active site to a nearby inactive one, i.e., a counter ion gets exchanged with the proton of a hydroxyl group located on a different molecule. Modeling this effect is crucial for the overall dynamic and the different ways to capture this effect will be discussed here.

4.5.1 M1a: Active and Inactive Molecules

The simplistic system can be extended, so that active molecules, B_s^1, and inactive molecules, B_s^0, are regarded. The following system of reaction equations (Scheme 4.8) illustrates how the polymer species can be separated and how their interactions can be modeled.

This scheme comprises twice the amount of molecular species than the simplistic one and introduces a new kinetic rate coefficient for the ion transfer reactions. The effort to solve such a system remains reasonable though and poses no problem.

$$\begin{aligned}
\text{Prop(s):} \quad & B_s^1 + AB \xrightarrow{k_p} B_{s+1}^1 \\
\text{Tran(s,r):} \quad & B_s^1 + B_r^0 \xrightarrow{k_t} B_s^0 + B_r^1 \\
\text{Mfeed:} \quad & \emptyset \xrightarrow{k_{feed}} AB
\end{aligned}$$

Scheme 4.8. Reaction equations considering that only active polymers may propagate and that polymers can activate/deactivate each other via ion transfer reactions.

4.5.2 M1b: Molecules with multiple Active Sites

If cross-activation reactions between molecules are considered, one also has to account for the possibility that the accepting hydroxyl group is located on a molecule that already has at least one deprotonated hydroxyl group. In that case, the accepting molecule will contain multiple active sites after a transfer reaction. This effect can be incorporated into the model by extending the representation of the polymer species by another dimension that denotes the number of active sites it contains, i.e., B_s^m. The reaction coefficients have to be adjusted accordingly.

$$\begin{aligned}
\text{Prop(m,s):} \quad & B_s^m + AB \xrightarrow{k_p \cdot m} B_{s+1}^m \\
\text{Tran(m,s,n,r):} \quad & B_s^m + B_r^n \xrightarrow{k_t \cdot m \cdot (r-n)} B_s^{m-1} + B_r^{n+1} \\
\text{Mfeed:} \quad & \emptyset \xrightarrow{k_{feed}} AB
\end{aligned}$$

Scheme 4.9. Reaction equations regarding propagation of polymers with multiple active sites and cross-activation reactions between polymers. The number of active sites cannot exceed the number of hydroxyl groups ($0 < m \leq s$ and $0 \leq n < r$)

In Scheme 4.9 every reaction rate coefficient was modified by multiplying it with the number of active sites, so that molecules with more active sites are proportionally more likely to undergo a reaction. The ion transfer reaction is additionally multiplied by the number of normal hydroxyl groups on the accepting molecule. This way, molecules with many inactive hydroxyl groups are more likely to increase their reactivity and if a molecule has only deprotonated hydroxyl groups, it cannot accept anymore counter ions.

This model is very hard to simulate because the two-dimensional state space becomes very big for molecules of the expected size. For the same reason, such systems are not supported by the used software. To avoid this problem, one can introduce a cut-off value for the maximum number of active sites. For example, in the extreme case where the cut-off value is one, the model reduces to the previously presented model M1a. This can be realized by splitting the 2-dimensional distribution into many 1-dimensional species

which represent polymers with different amounts of active sites. However, performing simulations can still be problematic in many cases because due to the fast ion transfer reactions all polymers species can interact with each other. This can lead to performance issues depending on the method of discretizing and lumping the chain length distribution.

4.5.3 M1c: Approximating the Expected Number of Active Sites

In order to overcome the limitation of the previous model, an approximation for the number of active sites per polymer was derived which depends on the polymers size alone. However, some harsh simplification assumptions have to be employed in order for this theory to hold true.

In order to understand the derivation, one must firstly look at the ion transfer reaction closely (Scheme 4.10).

$$\text{Tran(m,s,n,r):} \quad B_s^m + B_r^n \xrightarrow{k_t \cdot m \cdot (r-n)} B_s^{m-1} + B_r^{n+1} \quad \begin{pmatrix} \forall & 3 \leq s \leq \infty & 0 \leq m < s \\ \forall & 3 \leq r \leq \infty & 0 \leq n \leq r \end{pmatrix}$$

Scheme 4.10. Reaction equations that realize the cross-activation of polymers. The limitations to the number of hydroxyl groups (s and r) and to the number of active sites (m and n) are specified in brackets.

For a given polymer distribution that is unaffected by any other reaction an equilibrium will be eventually reached. Because polymers with many active sites are more likely to donate and polymers with many inactive hydroxyl groups are more likely to accept a counter ion, every hydroxyl group in the whole system will end up with the same probability to be deprotonated. In other words, the counter ions are distributed evenly over all hydroxyl groups in the system. Thus, the number of active sites (m) per polymer depends on the number of hydroxyl groups (s) it contains and on the elemental probability of every hydroxyl group to be active (p). Therefore, it can be regarded as a binomially distributed random variable and the probability for a B_s^m-polymer can be calculated with the respective probability mass function

$$f(m|s,p) = \begin{pmatrix} s \\ m \end{pmatrix} p^m (1-p)^{s-m}$$

with the binomial coefficient

$$\begin{pmatrix} s \\ m \end{pmatrix} = \frac{s!}{m!(s-m)!}$$

The elemental probability p is equal to the ratio of counter ions, K, to the overall number of hydroxyl groups, OH, in the system. Both quantities are known by the design of the experiment and the expected number of active sites per polymer can be calculated as the expectation value of the binomial distribution.

$$\mathbb{E}\left[f(m|s,p)\right] = s \cdot p = s \cdot \frac{K}{OH}$$

Interestingly, the number of hydroxyl groups rises with the amount of monomers that are added to the system, whereas the amount of counter ions is keep constant throughout the entire polymerization. Thus, the elemental probability decreases as the reaction time progresses.

Using this expectation value allows to model the number of active sites implicitly by modifying the propagation rate coefficient and discarding the superscript of the polymer species that was denoting the number of active sites. This results in the following set of reaction equations (Scheme 4.11).

$$\begin{aligned} \text{Prop(s):} \quad & B_s + AB \xrightarrow{k_p \cdot \mathbb{E}[f(m|s,p)]} B_{s+1} \\ \text{Mfeed:} \quad & \emptyset \xrightarrow{k_{feed}} AB \end{aligned}$$

Scheme 4.11. Reaction equations to model anionic propagation reactions by approximating the number of active sites per polymer.

Before creating a model in the framework of the simulation software, a simple example was tested to assess the applicability of the approximation. A discrete Poisson distribution was created to represent an artificial polymer size distribution. The set of ODEs derived from the ion transfer reactions was used to solve the IVP which converged towards an equilibrium distribution very quickly. As expected, the result was equivalent to the binomial distribution.

Figure 4.3 shows that simulating the ion transfer reactions indeed leads to binomially distributed active sites, but the equilibrium will inevitably be disturbed by other reactions, e.g., polymer propagation. Therefore, in the next test the dynamic of the propagation reaction is mimicked by simply adding the propagation rates to the ODEs. Here, the actual monomer concentrations is ignored (it is assumed to stay constant throughout the reaction and is incorporated in the reaction rate coefficient) and the modified differential

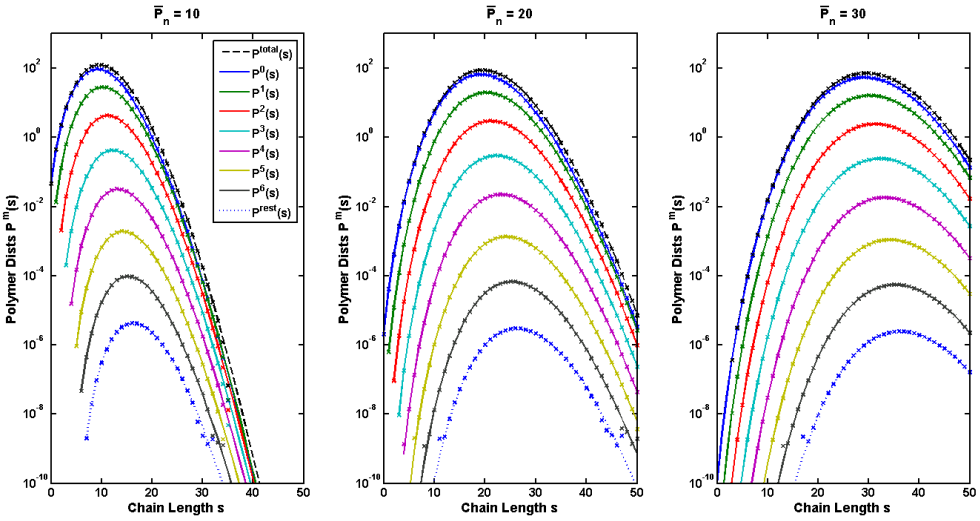

Figure 4.3. An illustration of the 2-dimensional polymer distribution, $P^m(s)$, where s is the number of hydroxyl groups and m the number of active sites. The solid lines show the polymer distributions after distributing the active sites binomially and the markers show the result of simulating the ion transfer reactions explicitly.

equations for the concentrations of the different polymers looks as follows.

$$\frac{dB_s^m}{dt} \rightarrow \frac{dB_s^m}{dt} + k_p \cdot m \cdot \left(B_{s-1}^m - B_s^m\right)$$

Initially, 30% of the polymers have one active site and the rest none, so the ion distribution does not start in the equilibrium state and it will be interesting to see how close the distribution gets to the equilibrium despite the constant disturbance by the propagation reactions.

Figure 4.4 shows the interplay of propagation and ion transfer reactions. For transfer rates much lower than the propagation rate, one can see that only the initially activated polymers grow and the inactive ones do not react. With higher ratios of transfer to propagation rates the binomial equilibrium is approached. Although it is hard to see, the number of polymers with 2 or more active sites rises considerably.

Lastly, the new model is tested by using the expectation value for the number of active sites, i.e., only the total polymer size distribution is modeled and polymers of equal size have the same propagation rate. The result is compared to the total polymer size distribution (summed over the number of active sites) obtained by simulating the ion transfer reactions explicitly with $k_p = k_t$. For this test a higher propagation rate was used, so that the average size increased from 10 to 20 monomeric hydroxyl groups.

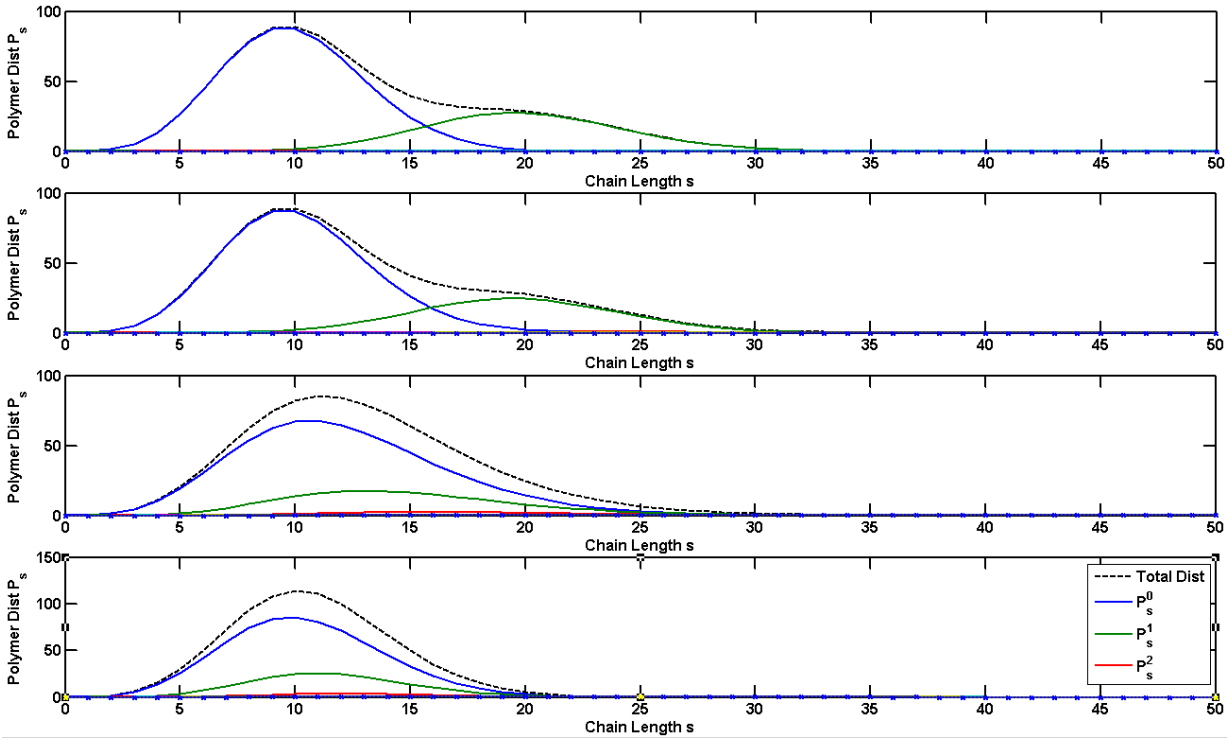

Figure 4.4. Testing the interaction of propagation and ion transfer reactions. The propagation rate was fixed, so that the average size of the polymers rises from 10 to 13, and the ion transfer rate was varied (from top to bottom: $k_t/k_p = 1e^{-8},\ 1e^{-6},\ 1e^{-4},\ 1e^{-2}$).

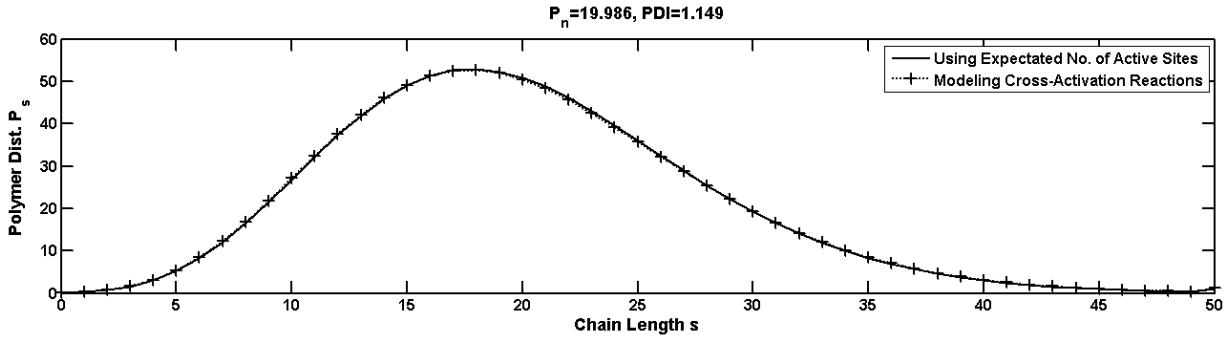

Figure 4.5. A comparison of a simple simulation using two different models. The markers show the result when modeling the number of active sites per polymer and the cross-activation reactions explicitly. The solid line is the result from using the expected number of active sites.

Figure 4.5 shows that the simplification is justified as long as the transfer reactions occur at least as fast as the propagation reactions. One has to be careful though with such statements because the rates for transfer and propagation rates are not comparable. Although both reaction types depend on the number of active sites of a reacting polymer,

the transfer rate depends additionally on the number of normal (inactive) hydroxyl groups of the accepting polymer, whereas the propagation rates depend on the number of epoxides in the system, i.e., the number of free monomers which was assumed to stay constant in this example. Therefore, it is not trivial to formulate a condition based on the reaction rate coefficients that permits the use of this approximation. However, it is safe to say that for every situation, there exists a transfer reaction rate coefficient that is high enough in order for the discussed approximation to be justified.

4.6 M2: Spontaneous Self-initiation of Monomers

Upon collision of an active molecule with a monomer two reactions may occur. Either the epoxide reacts with the active site to cause the ring to open and the monomer is bound covalently to its reaction partner or the counter ion is exchanged with the proton of the monomer's hydroxyl group. In the latter case, the donating molecule loses an active site and the accepting monomer can now undergo anionic propagation reactions itself. Therefore, it competes with other active molecules for the free monomers in the system. Such self-initiated monomers form a new type of polymer that can be differentiated from the primary polymers by the lack of the initiator derivative and the fact that it still contains an unopened epoxide ring. The left over epoxide ring can further react intermolecularly resulting in a combination reaction of two polymers or intramolecularly to produce a macromolecular cycle.

$$
\begin{aligned}
\text{Comb1(s,r):} \quad & B_s^1 + AB_r^0 \xrightarrow{k_p} B_{s+n}^1 \\
\text{Comb2(s,r):} \quad & AB_s^1 + AB_r^0 \xrightarrow{k_p} AB_{s+n}^1 \\
\text{Tran1(s,r):} \quad & B_s^1 + B_r^0 \xrightarrow{k_t} B_s^0 + B_r^1 \\
\text{Tran2(s,r):} \quad & B_s^1 + AB_r^0 \xrightarrow{k_t} B_s^0 + AB_r^1 \\
\text{Tran3(s,r):} \quad & AB_s^1 + B_r^0 \xrightarrow{k_t} AB_s^0 + B_r^1 \\
\text{Tran4(s,r):} \quad & AB_s^1 + AB_r^0 \xrightarrow{k_t} AB_s^0 + AB_r^1 \\
\text{Cyc1(s):} \quad & AB_s^1 \xrightarrow{k_{cyc}} B_s^1 \\
\text{Mfeed:} \quad & \emptyset \xrightarrow{k_{feed}} AB^0
\end{aligned}
$$

Scheme 4.12. A reaction scheme accounting for standard and self-initiated polymers (B_s^m and AB_s^m). This way, combination, cyclization, and ion transfer reactions have to be considered. This particular version does not regard multiply activated polymers.

How the system of reaction equations can be extended to capture this mechanism is shown in Scheme 4.12. Just one of the simplest versions of the model is illustrated. Of

course it can be adjusted in the same manner as models M-1b and M-1c in order to allow multiple activation of polymers. This is especially useful because this allows one to model the combination reaction between two active, self-initiated polymers ($AB_s^1 + AB_r^1 \longrightarrow AB_{s+r}^2$) which is not possible with the system above.

A cyclization reaction consumes the epoxide ring, but the number of hydroxyl groups and the number of active sites remain the same. A cyclic polymer of size s is modeled as B_s^0 or B_s^1 because it has the same reactivity as a normally initiated polymer. Therefore, primary and cyclic polymers are indistinguishable in the simulation result and the fraction of cyclic polymers cannot be used for comparison with experimental data. If such a comparison is desired, the model can be adjusted in various ways. Because the cyclization reaction is assumed to be irreversible a simple reaction counter (a feature of the simulation package PREDICI) can be introduced to the cyclization reaction. If the individual PSD for the cyclic polymers is of interest, a new polymer species for the cyclic product has to be defined, e.g., cB_s^1. This will result in a bigger state space and the performance of the simulations will decrease, but this is a viable option. It remains to say that these modifications only make sense if measurements of the cyclic byproduct are accurate.

4.7 M3: Thermal Ring-opening Reactions

As mentioned in Chapter 3, an epoxide ring is reactive enough to be subject of a nucleophilic attack by a hydroxyl group, if the energy input, e.g. temperature, is high enough. This can be accounted for by introducing additional reaction equations that represent the thermally induced side reactions. Disregarding all of the anionic ring-opening reactions, the system can be modeled with the following reaction equations (Scheme 4.13).

$$\begin{array}{rrcll}
\text{B-Comb(m,s,n,r):} & B_s^m + AB_r^n & \xrightarrow{k_{thr}\cdot(s-m)} & B_{s+n}^{m+n} & \left(\begin{array}{llll} \forall & 1 \le s \le \infty & 0 \le m < s \\ \forall & 1 \le r \le \infty & 0 \le n \le r \end{array}\right) \\
\text{AB-Comb(m,s,n,r);} & AB_s^m + AB_r^n & \xrightarrow{k_{thr}\cdot(s-m+r-n)} & AB_{s+n}^{m+n} & \left(\begin{array}{llll} \forall & 1 \le s \le \infty & 0 \le m < s \\ \forall & 1 \le r \le \infty & 0 \le n \le r \end{array}\right) \\
\text{Cyc2(s):} & AB_s^m & \xrightarrow{k_{cyc2}\cdot(s-m)} & B_s^m & \left(\begin{array}{llll} \forall & 1 \le s \le \infty & 0 \le m < s \end{array}\right)
\end{array}$$

Scheme 4.13. A reaction scheme for the thermal ring-opening reactions between all polymers. In this case, multiple active sites and self-initiation reactions are accounted for. The limitations to the number of hydroxyl groups (s and r) and to the number of active sites (m and n) are specified in brackets.

Scheme 4.13 shows the thermal variants for initiation (B-Comb(m,3,1,0)), self-initiation

(AB-Comb(1,0,1,0)), propagation (B-Comb(m,s,1,0) and AB-Comb(m,s,1,0)), combination (any other B-Comb or AB-Comb reaction) and cyclization reactions in a very compact form. The reaction rate depends on a kinetic rate coefficient for any thermal ring-opening reaction, k_{thr}, and the number of hydroxyl groups that have not been deprotonated before. For the combination of two self-initiated polymers (any AB-Comb) the hydroxyl groups of both polymers can participate in a ring-opening reaction, which is not the case for the combination of a normal with a self-initiated polymer.

It is possible to design experiments without introduction of anionic initiators. These can be used to estimate the thermal parameters independently from the anionic reactions.

4.8 M4: Primary and Secondary Hydroxyl Groups

During the ring-opening reaction of glycidol two kinds of hydroxyl groups can arise, primary and secondary ones. It is well known that primary hydroxyl groups show a higher reaction rate in conventional SN_2 substitution reactions.[107] This may also apply to the ring-opening reaction due to a nucleophilic attack, but it is unclear how big this difference in reactivity really is, especially since the reaction is carried out at elevated temperatures. It was also stated before that the counter ion will preferably stay on a primary hydroxyl group if present,[66] which leads to reduced amounts of dendritic and linear-1,3 subunits incorporated in the polymers. There are ways to incorporate different reactivities of functional groups into the model, but unfortunately not in every case and it usually is necessary to use an average composition of functional groups in the system.

How the information about the polymers' hydroxyl groups can be incorporated, will be illustrated for an idealized thermal polymerization reactions. Scheme 4.14 shows the base model for the process where no hydroxyl groups are deprotonated, but monomers cannot combine with each other, so that only one type of polymer exists and no polymer combination reactions have to be considered. However, the propagation rate is proportional to the number of hydroxyl groups on the reacting polymer.

$$\begin{array}{rrcl} \text{Prop(s):} & B_x + AB & \xrightarrow{k_{thr} \cdot x} & B_{x+1} \\ \text{Mfeed:} & \emptyset & \xrightarrow{k_{feed}} & AB \end{array}$$

Scheme 4.14. An ideal reaction scheme for a thermal ring-opening polymerization.

An obvious extension is to introduce a second dimension to the polymer distribution, counting primary and secondary hydroxyl groups at the same time. This can be seen in

Scheme 4.15.

$$
\begin{aligned}
\text{Prop11(p,s):} \quad & B_{p,s} + AB \xrightarrow{k_{thr}\cdot a_1\cdot b_1\cdot p} B_{p,s+1} \\
\text{Prop12(p,s):} \quad & B_{p,s} + AB \xrightarrow{k_{thr}\cdot a_1\cdot b_2\cdot s} B_{p+1,s} \\
\text{Prop21(p,s):} \quad & B_{p,s} + AB \xrightarrow{k_{thr}\cdot a_2\cdot b_1\cdot p} B_{p+1,s} \\
\text{Prop22(p,s):} \quad & B_{p,s} + AB \xrightarrow{k_{thr}\cdot a_2\cdot b_2\cdot s} B_{p+2,s-1} \\
\text{Mfeed:} \quad & \emptyset \xrightarrow{k_{feed}} AB
\end{aligned}
$$

Scheme 4.15. Ideal reaction scheme for the thermal ring-opening polymerization with differentiation between primary and secondary hydroxyl group.

One can see that the reaction rate coefficients in Scheme 4.15 are multiplied either by the number of primary (p) or the number of secondary hydroxyl groups (s). This leads to an interesting dynamic because, next to the type of the reacting functional group, the ring-opening direction becomes important. Therefore, the following four scenarios have to be considered.

1. A primary hydroxyl group reacts, while one primary and one secondary group arise.
2. A primary hydroxyl group reacts, while two primary groups arise.
3. A secondary hydroxyl group reacts, while one primary and one secondary group arise.
4. A secondary hydroxyl group reacts, while two primary groups arise.

Scheme 4.15 captures all four scenarios which have different reaction rates. Here, the different rates are calculated with 5 parameters, k_{thr}, a_1, a_2, b_1, and b_2. For simplicity one can assume $a_1 = b_1 = 1$ and adjust k_{thr} accordingly. Then one only has to vary 3 different parameters to cover all possible combinations of reaction rates.

The proposed model is again very hard to simulate because of the two dimensional polymer distributions. Even the simplest version of the model, illustrated above, becomes nearly impossible to solve when big polymers are regarded.

An alternative model incorporating the different reactivities of primary and secondary hydroxyl groups can be derived by calculating their global ratio in the whole system and assume that every hydroxyl group in the system has the same probability to be of either type. This way, the number of primary and secondary hydroxyl groups can be calculated for any polymer as a function of its size and the information about the global ratio. This

assumption can never be justified or evaluated, but it is the best way because it does not interfere with the softwares rules for designing the system of reaction equations.

Similar to the previous scheme, every propagation reaction is modeled as four separate reaction equations that account for the four different ring-opening scenarios. In this case, only the total number of hydroxyl groups per polymer is modeled, therefore, only one property index is used (chosen as x so that it is not confused with the previously used indexes). The produced polymer is the same for all four reactions because in every case that total number of hydroxyl groups is increased by one. The reaction rate coefficients are the key to differentiating the different reaction rates and their calculation will be explain in detail further below. The overall number of molecules that have been created through the individual reactions is recorded by introducing low molecular species, called "counters." These artificial species have a molecular mass of zero and are not allowed to react at any time, so that they do not effect the system as a normal molecular species does. However, their amounts can be used to modify the reaction rates. This is illustrated in the following reaction Scheme 4.16 that takes into account the thermal propagation reactions of primary and secondary hydroxyl groups.

$$
\begin{array}{lrcl}
\text{Prop11(x):} & B_x + AB & \xrightarrow{k_{11}(x,t)} & B_{x+1} + C_{11} \\
\text{Prop12(x):} & B_x + AB & \xrightarrow{k_{12}(x,t)} & B_{x+1} + C_{12} \\
\text{Prop21(x):} & B_x + AB & \xrightarrow{k_{21}(x,t)} & B_{x+1} + C_{21} \\
\text{Prop22(x):} & B_x + AB & \xrightarrow{k_{22}(x,t)} & B_{x+1} + C_{22} \\
\text{Mfeed} & \emptyset & \xrightarrow{k_{feed}} & AB
\end{array}
$$

Scheme 4.16. Another reaction scheme to model propagation reactions that act on primary or secondary hydroxyl groups. By using "counters" (C_{11}, C_{12}, C_{21}, and C_{22}), polymers can be modeled with only one dimension.

Here the modified reaction rate coefficients are especially important, because they depend on the reacting polymer's size and the time-dependent fraction of primary or secondary hydroxyl groups, defined as $f_p(t)$ and $f_s(t)$.

$$k_{11}(x,t) = k_{thr} \cdot a_1 \cdot b_1 \cdot x \cdot f_p(t) \tag{4.86}$$

$$k_{12}(x,t) = k_{thr} \cdot a_1 \cdot b_2 \cdot x \cdot f_p(t) \tag{4.87}$$

$$k_{21}(x,t) = k_{thr} \cdot a_2 \cdot b_1 \cdot x \cdot f_s(t) \tag{4.88}$$

$$k_{22}(x,t) = k_{thr} \cdot a_2 \cdot b_2 \cdot x \cdot f_s(t) \tag{4.89}$$

The fractions of the different hydroxyl groups at time t ($f_p(t)$ and $f_s(t)$) are defined in dependence of the the overall amounts of primary and secondary hydroxyl groups at that time ($C_p(t)$ and $C_s(t)$).

$$f_p(t) = \frac{C_p(t)}{C_p(t) + C_s(t)} \tag{4.90}$$

$$f_s(t) = \frac{C_s(t)}{C_p(t) + C_s(t)} \tag{4.91}$$

The overall amounts of the different hydroxyl groups depend the concentration of the "counters" at time t ($C_{11}(t)$, $C_{12}(t)$, $C_{21}(t)$, and $C_{22}(t)$). This relationship becomes clear upon comparison of scheme 4.15 to 4.16. In all cases the total number of hydroxyl groups is increased by one, and the produced "counter" gives information about the type of hydroxyl group that reacted and what types were created. That leads to the following interpretation:

- For every C_{11}, the number of secondary hydroxyl groups is increase by one.
- For every C_{12} or C_{21}, the number of primary hydroxyl groups is increased by one.
- For every C_{22}, the number of secondary hydroxyl groups is decreased and the number of primary hydroxyl groups is increased by two.

Therefore, the the overall amounts of different hydroxyl groups can be calculated as follows.

$$C_p(t) = C_p(0) + C_{12}(t) + C_{21}(t) + 2 \cdot C_{22}(t) \tag{4.92}$$

$$C_s(t) = C_{11}(t) - C_{22}(t) \tag{4.93}$$

$C_p(0)$ stands for the initial amount of primary hydroxyl groups, i.e. the total number of hydroxyl groups of all initiators. The initial amount of secondary hydroxyl groups is zero.

One flaw of this model becomes obvious when regarding this highly simplified model which assumes that monomers, AB, can only bind to initiators, B_3, and the resulting polymers, B_s ($3 < s$). Because initiators have three primary hydroxyl groups and this number is never reduced by any of the propagation schemes, every polymer in the system must also have at least three primary hydroxyl groups, but as the polymers grow, the overall fraction of primary hydroxyl groups decreases below one and the reaction rate for an initiator is slightly lowered as if an initiator could also contain secondary hydroxyl groups.

In this example, this small error can be avoided by excluding the initial amounts of primary hydroxyl groups $C_p(0)$ in Equation 4.92 and modifying the reaction rates, so that every polymer has at least three primary hydroxyl groups, e.g., $k_{11}(x,t) = [3 + (x-3) \cdot f_p(t)]$. However, if the model is extended by self-initiation, combination, and cyclization reactions, the formulations of the rate equations become much more complex since not every polymer has at least three hydroxyl groups. In that case, one has to differentiate between the different polymer species: (a) polymers with initiator (B_x) have at least three primary hydroxyl groups, (b) polymers with an unopened epoxide derivative (AB_x) have at least one, and (c) a cyclic polymer (cB_x) can have any amount of primary hydroxyl groups since a cyclization reaction may use up the only primary hydroxyl group of a self-initiated polymer. In order to use this information, this fixed amount of primary hydroxyl groups must be excluded from the calculation of the fractions (f_p and f_s). It turns out that the above scheme can easily be extended without introducing new counters and the formula for f_p and f_s also remains the same. However the model becomes somewhat unintuitive. This will be explained on the basis of Scheme 4.17.

The corresponding reaction rate coefficients have to be calculated in dependence on the type of the reacting polymer which is indicated in the superscript. The following equations show that not every hydroxyl group of the polymers can be secondary ones.

$$k_{11}^{B}(x,t) = k_{thr} \cdot a_1 \cdot b_1 \cdot \left[3 + (x-3) \cdot \hat{f}_p(t)\right] \tag{4.94}$$

$$k_{12}^{B}(x,t) = k_{thr} \cdot a_1 \cdot b_2 \cdot \left[3 + (x-3) \cdot \hat{f}_p(t)\right] \tag{4.95}$$

$$k_{21}^{B}(x,t) = k_{thr} \cdot a_2 \cdot b_1 \cdot (x-3) \cdot \hat{f}_s(t) \tag{4.96}$$

$$k_{22}^{B}(x,t) = k_{thr} \cdot a_2 \cdot b_2 \cdot (x-3) \cdot \hat{f}_s(t) \tag{4.97}$$

$$k_{11}^{cB}(x,t) = k_{thr} \cdot a_1 \cdot b_1 \cdot x \cdot \hat{f}_p(t) \tag{4.98}$$

$$k_{12}^{cB}(x,t) = k_{thr} \cdot a_1 \cdot b_2 \cdot x \cdot \hat{f}_p(t) \tag{4.99}$$

$$k_{21}^{cB}(x,t) = k_{thr} \cdot a_2 \cdot b_1 \cdot x \cdot \hat{f}_s(t) \tag{4.100}$$

$$k_{22}^{cB}(x,t) = k_{thr} \cdot a_2 \cdot b_2 \cdot x \cdot \hat{f}_s(t) \tag{4.101}$$

$$k_{11}^{AB}(x,t) = k_{thr} \cdot a_1 \cdot b_1 \cdot \left[2 + (x-2) \cdot \hat{f}_p(t)\right] \tag{4.102}$$

$$k_{12}^{AB}(x,t) = k_{thr} \cdot a_1 \cdot b_2 \cdot \left[2 + (x-2) \cdot \hat{f}_p(t)\right] \tag{4.103}$$

$$k_{21}^{AB}(x,t) = k_{thr} \cdot a_2 \cdot b_1 \cdot (x-2) \cdot \hat{f}_s(t) \tag{4.104}$$

$$k_{22}^{AB}(x,t) = k_{thr} \cdot a_2 \cdot b_2 \cdot (x-2) \cdot \hat{f}_s(t) \tag{4.105}$$

$$
\begin{aligned}
\text{B-Comb11(x,y):} \quad & B_x + AB_y \xrightarrow{k_{11}^{B}(x,t)} B_{x+y} + C_{11} \\
\text{B-Comb12(x,y):} \quad & B_x + AB_y \xrightarrow{k_{12}^{B}(x,t)} B_{x+y} + C_{12} \\
\text{B-Comb21(x,y):} \quad & B_x + AB_y \xrightarrow{k_{21}^{B}(x,t)} B_{x+y} + C_{21} \\
\text{B-Comb22(x,y):} \quad & B_x + AB_y \xrightarrow{k_{22}^{B}(x,t)} B_{x+y} + C_{22} \\
\text{cB-Comb11(x,y):} \quad & cB_x + AB_y \xrightarrow{k_{11}^{cB}(x,t)} cB_{x+y} + C_{11} \\
\text{cB-Comb12(x,y):} \quad & cB_x + AB_y \xrightarrow{k_{12}^{cB}(x,t)} cB_{x+y} + C_{12} \\
\text{cB-Comb21(x,y):} \quad & cB_x + AB_y \xrightarrow{k_{21}^{cB}(x,t)} cB_{x+y} + C_{21} \\
\text{cB-Comb22(x,y):} \quad & cB_x + AB_y \xrightarrow{k_{22}^{cB}(x,t)} cB_{x+y} + C_{22} \\
\text{AB-Comb11(x,y):} \quad & AB_x + AB_y \xrightarrow{k_{11}^{AB}(x+y,t)} AB_{x+y} + C_{11} \\
\text{AB-Comb12(x,y):} \quad & AB_x + AB_y \xrightarrow{k_{12}^{AB}(x+y,t)} AB_{x+y} + C_{12} \\
\text{AB-Comb21(x,y):} \quad & AB_x + AB_y \xrightarrow{k_{21}^{AB}(x+y,t)} AB_{x+y} + C_{21} \\
\text{AB-Comb22(x,y):} \quad & AB_x + AB_y \xrightarrow{k_{22}^{AB}(x+y,t)} AB_{x+y} + C_{22} \\
\text{Cyc11(x):} \quad & AB_x \xrightarrow{k_{11}^{cyc}(x,t)} cB_x + C_{11} \\
\text{Cyc12(x):} \quad & AB_x \xrightarrow{k_{12}^{cyc}(x,t)} cB_x + C_{12} \\
\text{Cyc21(x):} \quad & AB_x \xrightarrow{k_{21}^{cyc}(x,t)} cB_x + C_{21} \\
\text{Cyc22(x):} \quad & AB_x \xrightarrow{k_{22}^{cyc}(x,t)} cB_x + C_{22} \\
\text{Mfeed:} \quad & \emptyset \xrightarrow{k_{feed}} AB
\end{aligned}
$$

Scheme 4.17. An extension of the previous reaction scheme that incorporates self-initiation, polymer combination, and cyclization reaction. Artificial "counter" species (C_{11}, C_{12}, C_{21}, C_{22} and C_3) are used to calculate the global fraction of primary and secondary hydroxyl groups.

The interpretation of the "counters" remains the same, but the fractions $\hat{f}_p(t)$ and $\hat{f}_s(t)$ are calculated differently, so that the hydroxyl groups that are fixed to be primary ones are excluded. Therefore, the variable $\hat{C}_p(t)$ and $\hat{C}_p(t)$ are defined as follows.

$$\hat{C}_p(t) = C_{12}(t) + C_{21}(t) + 2 \cdot C_{22}(t) \tag{4.106}$$

$$\hat{C}_s(t) = C_{11}(t) - C_{22}(t) \tag{4.107}$$

The difference between equations 4.92 and 4.106 is that the first includes the number of hydroxyl groups introduced by the initiators ($C_p(0)$) and the latter does not. The hydroxyl groups located on free monomers is not regarded in either of the two models since the monomer addition reaction (Mfeed) no "counter" is used. Having these reduced amounts of primary and secondary hydroxyl groups allows the formulation of their fractions, which are defined as follows.

$$\hat{f}_p(t) = \frac{\hat{C}_p(t)}{\hat{C}_p(t) + \hat{C}_s(t)} \tag{4.108}$$

$$\hat{f}_s(t) = \frac{\hat{C}_s(t)}{\hat{C}_p(t) + \hat{C}_s(t)} \tag{4.109}$$

The peculiarity of Scheme 4.17 becomes obvious when inspecting the reaction equation of a self-initiation reaction closely. Depending on the direction in which the epoxide ring opens, the self-initiation reaction is modeled as either AB-Comb11(1,1) or AB-Comb12(1,1) and "counters" C_{11} or C_{12} are produced, respectively. The interpretation of these "counters" has not changed, so that either a primary hydroxyl group is replaced by a primary and a secondary one or a primary hydroxyl group is replaced by two primary ones. This basically means that before the reaction, none of the hydroxyl groups were counted and after the reaction either a secondary or a primary hydroxyl group are counted. That makes sense because the resulting dimer is considered to have one primary hydroxyl group and the type of the second one is calculated according to the above fractions. For the same reason, the cyclization reactions also produce the four different "counters", even though the total number of hydroxyl groups remains unchanged by this reaction. There are other ways to model this dynamic, but this way is the most efficient one because no group is counted unnecessarily, only four counters are required and propagation reactions can be interpreted as combination reactions.

Another interesting effect is introduced by to the symmetry of the AB-Comb reaction

equations. The reaction rate depends on the combined number of hydroxyl groups of both polymers because both molecules contain an epoxide derivative. By definition, two of these have to be primary hydroxyl groups. This is reflected in the calculation of the respective reaction rates (see equations 4.102-4.105).

It should be mentioned that the error that can be compensated this way is nearly negligible in comparison to the error that is introduced by averaging the types of hydroxyl groups in the first place. Also this error vanishes for big polymers since $x - 3 \approx x$ for high values of x.

The last improvement of the model captures the dynamic more realistically without adding additional kinetic parameters. The performance of the simulation is only influenced by the introduction of the new polymer species and the fact that multiple interpreter functions have to be compiled and called. The latter does not affect the software's performance much, but an almost three-fold increase of the parameter space can have a tremendous impact on the algorithm's stability. This effect is very hard to evaluate because it depends strongly on the way the polymer species can interact with each other. It is likely that the discretization schemes for the separate PSDs influence each other in a way that they become less efficient, i.e., more discretization points are required to guarantee a low modeling error.

In theory, this concept can also be applied to the anionic ring-opening reactions. It can be assumed that primary hydroxyl groups have a higher probability to be deprotonated by a counter ion. Since it is not desirable to model the very fast intramolecular ion transfer reaction, another global quantity representing the ratio of counter ions attached to primary or secondary hydroxyl groups has to be used in order to adjust the anionic reaction rates. Additionally, every propagation scheme mentioned above will have to be duplicated two more times, once anionic propagation reactions of active primary and once for active secondary hydroxyl groups. Since this model would have to be combined with the theory of treating multiply activated polymers as well, such a model will not be considered in this study. The complexity becomes way too high and too many approximation have to be applied at once. The success of such a model is very low and the result would be useless due to the many different error sources that contribute to it.

4.9 M5: Dendritic, Linear, and Terminal Subunits

It is also possible to keep track of the composition of the polymers by distinguishing between terminal, linear, and dendritic subunits. This may affect the steric hindrance and thereby the reaction rate at the given location of a polymer. One can assume that a terminal subunit is located at the surface of a polymer and that it can react easily with other molecules. This is not always true because for very big, hyperbranched polymers a terminal unit can be surrounded by other branches of the same polymer, so that the accessibility is still hindered. Because this case is very rare, it is assumed to have an insignificant effect on the reaction rates. A linear subunit, on the other hand, is always less accessible than a terminal one because there is less free space around a chain segment than there is at its end. Additionally, since a linear subunit is, by definition, part of the interior backbone, one can assume that the steric hindrance induced by other branches of the polymer is much higher. A dendritic subunit represents a branching point in the polymer and does not possess any hydroxyl group, therefore, it cannot participate in any more reactions. The information about the number of branching points is of high interest because it is very important for the polymer's properties which can also be used to estimate more precise reaction rates.

In order to capture the dynamic behavior correctly, the polymers' subunits have to be categorized into different types for which separate reaction equation with different rates have to be introduced. At the same time, the quantities of the subunits have to be updated differently for every reaction. In general, a terminal subunit is converted into a linear one upon reacting with a monomer which at the same time forms a new terminal subunit. In a similar manner, a linear subunit reacts to form a dendritic one. An initiator derivative of a polymer can be considered a subunit as well. This can be cumbersome because the extra hydroxyl groups can react as well, and one would have to introduce three separate polymer species which have an "initiator subunit" that contributes 0, 1, or 2 unreacted hydroxyl groups. However, there is a convenient alternative to model the initiator as a subunit. Due to the similarity of TMP to glycerol, the initiator can be regarded as an extra terminal subunit which can further react to form a linear and ultimately a dendritic subunit. This way an initiator is modeled as a low molecular species rather than a polymer that contains three hydroxyl groups, as has been done before. An initiator can then react with a monomer to from a dimer consisting of two terminal subunits. This way the reaction rates should be calculated accurately, but one has to keep in mind that the total number of subunits will no longer be equivalent to the number of used monomers (i.e. the

degree of polymerization). This is important for the calculation of the average degree of polymerization and for compliance with the mass balance condition since an initiator has a mass higher than that of a monomeric subunit.

Modeling the structure becomes more complex when self-initiation reactions are included because the epoxide derivative has to be considered as another type of subunit of the polymers. Upon a ring-opening reaction, this subunit is transformed into a linear one. Additionally, self-initiated polymers can undergo cyclization reactions which result in polymers with different constraints on the subunit composition as compared to the normally initiated polymers. Similarly to a combination reaction, the epoxide derivative turns into a linear subunit and the other reacting subunit is transformed either from terminal to linear or from linear to dendritic. The resulting polymer has as many dendritic as terminal subunits, whereas the acyclic form always has one terminal subunit more than it has dendritic ones. For a normally initiated polymer the number of terminal subunits exceeds the number of dendritic ones by two. How this will affect the reaction rates, will be discussed further below.

As an illustration, this extension is applied to an advanced model that already incorporates self-initiation and cyclization reactions. Since polymers can no longer be classified solely by the total number of hydroxyl groups, the nomenclature is changed so that the number of different subgroups are depicted instead. The initiators and monomers are represented as low molecular species I and M, respectively. A polymer that incorporates an initiator is given as $P_i(d, l, t)$, a self-initiated polymer as $P_m(d, l, t)$, and a cyclic polymer as $P_c(d, l, t)$. For each polymer three properties are modeled, d, l, and t, which depict the amount of dendritic, linear, and terminal subunits, respectively. The nomenclature is designed so that for each polymer the total number of hydroxyl groups, N_{OH}, can be calculated easily as follows.

$$N_{OH} = l + 2 \cdot t$$

Since the numbers of dendritic and terminal subunits are strictly related to each other, it is possible to discard one of the according property indexes (d or t) without loosing the ability to capture every possible structure. However, for a better understanding, all three properties will be regarded at this point.

As an example, Scheme 4.18 illustrates this concept for the thermal ring-opening polymerization under consideration of self-initiation, propagation, combination, and cyclization reactions. This model is still highly simplified because anionic reactions are not regarded and primary hydroxyl groups are not differentiated from secondary ones. In

general, these concepts could also be incorporated, but it is very complicated and the set of reaction equations would span many pages. However, at this point, only the differentiation between the different types of subunits is of interest.

Initiation:	$I + M$	$\xrightarrow{k_{thr}\cdot c_1\cdot 3}$	$P_i(0,0,2)$	
Self-Initiation:	$M + M$	$\xrightarrow{k_{thr}\cdot c_1\cdot 2}$	$P_m(0,0,1)$	
Prop11(d,l,t):	$P_i(d,l,t) + M$	$\xrightarrow{k_{thr}\cdot c_1\cdot 2t}$	$P_i(d,l+1,t)$	$(\forall\ 0 \le d = t-2,\ 0 \le l)$
Prop12(d,l,t):	$P_i(d,l,t) + M$	$\xrightarrow{k_{thr}\cdot c_2\cdot l}$	$P_i(d+1,l-1,t+1)$	$(\forall\ 0 \le d = t-2,\ 0 \le l)$
Prop21(d,l,t):	$P_m(d,l,t) + M$	$\xrightarrow{k_{thr}\cdot c_1\cdot 2t}$	$P_m(d,l+1,t)$	$(\forall\ 0 \le d = t-1,\ 0 \le l)$
Prop22(d,l,t):	$P_m(d,l,t) + M$	$\xrightarrow{k_{thr}\cdot c_2\cdot l}$	$P_m(d+1,l-1,t+1)$	$(\forall\ 0 \le d = t-1,\ 0 \le l)$
Prop31(d,l,t):	$P_c(d,l,t) + M$	$\xrightarrow{k_{thr}\cdot c_1\cdot 2t}$	$P_c(d,l+1,t)$	$(\forall\ 0 \le d = t,\ 0 \le l)$
Prop32(d,l,t):	$P_c(d,l,t) + M$	$\xrightarrow{k_{thr}\cdot c_2\cdot l}$	$P_c(d+1,l-1,t+1)$	$(\forall\ 0 \le d = t,\ 0 \le l)$
I-Comb(x,y,z):	$I + P_m(x,y,z)$	$\xrightarrow{k_{thr}\cdot c_1\cdot 3}$	$P_i(x,y+1,z+1)$	$(\forall\ 0 \le x = z-1,\ 0 \le y)$
M-Comb(x,y,z):	$M + P_m(x,y,z)$	$\xrightarrow{k_{thr}\cdot c_1}$	$P_m(x,y+1,z)$	$(\forall\ 0 \le x = z-1,\ 0 \le y)$
Comb11(d,l,t,x,y,z):	$P_i(d,l,t) + P_m(x,y,z)$	$\xrightarrow{k_{thr}\cdot c_1\cdot 2t}$	$P_i(d+x,l+y+2,t+z-1)$	$\begin{pmatrix} \forall\ 0 \le d = t-2,\ 0 \le l \\ \forall\ 0 \le x = z-1,\ 0 \le y \end{pmatrix}$
Comb12(d,l,t,x,y,z):	$P_i(d,l,t) + P_m(x,y,z)$	$\xrightarrow{k_{thr}\cdot c_2\cdot l}$	$P_i(d+x+1,l+y,t+z)$	$\begin{pmatrix} \forall\ 0 \le d = t-2,\ 0 \le l \\ \forall\ 0 \le x = z-1,\ 0 \le y \end{pmatrix}$
Comb21(d,l,t,x,y,z):	$P_m(d,l,t) + P_m(x,y,z)$	$\xrightarrow{k_{thr}\cdot c_1\cdot(2t+2z)}$	$P_m(d+x,l+y+2,t+z-1)$	$\begin{pmatrix} \forall\ 0 \le d = t-1,\ 0 \le l \\ \forall\ 0 \le x = z-1,\ 0 \le y \end{pmatrix}$
Comb22(d,l,t,x,y,z):	$P_m(d,l,t) + P_m(x,y,z)$	$\xrightarrow{k_{thr}\cdot c_2\cdot(l+y)}$	$P_m(d+x+1,l+y,t+z)$	$\begin{pmatrix} \forall\ 0 \le d = t-1,\ 0 \le l \\ \forall\ 0 \le x = z-1,\ 0 \le y \end{pmatrix}$
Comb31(d,l,t,x,y,z):	$P_c(d,l,t) + P_m(x,y,z)$	$\xrightarrow{k_{thr}\cdot c_1\cdot 2t}$	$P_c(d+x,l+y+2,t+z-1)$	$\begin{pmatrix} \forall\ 0 \le d = t,\ 0 \le l \\ \forall\ 0 \le x = z-1,\ 0 \le y \end{pmatrix}$
Comb32(d,l,t,x,y,z):	$P_c(d,l,t) + P_m(x,y,z)$	$\xrightarrow{k_{thr}\cdot c_2\cdot l}$	$P_c(d+x+1,l+y,t+z)$	$\begin{pmatrix} \forall\ 0 \le d = t,\ 0 \le l \\ \forall\ 0 \le x = z-1,\ 0 \le y \end{pmatrix}$
Cyc1(d,l,t):	$P_m(d,l,t)$	$\xrightarrow{k_{cyc}\cdot c_1\cdot 2t}$	$P_c(d,l+2,t-1)$	$(\forall 0 \le d = t,\ 0 \le l)$
Cyc2(d,l,t):	$P_m(d,l,t)$	$\xrightarrow{k_{cyc}\cdot c_2\cdot l}$	$P_c(d+1,l,t)$	$(\forall 0 \le d = t,\ 0 \le l)$
Mfeed:	$\emptyset$	$\xrightarrow{k_{feed}}$	M	

Scheme 4.18. A reaction scheme that regards the polymers' composition of monomeric subunits.

The described reaction scheme again requires a polymer species to be modeled with at least two property indexes which cannot be realized in the chosen software framework. Therefore, an alternative way to incorporate the information about the location of the hydroxyl groups, i.e., at the core or at the surface of the molecule, will be presented here.

The problem will be avoided in the same manner as the one in the previous section where primary and secondary hydroxyl groups were distinguished. In this case, the overall distribution of dendritic, linear, and terminal subunits has to be modeled in order to modify the reaction rates accordingly. This results in an accurate calculation of the overall reactivity of the system, but the history of individual molecules is lost which in turn can lead to an error that cannot be evaluated with certainty.

In agreement with the modeling strategy described in the previous section, the following set of reaction equations can be formulated (Scheme 4.19).

The reaction rate coefficients are modified to contain information about the overall fraction of linear and terminal subunits. The underlying assumption is that every hydroxyl groups has the same probability to either belong to a terminal or to a linear subunit. The error induced by this assumption is unpredictable.

$$k_i = k_{thr} \cdot c_1 \cdot 3 \tag{4.110}$$

$$k_{si} = k_{thr} \cdot c_1 \cdot 2 \tag{4.111}$$

$$k_{11}(s,t) = k_{thr} \cdot c_1 \cdot s \cdot f_T(t) \tag{4.112}$$

$$k_{12}(s,t) = k_{thr} \cdot c_2 \cdot s \cdot f_L(t) \tag{4.113}$$

$$k_{21}(s,t) = k_{thr} \cdot c_1 \cdot s \cdot f_T(t) \tag{4.114}$$

$$k_{22}(s,t) = k_{thr} \cdot c_2 \cdot s \cdot f_L(t) \tag{4.115}$$

$$k_{31}(s,t) = k_{thr} \cdot c_1 \cdot s \cdot f_T(t) \tag{4.116}$$

$$k_{32}(s,t) = k_{thr} \cdot c_2 \cdot s \cdot f_L(t) \tag{4.117}$$

$$k_1^c(s,t) = k_{cyc} \cdot c_1 \cdot s \cdot f_T(t) \tag{4.118}$$

$$k_2^c(s,t) = k_{cyc} \cdot c_2 \cdot s \cdot f_L(t) \tag{4.119}$$

k_p and k_c are the general rate coefficients for inter- and intramolecular ring-opening reactions that involve an arbitrary hydroxyl group and an epoxide derivative. c_1 and c_2 are additional parameters used to realize the different reactivities of hydroxyl groups based on their location on the involved polymer. $f_t(t)$ and $f_L(t)$ denote the global fraction

Init:	$I + M$	$\xrightarrow{k_i}$	$P_i(2) + \{C_T + C_T\}$
Self-Init:	$M + M$	$\xrightarrow{k_{si}}$	$P_m(1) + \{C_L\}$
Prop11(s):	$P_i(s) + M$	$\xrightarrow{k_{11}(s,t)}$	$P_i(s+1) + \{C_L\}$
Prop12(s):	$P_i(s) + M$	$\xrightarrow{k_{12}(s,t)}$	$P_i(s+1) + \{C_T + C_D - C_L\}$
Prop21(s):	$P_m(s) + M$	$\xrightarrow{k_{21}(s,t)}$	$P_m(s+1) + \{C_L\}$
Prop22(s):	$P_m(s) + M$	$\xrightarrow{k_{22}(s,t)}$	$P_m(s+1) + \{C_T + C_D - C_L\}$
Prop31(s):	$P_c(s) + M$	$\xrightarrow{k_{31}(s,t)}$	$P_c(s+1) + \{C_L\}$
Prop32(s):	$P_c(s) + M$	$\xrightarrow{k_{32}(s,t)}$	$P_c(s+1) + \{C_T + C_D - C_L\}$
I-Comb(r):	$I + P_m(r)$	$\xrightarrow{k_i}$	$P_i(2+r) + \{C_L + C_T\}$
M-Comb(r):	$M + P_m(r)$	$\xrightarrow{k_{si}}$	$P_m(1+r) + \{C_L\}$
Comb11(s,r):	$P_i(s) + P_m(r)$	$\xrightarrow{k_{11}(s,t)}$	$P_i(s+r+1) + \{C_L + C_L - C_T\}$
Comb12(s,r):	$P_i(s) + P_m(r)$	$\xrightarrow{k_{12}(s,t)}$	$P_i(s+r+1) + \{C_D\}$
Comb21(s,r):	$P_m(s) + P_m(r)$	$\xrightarrow{k_{21}(s+r,t)}$	$P_m(s+r+1) + \{C_L + C_L - C_T\}$
Comb22(s,r):	$P_m(s) + P_m(r)$	$\xrightarrow{k_{22}(s+r,t)}$	$P_m(s+r+1) + \{C_D\}$
Comb31(s,r):	$P_c(s) + P_m(r)$	$\xrightarrow{k_{31}(s,t)}$	$P_c(s+r+1) + \{C_L + C_L - C_T\}$
Comb32(s,r):	$P_c(s) + P_m(r)$	$\xrightarrow{k_{32}(s,t)}$	$P_c(s+r+1) + \{C_D\}$
Cyc1(s):	$P_m(s)$	$\xrightarrow{k_1^c(s,t)}$	$P_c(s+1) + \{C_L + C_L - C_T\}$
Cyc2(s):	$P_m(s)$	$\xrightarrow{k_2^c(s,t)}$	$P_c(s+1) + \{C_D\}$
Mfeed:	$\emptyset$	$\xrightarrow{k_{feed}}$	M

Scheme 4.19. A reaction scheme that differentiates between ring-opening reactions that involve linear or terminal subunits. The terms in curly brackets represent "counters" which are used to calculate accurate reaction rates.

of hydroxyl groups located on terminal or linear subunits at time t, respectively. These fractions can be calculated with the amounts of "counter" species that were produced. In the software "counters" are implemented in a way that they can never be used up by a reaction, but in this case it is important to also track the loss of subunits. Therefore, Scheme 4.19 includes "counters" that indicate the loss of a specific subunit, e.g., for every "counter" $\{C_L + C_L - C_T\}$ two linear subunits are created and one terminal subunit is eliminated. The "counter" is written in curly brackets because it is actually implemented as a single species which is used to calculate the total amount of linear and terminal

subunits as follows. All amounts are actually time-dependent, but the time parameter was omitted for clarity.

$$C_T = 2\{C_T + C_T\} + \{C_T + C_D + C_L\} + \{C_L + C_T\} - \{C_L + C_L - C_T\} \tag{4.120}$$

$$C_L = \{C_L\} + \{C_L + C_T\} + 2\{C_L + C_L - C_T\} - \{C_T + C_D - C_L\} \tag{4.121}$$

Knowing the total amounts of terminal and linear subunits in the system at any time t, allows one to easily calculate the fractions of hydroxyl groups that are located on the surface, $f_T(t)$, or on the backbone, $f_L(t)$. These are the factors that are used in Equations 4.112 to 4.119.

$$f_T(t) = \frac{2C_T(t)}{C_L(t) + 2C_T(t)} \tag{4.122}$$

$$f_L(t) = \frac{C_L(t)}{C_L(t) + 2C_T(t)} \tag{4.123}$$

As it was shown for the treatment of primary and secondary hydroxyl groups, the constraints to the number of different subunits can be incorporated by reformulating C_T and C_L, so that not every subunit is counted. Because normally initiated polymers have at least two terminal subunits, self-initiated ones only one, and cyclic polymers can contain any number of terminal units, the reaction rates have to be adjusted. This can be done easily in the same manner as it was discussed earlier, therefore, this extension will not be rewritten for the new scheme.

Similarly to the previous section, it is questionable whether an extension of this model to capture anion reactions is reasonable. In theory, it is possible, but the problem becomes extremely hard to simulate, once the subunits are additionally categorized by their activity. Using more than one global quantity is very erroneous and is not advised. Even if the simulation does not have to be aborted due to stability problems of the underlying algorithm, the results are nearly useless because they are just a product of the additive errors created by the averaging of the important structural properties of the molecules.

For the sake of describing the anionic ring-opening polymerization, a different approach will be used where the structural properties are approximated with a simple and uniform function depending on the actual size of the polymer. However, the model discussed in this section was tested for a simpler version of the process, where no anionic initiators were used. In that case, the described approximation strategy is feasible and the dependence of the thermal reaction rates on the molecular structure can be analyzed in detail.

4.10 M6: Approximating the Shape of the Polymers

Another way to incorporate the molecules' structure is to derive a general formula for the reaction rate of a polymer based on its size. This formula will realize a variety of additive effects, such as number of hydroxyl groups, surface area of the molecule, average fraction of primary or secondary hydroxyl groups, average fraction of linear or terminal subunits or the inhibited mobility of large molecules. Attempting to find an exact formula for the combined effect of all these aspects is futile, but a general expression that mimics the trend of the size dependency is feasible. The expression must be basic enough to provide good performance of the software and at the same time it must be variable enough to cover a wide range of different concepts. The advantage of this analysis is that the overall trend for the polymer size dependency of the reaction rates can be directly assessed by the parameter estimation procedure that is provided by the software package. In other words, the parameters which produce simulated results that describe the experimental data best indicate how the reaction rates depend on the polymers' size. In this study, a rate of a reaction between molecules of different type (i.e. A and B) and of different size (i.e. number of hydroxyl groups s and r) is generally described by the following formula:

$$R_{AB}(s,r) = A(s) \cdot B(r) \cdot k \cdot s^x \cdot r^y$$

Here, $A(s)$ and $B(s)$ denote the concentrations for the reaction partners, k is a fixed reaction coefficient, and x and y are additional parameters that dictate the polymer size dependence of the reaction rate. To capture a wide variety of effects that contribute to the polymer size dependency, the interval for the exponents is limited to $[-1, 1]$. This way, the important special cases where $x, y \in \{-1, 0, 1\}$ are incorporated in the general formulation. It will be very interesting to see which combinations of values for the exponents will produce results closest to the experimental data.

In order to adopt this representation of the reaction rates, the schemes for the thermal and anionic reactions have to be modified. In order to keep the computational effort reasonable, polymer combination reactions will not be tested, but the limits of simulating the number of active sites explicitly will be analyzed. The following set of reaction equations describes the anionic an thermal propagation reactions, a simplified self-initiation and a simplified ion transfer to monomer reaction, as well as the ion transfer reactions between polymers that may or may not result in binomially distributed counter ions.

As shown in Scheme 4.20, the anionic propagation rate coefficient is multiplied by

$$
\begin{array}{rrcl}
\text{Prop1(m,s):} & B_s^m + AB & \xrightarrow{k_p \cdot m \cdot s^\alpha} & B_{s+1}^m \\
\text{Prop2(m,s)} & B_s^m + AB & \xrightarrow{k_{thr} \cdot s^\theta} & B_{s+1}^m \\
\text{Self-Init} & AB + AB & \xrightarrow{k_{thr} \cdot 2} & B_2^0 \\
\text{TTP(m,s,n,r)} & B_s^m + B_r^n & \xrightarrow{k_t \cdot m \cdot s^\gamma \cdot r^\beta} & B_s^{m-1} + B_r^{n+1} \\
\text{TTM(m,s)} & B_s^m + AB & \xrightarrow{k_t \cdot m \cdot s^\gamma} & B_s^{m-1} + B^1 \\
\text{Mfeed} & \emptyset & \xrightarrow{k_{feed}} & AB
\end{array}
$$

Scheme 4.20. A reaction scheme to model thermal and anionic propagation reactions. It also includes a simplified self-initiation and transfer to monomer reactions. The system includes 4 kinetic rate coefficients and 4 additional parameters defining the polymer size dependencies of the reaction rates.

the number of active sites, m, and the polymer size dependency factor, s^α. The thermal propagation rate is modeled independently of the number of active sites, but there must be at least one inactive hydroxyl group ($m < s$). The thermal rate coefficient is multiplied by s^θ indicating that the polymer size dependency may differ from that of the anionic reactions. It would be more precise to write the modified rate coefficient for the thermal propagation reaction as $k_{thr} \cdot (s - m) \cdot s^{\theta'}$, but assuming that m will be much smaller than s in the vast majority of the reactions, the approximation $(s - m) \cdot s^{\theta'} \approx s^\theta$ can be used. This means that the affinity of thermal reactions to act upon polymers with many hydroxyl groups ($s >> 1$) is encoded in the exponent θ together with the other possible effects described above. Probably the most interesting effect is induced by the ion transfer reactions between polymers (labeled TTP in the scheme) because these are the only reactions that depend on the sizes and structures of two molecules. These reactions dictate how the active sites will be distributed over the hydroxyl groups in the system. Multiplying the rate coefficient by the number of active sites of the donating polymer (m) ensures that the degree of activity is somewhat flattened, whereas a negative value for α counteracts this effect by making big polymers less likely to decrease their activity. And of course, high values of β will cause big polymers to be more likely to bind one or more counter ions.

One should keep in mind that not all combinations of parameter values are reasonable from a chemical point of view and that the model has been designed with specific expectations. However, since the dependencies are very unclear at this point due to the unsubstantiated state of knowledge about the elemental mechanisms and their complex interactions, even a surprising or unrealistic result can disclose research directions that

could not be thought of before.

4.11 Alternative Modeling Approaches

The main difficulty for this study was connected to the fact that the reaction rates are assumed to be dependent on the polymers' structure, i.e. the number of different hydroxyl groups it contains. The only exact way to account for this is to model every type of polymer as an individual species. Therefore, a polymer species is defined by the number, the type, and the location of every reacting group of the molecule, i.e., reacting groups can be an epoxide, a primary hydroxyl on the surface (terminal subunit), a secondary hydroxyl on the surface, a primary hydroxyl on the backbone (linear subunit), a secondary hydroxyl on the backbone, a primary alkoxide (deprotonate hydroxyl) on the surface, a secondary alkoxide on the surface, a primary alkoxide on the backbone or a secondary alkoxide on the backbone. The basic approach of this study was that the reaction rate of a polymer species can be expressed as a function of all its reacting groups. Calculating these rates explicitly would require knowledge about the exact numbers of the different reacting groups for every polymer at any time. Additionally, the polymers' composition is likely to change dynamically, e.g., through an ion transfer reaction. Therefore, kinetic rates have to be calculated not only for propagation and combination reactions, but also for inter- and intramolecular ion transfer reactions. This enormous task needs to repeated in every step of the simulation and estimating every kinetic parameter separately on the basis of measurement data is simply impossible. The strategy that was pursued in this study and many others as well, is to approximate the relationship between the different reaction rates by a function that depends on a much lower number of parameters, e.g., only on the total number of hydroxyl groups.

In the deterministic approach, the rate equations are translated into a set of ODEs, one for each polymer species, which is used to solve an IVP. For the IVP to be solvable in a reasonable time, the number of polymer species must be restricted. The maximum number of ODEs cannot be assessed without knowing the exact dynamics of the process. However, with regard to the system at hand, several hundred equations do not pose a big problem and even a few thousands can be solved in an efficient manner. This is where the integration method implemented in the simulation software becomes very beneficial because it is optimized for the approximation of polymer size distributions. To illustrate this one can think of a PSD with a maximum polymer size of M. Normally, simulating the changes

in all M polymer species would require as many ODEs, but the software approximates the PSD with a series of polynomials. Therefore, instead of calculating the changes for the concentrations of every polymer of every size, the changes for every polynomial coefficient are used. Although the polynomials have to be adapted in every step to ensure that the overall modeling error stays below a predefined tolerance limit, the number of differential equations is usually much lower than M. The drawback of this representation is that the PSD has to be smooth, just like the polynomials that are used to model it. Additionally, this approximation only works for one-dimensional polymer species.

An alternative to the deterministic approach is a stochastic simulation, e.g., a variation of Gillespie's stochastic simulation algorithm (SSA).[108] The methods do not restrict the dimensions of the state space, but a large state space will result in a large number of "reaction events" and the time step length will become very small. Even though there are ways to improve the performance of these algorithms, the computational effort will always exceed that of a comparable deterministic simulation. However, simulations of very complex systems are always realizable and by averaging over many randomly simulated trajectories, the results become similarly accurate as the experimental data.

Although stochastic simulations are possible, they cannot be optimized to reproduce the experimental data. The biggest advantage of a deterministic approach is that the difference between simulated and experimental results can be formulated as an objective function which depends on the kinetic parameters of the underlying, deterministic model. This objective function can then be optimized with the help of sophisticated, mathematical methods.[10] Stochastic simulations will always create a substantial sampling error introduced by averaging the randomly created output. Because of that error, it is not possible to formulate an objective function in dependence on the model's parameters and optimizing them requires less robust methods, such as maximum likelihood estimators. These methods are proven to converge, but they are not guaranteed to do so in a reasonable time and an optimum might never be reached. In summary, Monte-Carlo methods are very useful in cases where input parameters are known and one is interested in the outcome of a fixed system, but they are not useful for finding optimal parameters that produce an output that is known beforehand. There exist some approaches to combine stochastic and deterministic simulations by splitting the dynamics and treating the different aspects of the process separately in a controlled manner.[100] This methodology also does not permit the use of parameter estimation procedures, but it could be used to improve the simulation if the deterministic dynamic has already been pre-optimized.

As for the simplification strategies, this chapter clearly shows the vast number of possibilities that exist and there are many other concepts that can be employed to reduce the model to a reasonable size. This study relies on polymer size dependent reaction coefficients, pseudo two-dimensional polymer species, approximating the average number of active sites per polymer, and global "counter" species to model the ratios between different types of reacting groups. Some properties could not be captured with this approach, such as real multi-dimensional polymer species, mixing inhomogeneities, residual water contamination, post-processing effects, or perturbations induced by the sample recovery. It was decided to not include these problems in the model because either they are assumed to be less significant than the measurement error or they simply cannot be quantified at all.

For some mechanisms more detailed information has to be gathered in order to properly approximate their effects. These include the reduced mobility of big molecules in comparison to small ones and the cyclization rate of self-initiated polymers. It is widely known that large molecules are more strongly effected by the reactor's viscosity. This effect has been observed in free radical polymerizations,[109] and is often referred to as autoacceleration or Trommsdorff-effect. In biological systems the hindered mobility of macromolecules in cells is referred to as macromolecular crowding. In every case it is a result from the Brownian motion of the molecules.[110] With increasing viscosity, the large molecules entangle and block each other, which limits the space they can travel in. This does not apply to small molecules which can still move freely through the remaining solution and their travel distance can actually be increased due to the excluded volume of the big molecules. A similar effect can be observed for polymers close to a solid surface such as the outer wall of a reactor.[111] The other issue that might be addressed after further investigation regards the intramolecular reactions, i.e., if an epoxide reacts with a reacting group of the same molecule. Jacobson and Stockmayer have postulated the ring formation reaction to depend on the number of bonds that separate the involved functional groups in a non-linear way.[112] However, this theory was solely based on randomly coiled, linear polymers with Gaussian end-to-end distances and only two reacting groups. A modification of this approach was used by Dušek et al.[113] for hyperbranched polymers produced in random polycondensation reactions of AB_m-type monomers. In their work they used two extreme cases, one for a perfect dendrimer and one for a linear chain, and averaged the cyclization rates accordingly. However, it remains a very harsh simplification and it is by no means appropriate to assume Gaussian end-to-end distances between the

functional groups of a branched molecule. The described problems could be approximated after a thorough investigation with molecular dynamics simulations, but this is not in the scope of this study.

5. EXPERIMENTAL DESIGN AND DATA PROCESSING

This study was part of a project that aimed to improve the synthesis of dendritic polyglycerol. This main focus of this thesis is the mathematical representation of the chemical mechanisms and how the process can be simulated. Although the experiments were exclusively conducted by the collaboration partners, the design of new experiments and the general research direction were strongly affected by the simulation results. After the initial series of experiments was computationally analyzed, new experiments were explicitly designed to prove or disprove the preliminary results.

This chapter describes and discusses the experiments and the measurement data from a process engineering point of view. The first section briefly summarizes the general set-up of the experiments and describes the measurements that were performed to assess the quality of a sample. The second section focuses on the conducted experiments and the reasoning behind their design. Since many of the performed experiments were designed on the basis of the simulations, this section includes some generalized results from the computational analysis. However, details about the simulations are presented and discussed in the next chapter. In the last section of this chapter the interpretation of the measurement data is presented. This was very crucial for the simulation study because the parameter estimation procedure is based on this data and is highly sensitive to experimental errors. Great care was taken while processing the raw data into a formate that can be compared to the simulated output. The analysis of the experimental data constitutes an important part of the simulation study and thus, details about the measurements are reported and discussed as well.

5.1 Experimental Detail

All experiments were conducted by Florian Paulus who is part of the work group of Prof. Dr. Rainer Haag in the department of organic chemistry at the Free University Berlin.

A 1 liter reaction vessel was used with an anchor stirrer that ran constantly at high speed to ensure a well distributed polymer mixture. The reactor was placed in an oil bath

to keep the temperature constant throughout the reaction.

In a preprocessing step the initiators were prepared by dissolving trimethylolpropane (TMP or 2-(hydroxymethyl)-2-ethylpropane-1,3-diol) in methylpyrrolidone (NMP or 1-methyl-2-pyrrolidone). Additionally, potassium *tert*-butoxide (potassium 2-methylpropan-2-olate) was utilized as cation exchanger to deprotonate 10% of all hydrolyl groups of the TMP molecules. After that, the exchange product methanol was extracted and the apparatus was set up.

Glycidol (oxiranylmethanol or 2,3-epoxy-1-propanol) was used as cyclic monomer. Before adding it to the reactor, it was dissolved in tetrahydrofuran (THF or oxolane) and stored in a separate tank at room temperature that was connected to the reactor through a precision dosing pump.

While the continuously stirred reactor was running at an elevated temperature, the highly diluted monomers were added to the reactor over 18 hours. Once the dissolved monomers enters the heated system, the THF is distilled nearly instantly and was completely recovered after the reaction. Therefore, the system was not perturbed by this solvent at all.

For most experiments a pipette was used to extract a sample of ca. 0.3 mL every 2 hours. In order to obtain a sample, the stirrer had to be stopped and the monomer addition halted for a brief moment. The unavoidable error introduced by this perturbation of the running reactor is nearly impossible to be assessed. In some of the early experiments only one sample from the final product was taken after the reaction was completed, but most of the experiments were repeated with sampling at various time points.

Every sample was analyzed with the SEC, MALDI-TOF, and NMR techniques. The settings for the instruments were varied in some cases. Further details can be taken from the discussion of the experimental data.

5.2 Design of Experiments

The initial design of the experiments was adopted from previous studies.[8,9,114] The most important characteristic of the synthesis is the capability to control the average molecular weight of the final product by varying the ratio between the amounts of monomer and initiator. Therefore, the first series of experiments was designed with different monomer-to-initiator ratios to assess the controllability and its limitations. Slowly adding highly diluted monomers to reactor that was initiated with anionic core-forming molecules has

already been proven beneficial because monomer combinations could be avoided to a great extend.[106,115] This concept has also been adopted by this study. To avoid side effect of the monomer addition technique to affect the parameter estimation, the total amount of monomers and the addition rate was not changed for the initial series of experiments. Instead, the initial amount of initiators was altered in order to adjust the monomer-to-initiator ratio as desired. This way, also the total number of deprotonated hydroxyl groups in the system was altered, i.e., in all cases 10% of the hydroxyl groups were affected. This percentage was chosen because it could be shown that higher values lead to precipitation of the initiators. Furthermore, keeping the amount initiators with two or three deprotonated hydroxyl groups low helped estimating the anionic ring-opening reaction rates correctly. This was achieved by a low percentage of deprotonation, but one has to keep in mind that this also introduced a significant amount of "inactive" initiators without deprotonated hydroxyl groups. The last process parameter of interest was the reaction temperature which was fixed to 120 °C in accordance to the experiences by the work group of Prof. Haag.

The first series of experiments was compared to simulations of a very general model which included many parameters. These parameters were optimized to produce simulations that were as close as possible to the measured data. The main purpose of this parameter estimation was to gain a general insight into the chemical mechanisms and to assess which of them were essential to reproduce the experiments. The results from the simulation study can be briefly summarized in the following findings.

- Big polymers grow faster than small ones.
- Modeling multiply activated polymers with up to three deprotonated hydroxyl groups has a great impact on the simulated output.
- Considering thermal ring-opening reactions in the model does not help in describing the experimental data better.
- The concentration of monomers may become very high; at least in the simulations that best described the measurement data.
- Adding more monomers in the beginning and less at the end of the reaction improves the average molecular weight of the final product.

These conclusions had to be treated carefully because, firstly, the overall agreement between simulations and experiments was not very good and, secondly, the results were

somewhat contradictory because one would assume a high concentration of monomers to prompt thermal ring-opening reactions. The preliminary hypotheses were evaluated by designing two new series of experiments.

The first new series of experiments was designed to prove or disprove the new monomer addition technique that was suggested to improve the quality of the final product. For the limiting case with the lowest amount of initiator, the monomer addition technique was altered in two different ways. In both cases, the total reaction time (18 hours) was split into two hour intervals and the monomer addition rate was fixed for ever time interval individually. To test the hypothesis from the simulated results, most of the monomers were added in the first time interval. For subsequent time intervals, the monomer addition rate was decreased in a strictly monotonic manner, so that the total amount of added monomers was the same as described in the previous section. For comparison, an opposing monomer addition technique was tested as well. In this case, the sequence of reaction rates was reversed in time, so that only a few monomers were added at the beginning and the majority was added in the last time interval. The fact, that both new experiments resulted in products of lower average molecular weight, showed that an essential mechanism had to be missing in the model.

Another series of experiments was designed to assess the importance of thermally induced ring-opening reactions. The experiments were conducted without any initiators, so that no anionic ring-opening reactions could occur. Therefore, any polymer growth the could be detected must have been induced by thermal reactions. The reactor was set up in the same way as described in the previous section and the monomers were added with a constant rate over 18 hour. By preventing the anionic ring-opening reactions as well as any ion exchange between polymers from occurring, the thermal reactions could be analyzed with greater detail. This permitted the evaluation of the temperature dependencies which were expressed by the Arrhenius parameters of the thermal ring-opening reaction rate coefficients. Further details about the modeling concepts used to describe the thermal ring-opening polymerization are discussed in the next chapter. The purpose of this series of experiments was to fix the kinetic parameters of the thermal reactions in the overall model and then estimate the remaining anionic reaction rates separately.

Table 5.1 summarizes the conducted experiments and lists the values for the key parameters.

Table 5.1. Summary of the conducted experiments and their key parameters.

ID	NMP[a]	TMP[b]	deprot.	Temp.[c]	THF[a]	Gly[b]	M. feed[d]
PG0_90	10	0	n/a	90	225	100	$f(t) \propto t$
PG0_105	10	0	n/a	105	225	100	$f(t) \propto t$
PG0_120	10	0	n/a	120	225	100	$f(t) \propto t$
PG2500	10	5.36	10%	120	225	100	$f(t) \propto t$
PG5000	10	2.68	10%	120	225	100	$f(t) \propto t$
PG10k	10	1.34	10%	120	225	100	$f(t) \propto t$
PG20k	10	0.67	10%	120	225	100	$f(t) \propto t$
PG20k_f	10	0.67	10%	120	225	100	$f(t) \propto \log_{20}(t)$
PG20k_s	10	0.67	10%	120	225	100	$f(t) \propto 20^t$

[a] values in [mL]
[b] values in [g]
[c] values in [°C]
[d] This function illustrates the general time dependency and not the actual values.

5.3 Interpretation and Processing of Measured Data

In order to characterize the polymer samples obtained in the experiments different measurement techniques were utilized. SEC was used to determine the most important properties, i.e., number- and weight-average molecular weight. MALDI-TOF mass spectrometry was performed to assess the whole PSD for different species of polymers due to the fact that self-initiated polymers lack the initiator derivative and therefore form a different series of peaks in the mass spectrum. However, as will be discussed later, the distributions obtained by the MALDI-TOF technique produce average molecular weights that differ drastically from the more reliable values determined by SEC. Furthermore, the mass spectrum of the MALDI measurements appears to change only slightly over the different stages of the polymerization which is not to be expected. For these reasons and because SEC is widely accepted as the most accurate measurement technique for determining average molecular weights, the computational validation of the mathematical models was solely based on the SEC data. However, it must be noted that this measurement technique is also not completely free of errors. By using the universal calibration technique to determine the relationship between elution time and molecular mass. The results might be erroneous for randomly branched polymers because evaluation of the intrinsic viscosity based on the molecular mass is not clearly defined. To compensate for this error two different standards were used for the calibration, i.e., one linear and one perfectly branched polymer standard, but the error could not be quantified.

5.3.1 Size Exclusion Chromatography

Size exclusion chromatography (SEC) is often referred to as gel permeation chromatography (GPC) in literature and is known to be the most reliable method for measuring average molecular masses and dispersities of polymer samples. However, there still remain issues with the measurement technique that are related to the fact that the measured signal is actually corresponding to the intrinsic viscosity of the molecules rather than the molecular mass. The relation between intrinsic viscosities $[\nu]$ and molecular mass M is given by the Mark-Houwink equation:

$$[\nu] = KM^a \tag{5.1}$$

Unfortunately, the Mark-Houwink-Sakurada constants K and a are unknown for the studied polymers. Therefore, monodisperse samples of a comparable substance with well-defined molecular weight have to be used for a universal calibration. This type of calibration is specific for the column, solvent, and flow rate that were used for the measurement. This method works very well for linear polymers, but for branched polymers additional problems arise because the molecular structure yields different intrinsic viscosities in comparison to the standard. This problem can be counteracted by using a calibration standard with a similarly branched structure. For the analysis of hyperbranched polymers, it is not possible to find a substance with the same structural properties because of the variance in the branching density. Instead, two different standards, with linear and symmetrically branched structures, were used to calibrate the SEC column with the expectation that the hyperbranched polymers can be analyzed by combining the two calibration techniques. For the first experiments only the linear pullulan samples were used for the calibration, but in the later stage of the study samples of branched dextran molecules were considered as well.

Figure 5.1 shows the different standards used to calibrate our SEC column. One can see a difference, but it is within measurement error tolerance. For the further processing of the data the pullulan standard was used because the low molecular polymers seem to be depicted better and using the branched standard would make it impossible to identify signals at high elution times. This can be attributed to the fact that a single repeat unit of pullulan is structurally closer to that of glycerol than dextran.

Figure 5.2 illustrates how elution time diagrams can be translated into a weighted, continuous MMD. Such a distribution can also be used for parameter estimation in the PREDICI software. However, the average molecular weights ($\overline{M}_n$ and $\overline{M}_w$) are expected to

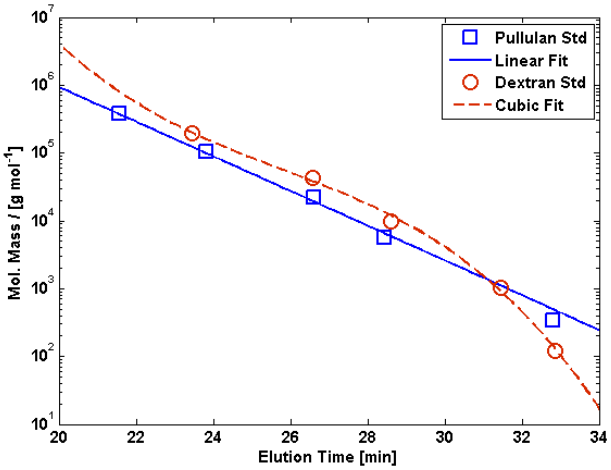

Figure 5.1. Comparison of the two standards used to calibrate the SEC apparatus. The markers indicate the measurements for the samples and the lines represent the corresponding regression curves.

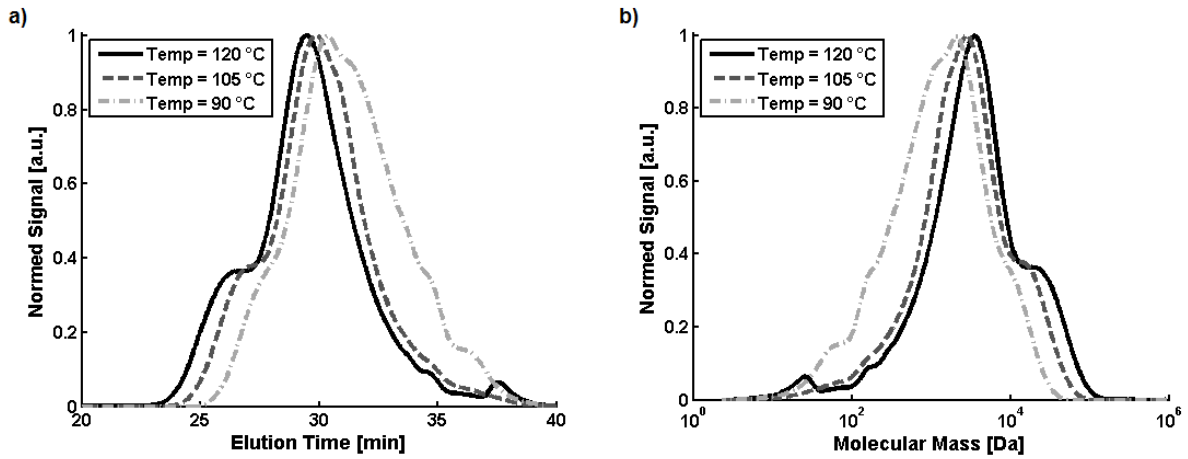

Figure 5.2. Comparison of the final SEC measurements at different temperatures. The left side shows the elution time diagrams, and the translated MMD are displayed on the right hand side.

be much more accurate than the actual distribution. Therefore, the optimization will be solely based on the averages. Another advantage is that comparing simulated to experimental data is much more time consuming when using whole distributions because this might interfere with the software's polymer size discretization scheme. The average values, on the other hand, can be calculated via the distribution moments which are available at every time step automatically.

Figure 5.3 shows the time profiles of $\overline{M}_n$ and $\overline{M}_w$ calculated from the measurements at various reaction times of the experiments without initiators (PG0_90, PG0_105 and

PG0_90). All three experiments included the same amount of monomers which were added over 18 h at a constant rate.

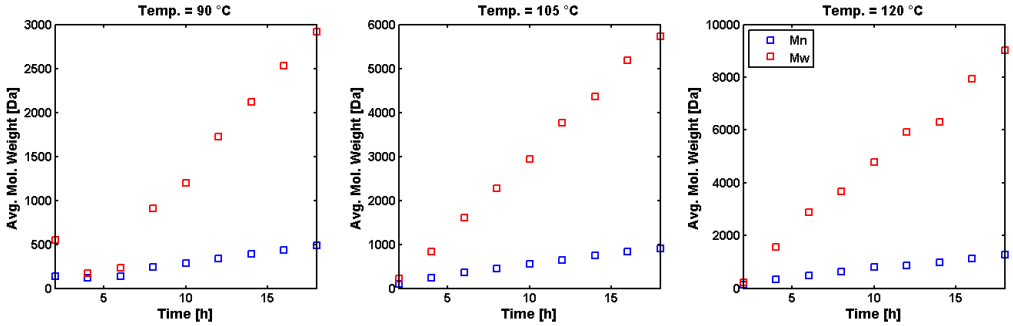

Figure 5.3. Time profiles of $\overline{M}_n$ and $\overline{M}_w$ at different temperatures.

One can clearly see that low temperatures result in much lower average molecular weights. The polydispersity (quotient of $\overline{M}_w$ and $\overline{M}_n$) takes quite high values in all three experiments. A polydispersity index lower than 1.6 is considered to account for a narrow MDW, whereas the values achieved here are larger than 6 indicating very broad distributions.

Figure 5.4 shows the time profiles of $\overline{M}_n$ and $\overline{M}_w$ calculated from the measurements at various reaction times of the experiments with different amounts of initiators (PG2500, PG5000, PG10k and PG20k). In all these experiments 100g of monomers were added over 18h at a constant rate and the reaction temperature was 120 °C in every case. For PG5000 and PG10k only the final sample was taken.

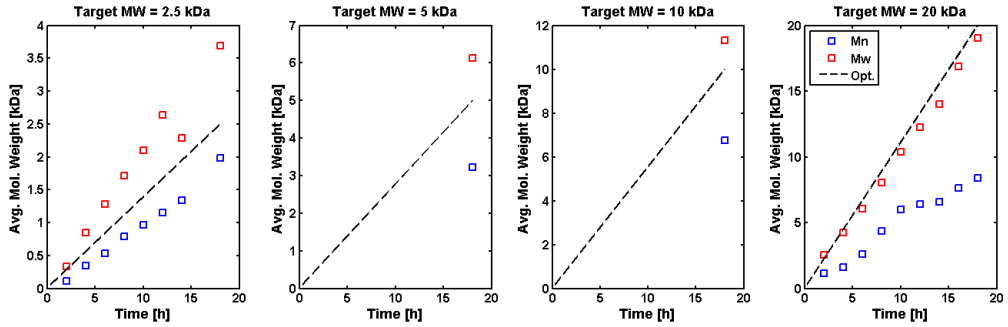

Figure 5.4. Time profiles of $\overline{M}_n$ and $\overline{M}_w$ for experiment with different amounts of initiators (target molecular weight is determined via the ratio of monomers to initiators added). The markers shows the measured values and the black, dashed line indicates the theoretically optimal trajectory for an ideal polymerization. The reaction temperature was 120 °C in all four experiments.

By adding initiators to the reactor, one can control the theoretical molecular weight of

the polymers at the end of the reaction. If all monomers exclusively bind to the initiators, i.e., no self-initiations occur and all monomers are used up at the end, the average molecular weight is defined by the ratio of monomers to initiators. If one further assumes that the monomers are distributed evenly over all initiators then the final polymer sample would only contain molecules with the same molecular weight which can be calculated via the ratio of used monomers and initiators together with the molar masses of a monomer and an initiator. With this the naming of the experiments' IDs becomes apparent since the targeted molecular weights are 2.5 kDa, 5 kDa, 10 kDa, and 20 kDa. The ideal time profile for $\overline{M}_n$ and $\overline{M}_w$ can also be plotted as a straight line that is proportional to the amount of added monomers. In Figure 5.4, this optimal trajectory is illustrated as a black, dashed line.

Figure 5.5 shows the SEC results for the experiments where the monomer addition technique was altered.

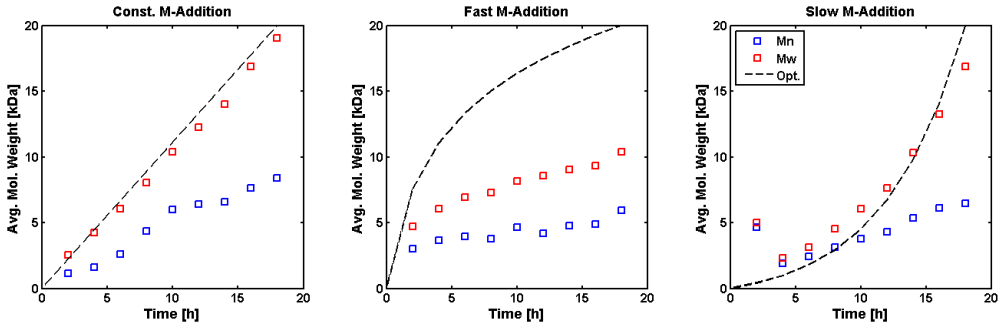

Figure 5.5. Time profiles of $\overline{M}_n$ and $\overline{M}_w$ for experiments with different monomer addition techniques. The amount of initiators was chosen so that the targeted molecular weight was 20 kDa and the reaction temperature was 120 °C in all three experiments.

One can observe a lower $\overline{M}_n$ for both alterations of the monomer addition technique. Interestingly, a fast monomer addition seems to lower the polydispersity index for the final product at the cost of the average molecular weight. In any case, it appears that a steep increase in monomer molecules will evidently result in the formation of self-initiated polymers. It seems that it would be best to give the monomers as much time as possible to bind to the existing molecules which suggests the flow rate should be kept at a minimum throughout the reaction. Therefore, a constant monomer addition appears to be the best option for preventing self-initiation reactions.

5.3.2 MALDI-TOF Mass Spectrometry

As mentioned above, mass spectrometry is a very promising measurement technique because the spectra are very detailed and one can observe clear peaks that can be correlated to polymers of different molecular weights. It is even possible to identify distinct series of peaks for different types of polymers, i.e., whether they stem from a growing initiator or they were created through spontaneous monomer combination.

In order to integrate the peaks in the signal, two different methods were employed. In the early stages of this study, only the software provided by the instrument's manufacturer was used. This required one to manually select every peak used to calculate average molecular weights ($\overline{M}_n$, $\overline{M}_w$, M_p) and the polydispersity index (PDI). Since these average values differed drastically from the ones obtained by the SEC measurement technique, the raw data was analyzed more carefully so that the unknown error induced by the automated procedure of the provided software could be avoided. Extracting discrete MMD was done with the help of the software OpenMS[116] that was developed by another work group at the Free University of Berlin.

The OpenMS processing pipeline TOPAS was used to apply the following sequence of data processing tools. Firstly, a noise filtration was utilized, followed by an automated baseline reduction. In the last step the build-in peak picking procedure was used to obtain the final MMD. After discussing our data with the developers of the peak picking methodology, the parameters were adjusted in a way that every significant peak is included while minimizing the number of artificially introduced peaks. Once good parameter values were identified, the same set was used to analyze all subsequent MALDI datasets. The results have always been checked to make sure no significant signal was discarded by accident. Figures 5.6 and 5.7 illustrate all steps in the pipeline.

The MMD was also transformed into size distributions for the various polymer species. For this a MATLAB script was written where a mass function was defined for every type of polymer, e.g., polymers with or without initiator, water-initiated polymers, and fragmented polymers. The general formula for the mass of a polymer was defined as the following size dependent expression.

$$M(P_s) = s \cdot 74.08 + 22.99 + X$$

This incorporates the molar mass of glycidol (74.08 g/mol) and sodium (22.99 g/mol) which was used to ionize the sample. The additional term X is directly related to the type of polymer. For example, a self-initiated polymer and its cyclic counterpart both have no

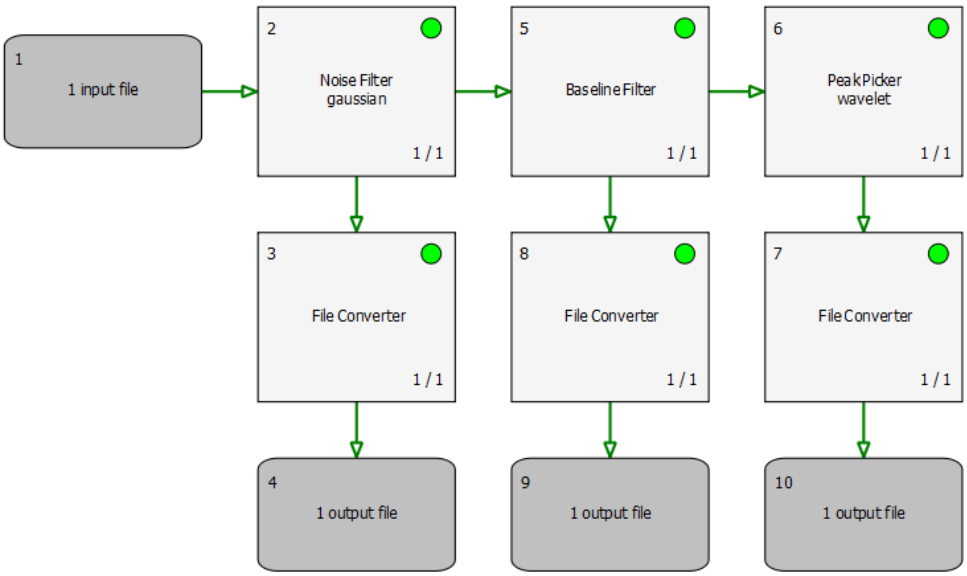

Figure 5.6. Illustration of the data processing pipeline used to transform the raw MALDI-TOF data into discrete MMDs.

extra mass ($X = 0$) whereas the normally initiated polymers' mass is increased by the molar mass of an initiator ($X = 134.17$). Additional values for X were analyzed in order to find the extent of contamination with water ($X = 18$) and whether polymers might have broken apart while in the measurement apparatus. In some cases, water contamination could not be ruled out, but the samples actually used for the parameter estimation nearly exclusively contained peak series associated with the primary and secondary polymer species.

Figure 5.8 shows a typical mass spectrum. Upon examination of the magnified region, one can observe multiple series of peaks that seem to be offset by specific values. Different Values for the offset were tested to analyze the polymer's composition in greater detail. The three offsets that can be used to identify most of the peaks are 10, 24 and 42. These values can be associated with TMP-initiated polymers ($22.9 + 134.17 - 2 \cdot 74.08 = 8.91$), glycidol-initiated polymers (22.9, the mass of a counter ion) and water-initiated polymers ($22.9 + 18.02 = 40.92$). One can even start to speculate that the water-initiated polymers could represent the self-initiated polymers that have not yet undergone cyclization. This would mean that the epoxide of these polymers was opened in the presence of water in the post-processing and measurement steps.

Another uncertainty arose from the peak picking procedure in combination with the chosen parameters. After noting that the isotopes of molecules were resulting in highly overlapping peaks in the spectrum, the peaks of the isotopes merged and averaged. This

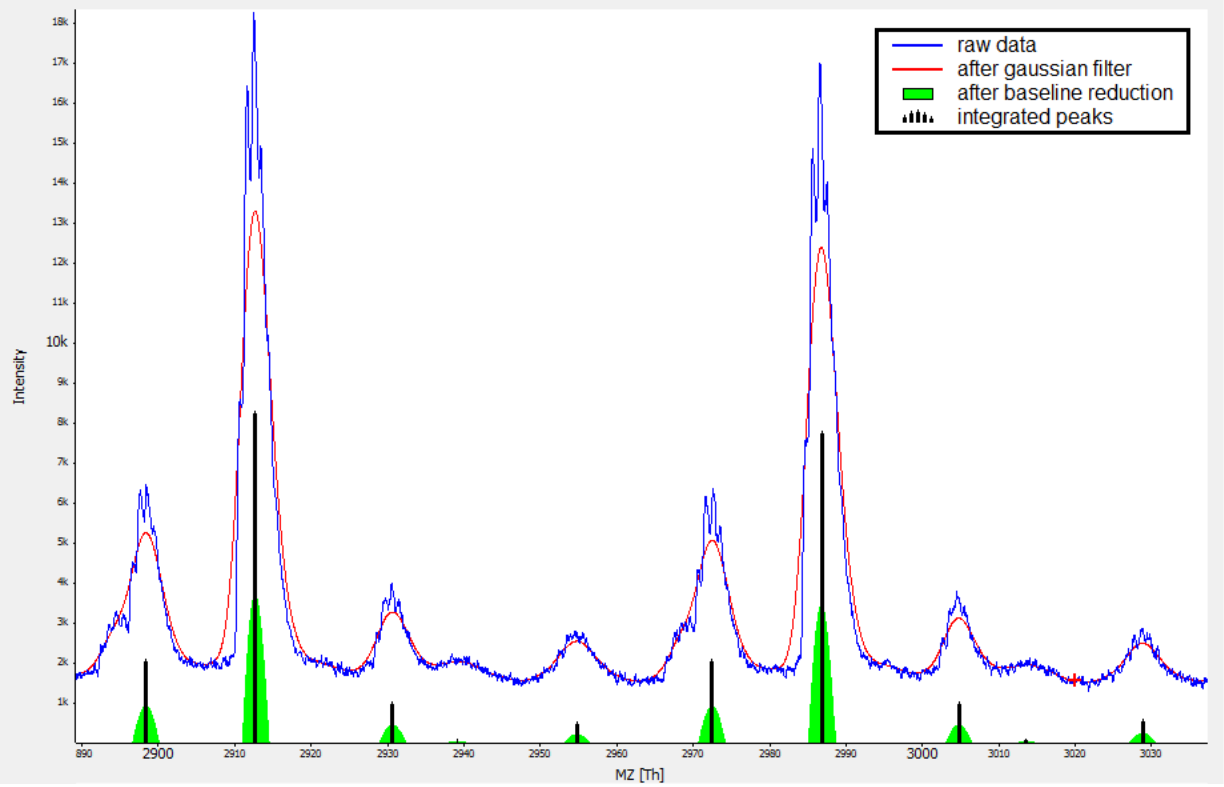

Figure 5.7. An illustration for the processing of the MALDI-TOF data. The blue line shows the original signal and the red line the intermediate result after applying the Gaussian noise filter. The green area is the result of the baseline reduction and the black bars represent the final discrete MMD. The distance between the two large peaks is equal to the molecular weight of a monomer.

was realized by choosing the noise filter parameter so that the isotopes were combined to one peak. In general that is not problematic because these peaks were likely to arise from the same polymer and would be summed later on anyways. Therefore, the integral should be correctly calculated, but the averaged mass of the peak could be perturbed so that the assignment from molecular mass to the polymer size was ambiguous. To compensate for this error induced by the peak picking method, the mass formula was kept variable by introducing a range of mass values for monomers ($[73.5, 75.5]$) and introduced a more general mass offset that represents X plus the mass of a counter ion. The highest value of the offset is the monomer's mass because otherwise the masses tested would be repeated. For every processing trial, more than 10000 combinations of values were tested and the ones that contributed the majority of the signals were chosen for further processing.

Figure 5.9 shows an example for the identification of the polymer size distributions. The first three depict normally initiated, self-initiated and water-initiated polymers,

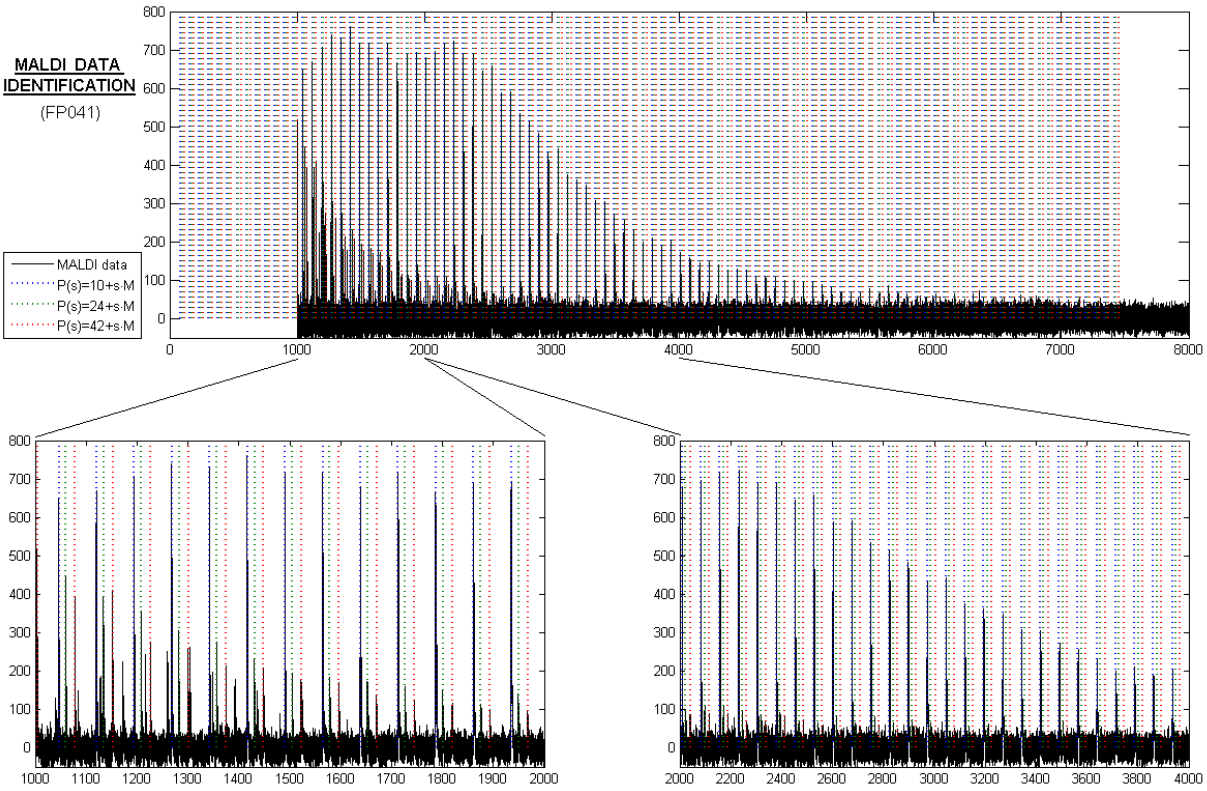

Figure 5.8. Illustration of a typical MALDI-TOF signal (black) along with the theoretical masses of normal, self-initiated, and water-contaminated polymers of different sizes (blue, green, and red dotted lines). In the magnified region one can easily assign the main peaks to the different polymer species.

respectively, and the other values were determined by the strategy explained above. This sample was chosen because it contains considerable amounts of water-contaminated polymers. For the same reason, this sample was not used for the model validation or the parameter estimation. Other samples did not show such high amounts of water-initiated polymers.

Unfortunately, there is no explanation for the low average molecular weights calculated with the MALDI measurements. For example, the data displayed in Figure 5.9 indicate an average molecular weight of less than 3 kDa whereas the SEC measurements show a value of almost 5 kDa. A similar comparison can be drawn for all measurements. Therefore, the MALDI data clearly contradicts the SEC measurements, which is known to be the most reliable technique to determine average molecular weights. The MALDI data also do not indicate a strong polymer growth, i.e., the values for $\overline{M}_n$ do not change significantly over time, which is very unrealistic from an engineering point of view. For these reasons, the

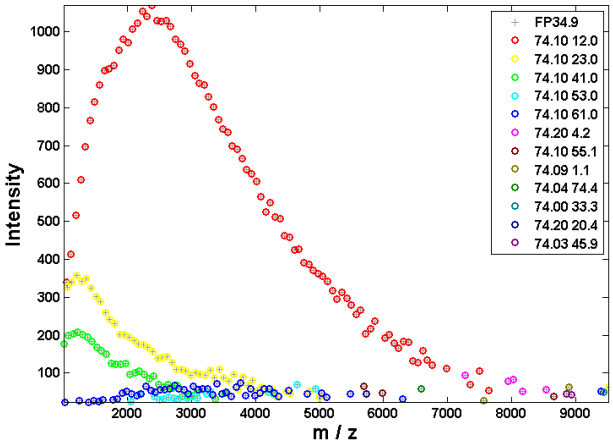

Figure 5.9. A typical result for the translation of the raw MALDI signal into discrete MMDs. One can identify three distinct series that account for normal, self-initiated, and water-initiated polymers. A fourth, unidentified series shown as blue markers can also be seen, but the very low intensities suggest that these signals are due to noise effects.

MALDI data was not used to validate the models.

6. RESULTS AND DISCUSSION

The developed models were validated by estimating the optimal kinetic reaction coefficients with which the experimental data could be reproduced most accurately. Since a deterministic approach was used to formulate the kinetic model, well-known mathematical optimization methods can be applied, but the optimization problem remains a difficult task. As a prerequisite for the parameter estimation procedure to work, i.e., to ensure its convergence towards the optimal solution, the model has to be simplified. Chapter 4 describes the concepts that were applied to simplify the model, so that it can be used for the estimation of kinetic parameters. There are alternative ways to develop a model that can be used to simulate and predict the outcome of chemical processes, but the chosen approach has many advantages and can be considered a natural choice. However, as mentioned before, the problem remains very hard to solve and simplifying the model can be done in many ways. Not every possible model was tested, but the most reasonable simplifications for this type of process were applied. This chapter reports and discusses the results of the parameter estimation procedures and elaborates the development of the model from the early stages of this study towards the final model that can be used for predicting the outcome of the synthesis.

The complexity of the process can be illustrated by the possible propagation reactions between a normally initiated polymer, P, and a monomer, M. The reaction rate is assumed to depend on the numbers of the different types of hydroxyl groups, where they are located on the polymers and whether they are deprotonated or not. In order to calculate the reaction rates correctly, the polymer species have to be specified by the number of hydroxyl groups they carry. The hydroxyl groups can be located either on a linear or a terminal subunit (denoted by property indexes l and t, resp.), be primary or secondary (denoted by subscript p and s, resp.), and they may be deprotonated or not (denoted by superscript 1 and 0, resp.). Regarding all possible combination of these three properties one ends up with 8 (2^3) different types of hydroxyl groups and almost every combination of hydroxyl groups may occur in the polymers. Details on the restrictions for these indexes will not be discussed here, e.g., the number of terminal, primary hydroxyl groups must be 3 or greater

due to the structure of the initiator.

$$
\begin{aligned}
\text{Prop1\_}L_p^1\text{:}\quad & P(l_p^1,l_s^1,t_p^1,t_s^1,l_p^0,l_s^0,t_p^0,t_s^0)+M \xrightarrow{k_{1,L,1,p}\cdot l_p^1} P(l_p^1-1,l_s^1,t_p^1,t_s^1+1,l_p^0,l_s^0,t_p^0+1,t_s^0)\\
\text{Prop1\_}L_s^1\text{:}\quad & P(l_p^1,l_s^1,t_p^1,t_s^1,l_p^0,l_s^0,t_p^0,t_s^0)+M \xrightarrow{k_{1,L,1,s}\cdot l_s^1} P(l_p^1,l_s^1-1,t_p^1,t_s^1+1,l_p^0,l_s^0,t_p^0+1,t_s^0)\\
\text{Prop1\_}T_p^1\text{:}\quad & P(l_p^1,l_s^1,t_p^1,t_s^1,l_p^0,l_s^0,t_p^0,t_s^0)+M \xrightarrow{k_{1,T,1,p}\cdot t_p^1} P(l_p^1,l_s^1,t_p^1-1,t_s^1+1,l_p^0,l_s^0,t_p^0+1,t_s^0)\\
\text{Prop1\_}T_s^1\text{:}\quad & P(l_p^1,l_s^1,t_p^1,t_s^1,l_p^0,l_s^0,t_p^0,t_s^0)+M \xrightarrow{k_{1,T,1,s}\cdot t_s^1} P(l_p^1,l_s^1,t_p^1,t_s^1,l_p^0,l_s^0,t_p^0+1,t_s^0)\\
\text{Prop2\_}L_p^1\text{:}\quad & P(l_p^1,l_s^1,t_p^1,t_s^1,l_p^0,l_s^0,t_p^0,t_s^0)+M \xrightarrow{k_{2,L,1,p}\cdot l_p^1} P(l_p^1-1,l_s^1,t^1,p+1,t_s^1,l_p^0,l_s^0,t_p^0+1,t_s^0)\\
\text{Prop2\_}L_s^1\text{:}\quad & P(l_p^1,l_s^1,t_p^1,t_s^1,l_p^0,l_s^0,t_p^0,t_s^0)+M \xrightarrow{k_{2,L,1,s}\cdot l_s^1} P(l_p^1,l_s^1-1,t_p^1+1,t_s^1,l_p^0,l_s^0,t_p^0+1,t_s^0)\\
\text{Prop2\_}T_p^1\text{:}\quad & P(l_p^1,l_s^1,t_p^1,t_s^1,l_p^0,l_s^0,t_p^0,t_s^0)+M \xrightarrow{k_{2,T,1,p}\cdot t_p^1} P(l_p^1,l_s^1,t_p^1,t_s^1,l_p^0,l_s^0,t_p^0+1,t_s^0)\\
\text{Prop2\_}T_s^1\text{:}\quad & P(l_p^1,l_s^1,t_p^1,t_s^1,l_p^0,l_s^0,t_p^0,t_s^0)+M \xrightarrow{k_{2,T,1,s}\cdot t_s^1} P(l_p^1,l_s^1,t_p^1+1,t_s^1-1,l_p^0,l_s^0,t_p^0+1,t_s^0)\\
\text{Prop1\_}L_p^0\text{:}\quad & P(l_p^1,l_s^1,t_p^1,t_s^1,l_p^0,l_s^0,t_p^0,t_s^0)+M \xrightarrow{k_{1,L,0,p}\cdot l_p^0} P(l_p^1,l_s^1,t_p^1,t_s^1,l_p^0-1,l_s^0,t_p^0+1,t_s^0+1)\\
\text{Prop1\_}L_s^0\text{:}\quad & P(l_p^1,l_s^1,t_p^1,t_s^1,l_p^0,l_s^0,t_p^0,t_s^0)+M \xrightarrow{k_{1,L,0,s}\cdot l_s^0} P(l_p^1,l_s^1,t_p^1,t_s^1,l_p^0,l_s^0-1,t_p^0+1,t_s^0+1)\\
\text{Prop1\_}T_p^0\text{:}\quad & P(l_p^1,l_s^1,t_p^1,t_s^1,l_p^0,l_s^0,t_p^0,t_s^0)+M \xrightarrow{k_{1,T,0,p}\cdot t_p^0} P(l_p^1,l_s^1,t_p^1,t_s^1,l_p^0,l_s^0,t_p^0,t_s^0+1)\\
\text{Prop1\_}T_s^0\text{:}\quad & P(l_p^1,l_s^1,t_p^1,t_s^1,l_p^0,l_s^0,t_p^0,t_s^0)+M \xrightarrow{k_{1,T,0,s}\cdot t_s^0} P(l_p^1,l_s^1,t_p^1,t_s^1,l_p^0,l_s^0,t_p^0+1,t_s^0)\\
\text{Prop2\_}L_p^0\text{:}\quad & P(l_p^1,l_s^1,t_p^1,t_s^1,l_p^0,l_s^0,t_p^0,t_s^0)+M \xrightarrow{k_{2,L,0,p}\cdot l_p^0} P(l_p^1,l_s^1,t_p^1,t_s^1,l_p^0-1,l_s^0,t_p^0+2,t_s^0)\\
\text{Prop2\_}L_s^0\text{:}\quad & P(l_p^1,l_s^1,t_p^1,t_s^1,l_p^0,l_s^0,t_p^0,t_s^0)+M \xrightarrow{k_{2,L,0,s}\cdot l_s^0} P(l_p^1,l_s^1,t_p^1,t_s^1,l_p^0,l_s^0-1,t_p^0+2,t_s^0)\\
\text{Prop2\_}T_p^0\text{:}\quad & P(l_p^1,l_s^1,t_p^1,t_s^1,l_p^0,l_s^0,t_p^0,t_s^0)+M \xrightarrow{k_{2,T,0,p}\cdot t_p^0} P(l_p^1,l_s^1,t_p^1,t_s^1,l_p^0,l_s^0,t_p^0+1,t_s^0)\\
\text{Prop2\_}T_s^0\text{:}\quad & P(l_p^1,l_s^1,t_p^1,t_s^1,l_p^0,l_s^0,t_p^0,t_s^0)+M \xrightarrow{k_{2,T,0,s}\cdot t_s^0} P(l_p^1,l_s^1,t_p^1,t_s^1,l_p^0,l_s^0,t_p^0+2,t_s^0-1)
\end{aligned}
$$

Scheme 6.1. Most exact representation of the propagation reactions.

Scheme 6.1 illustrates all possible propagation reactions for a normally initiated polymer. Every of the eight types of hydroxyl groups can undergo two types of ring-opening reactions (denoted by Prop1 and Prop2), i.e., depending on which carbon-oxygen bond is broken, either two primary or one primary and one secondary hydroxyl groups are added to the reacting polymer. This scheme in itself is not useful because the explicit modeling of the active centers requires one to model ion transfer reactions between hydroxyl groups. In this very detailed approach, even the intramolecular exchange reactions have to be modeled and the distribution of the counter ions over all hydroxyl groups has to be simulated which induces another extremely complex dynamic. Upon regarding intermolecular ion transfer reactions as well as reactions between pairs of monomers, a second polymer type has to

be introduced which accounts for the self-initiated polymers. Due to the presence of an unopened epoxide derivative of these secondary polymers further reactions have to be considered. Polymers still containing an epoxide can undergo combination reactions with other polymers or form a macromolecular cycle, depending on whether the ring-opening reaction occurs inter- or intramolecularly, respectively. Combination reactions can be formulated in a similar manner as the propagation scheme above with slight modifications. First-order cyclization reactions can be formulated to transform secondary polymers into a new, tertiary polymers, which are very similar to the primary ones. After all, propagation and combination reactions have to be modeled for every pair of molecules where at least one of them is either a monomer or a self-initiated polymer. Ion transfer reactions have to be considered for every pair of polymers and monomers and, additionally, secondary polymers can undergo cyclization reaction.

With this one should have a very potent model that should be able to describe the vast majority of elemental ring-opening and ion transfer reaction, but it still includes the most basic assumptions, such as independence from the location in space and reduced mobility due to the molecules' size.

The introduction of this "best model," as it will be referred to from now on, shows how complicated the problem can actually be. Solving a system like that is close to impossible, but there are ways to simplify it in order to perform simulations while still being able to reproduce the experiments accurately enough.

6.1 Simplification Strategy

Before going into the details of the simplification assumptions, one has to assess the possibilities for modeling the process. The choice of the software dictates the concepts that can be applied. The most important limitation by the software is that polymer species are not permitted to have more than one property index, so the main task will be to reduce the dimensions of all polymer species from eight to one.

The first idea that comes to mind is not to model the differences between the four types of hydroxyl groups as separate indexes. This approach is as harsh as it is effective, since the number of dimensions is instantly reduced to two, i.e., the total number of hydroxyl groups and the total number of counter ions attached to the polymer. However, the information about the structural composition of the polymers will not be disregarded completely. The first model used the more generic concept that was described in section 4.10. In cases

that allow the incorporation of the polymers' structure, the average polymer composition was calculated as described in the sections 4.8 and 4.8. In general, it is obvious that polymers with more counter ions are more reactive. Additionally, one can safely assume that the reactivity of a molecule rises with an increasing number of hydroxyl groups. The cyclization rate may pose an exception to this rule since it is a first-order reaction and the probability for an epoxide to get into contact with a hydroxyl group could be lowered by the overall size of the molecule. The increase might not be linear though because bigger polymers will accumulate secondary hydroxyl groups and linear subunits. In both cases the increase in reactivity will be less than proportional to the total number of hydroxyl groups of a reacting polymer. Therefore, a non-linearly dependency of the reactivity to the total number of hydroxyl groups is proposed. That is, the reactivity is proportional to s^α, where s is the number of hydroxyl groups and $\alpha \leq 1$ an additional parameter.

Since a two-dimensional system is still too complicated to be modeled in the software framework, the maximal number of active sites per polymer and the expected number of active sites per polymer were analyzed in detail. Since the experimental set-up dictates that 10% of all hydroxyl groups had to be deprotonated and every initiator contains three of them, the average number of active sites per initiator is below one and a significant number of polymer cannot have any active site. Assuming that the ion-proton exchange reactions were allowed to reach an equilibrium state in the pre-processing phase, one can calculate the theroetical number of initiators with zero, one, two, or three deprotonated hydroxyl groups through a binomial distribution $\mathcal{B}(3, 0.1)$. Table 6.1 gives the theoretical distribution of initiators with different degrees of activation.

Table 6.1. Theoretical number of active sites per initiator.

Active Sites per Initiator (m)	**0**	**1**	**2**	**3**
Fraction of Initiators I^m	0.729	0.243	0.027	0.001

It becomes evident that initially the fraction of twice and trice deprotonated molecules is very low (2.8%) and the average number of active sites per initiator is $3 \cdot 0.1 = 0.3$. The calculation becomes more complex after adding the monomers. The ideal polymerization is defined by the following conditions:

- counter ions are exchanged rapidly between initiators and/or polymers
- counter ions are never transfered to monomers
- monomers only bind to initiators or polymers and never to other monomers

- all polymers grow at the exact same rate.

This will lead to an ideal product consisting of I many identical polymers of size M/I, where M and I denote the total amounts for monomers and initiators, respectively. The number of counter ions stays constant throughout the polymerization and is given as $0.1 \cdot 3 \cdot I$ (10% of all initiators' hydroxyl groups). The total number of hydroxyl groups, on the other hand, rises with every added monomer. The exact amount can be calculated as $3I + M$. Assuming again that the ion exchange reaction have reached an equilibrium state, the number of active sites per polymer is binomially distributed as well with $K\ \mathcal{B}(n, p)$, where the number of hydroxyl groups per polymer is given as $n = M/I + 3$ and the elemental probability of every hydroxyl group to be active is $p = 0.3I/(3I + M)$.

For example, Table 6.2 shows the fractions of polymers with 0 to 3 active sites after adding 97 times more monomers than initiators.

Table 6.2. Theoretical number of active sites per polymer for the final product of an ideal polymerization.

Active Sites per Polymer (m)	**0**	**1**	**2**	**3**	**>3**
Fraction of Polymers P_s^m	0.7405	0.2228	0.0332	0.0033	< 2.52e-04

Again, one can see that the total amount of polymers with more than one active site is very low (3.67%) and the average number of active sites per polymer remains the same as before (0.3).

Side effects, introduced by self-initiation of monomers and size-dependent polymer growth, result in a mixture of differently sized polymers, in which case, it is not obvious how the counter ions are distributed. However, one can make some general observations. The average number of active sites per polymer should always be lower in comparison to the ideal case because self-initiation reactions will increase the number of polymers. Bigger polymers will have a higher probability to accept counter ions through a transfer reaction. This may lead to many small polymers without active sites and some big polymers with many active sites, so that the overall number of polymers with more than one active site is increased.

Two different approaches for modeling the number of active sites per polymer will be pursued. Firstly, the ion transfer dynamic will be simulated explicitly by using the ion transfer reaction schemes introduced in the previous chapter. Polymers with different degrees of polymerization are modeled as separate polymer species and reactions that would lead to polymers with more active sites than a predefined cut-off value are disregarded.

In the second approach, the reaction rates are calculated proportionally to the expected number of active sites per polymer. The underlying assumption is that the ion transfer reactions occur so fast that a quasi equilibrium is reached at all time, even if the polymer size distribution is altered by the propagation and combination reactions.

Another drastic simplification assumption is that the cyclization reaction is so fast that a combination of two monomers is followed by a cyclization before any other reaction can take place. This way, self-initiated polymers will not have to be accounted for because they will by transformed into cyclic polymers before they can undergo any other reaction. Not only does this reduce the amount of the polymer species that have to be modeled, it also simplifies the polymer growth dynamic by preventing combination reactions induced by self-initiated polymers. As a result, expoxide rings are assumed to be present exclusively on the monomers. This assumption was unavoidable for the explicit modeling of the ion transfer reactions due to the computational effort to simulate polymer combination reactions. However, in the case where the number of active sites per polymers was approximated combination reactions could be analyzed and the cyclization rate could be estimated as well.

6.2 Explicit Modeling of Ion Transfer Reactions

For the first approach, modeling the number of active sites per polymer explicitly was avoided by introducing a cut-off value, M, and ignoring all reactions that would produce a polymer with more than M active sites. This effects mostly ion transfer reactions, but also combination reactions where the sum of both the reacting molecules' active sites is bigger than M. A convenient choice of M is 1. This way polymers are considered to be either active or inactive. However, this will prevent combination and ion transfer reactions between two active polymers. Since this might alter the results drastically, an alternative cut-off value of 3 was tested as well. This will still prevent reactions between twice activated polymers and between once and trice activated ones, but because polymers of higher degrees of activation are proportionally more likely to donate a counter ion, the number of twice and trice activated polymers can be assumed to be very low. It should be mentioned though that increasing the cut-off value will increase the complexity of the system in a quadratic manner and for some combinations of parameter values, the simulations take too long and have to be aborted by the user or by the operating system if the computers resources are exhausted (out of memory). For this reason, the broad parameter variation

analysis was done with the cut-off value of 1 and this information was used to test the much more complex model in the promising region.

Scheme 6.2 illustrates the complete set of reaction equations used for this approach with a slight adjustment. For clarity, initiators are defined as B_3^m (with $m \in 0, 1, 2, 3$ denoting its degree of activation), and there is no distinction between standard polymers and cyclic polymers with the same amount of hydroxyl groups. In the actual model, initiators were defined as four separate low molecular species and the polymers were defined through the number of monomers they incorporate rather than the number of hydroxyl groups they contain. In order to fulfill the mass balance equation, standard and cyclic polymers had to be distinguished, e.g., standard polymers are $P1(s) \equiv B_{s+3}^1$ and cyclic polymers $Q1(s) \equiv B_s^1$. This also had to be considered in the size-dependent formulation of the reaction rate coefficients, e.g., the thermal propagation rate of $P1(s)$ is defined as $k_{thr} \cdot (s+3)^\theta$.

Despite all of the simplifications applied to this model, it is still extremely powerful and incorporates many elemental mechanisms of the process. This is depicted in the high number of parameters used to calculate the kinetic reaction rates. They can be summarized as follows:

- k_p is the effective kinetic rate coefficient of any deprotonated hydroxyl group to participate in a ring-opening reaction with the epoxide of a monomer.

- α defines the relationship between the anionic ring-opening reaction rates to the reacting polymer's size. This parameter combines the effects of reduced mobility, increased steric hindrance, and higher ratios of secondary to primary hydroxyl groups.

- k_{thr} is the effective kinetic rate coefficient of any normal hydroxyl group to participate in a ring-opening reaction with the epoxide of a monomer. This parameter is assumed to be significantly smaller than k_{p1}.

- θ defines the relationship between the thermal ring-opening reaction rates to the reacting polymer's size. In contrast to α, θ realizes that bigger polymers are more likely to undergo thermal ring-opening reactions due to the presence of more hydroxyl groups. This is an additional effect to the ones mentioned for α, with the result that one can expect θ to be larger than α and $\theta = 1 + \alpha$ is a reasonable hypothesis.

- k_t is the effective kinetic rate coefficient of any deprotonated hydroxyl group to exchange the attached counter ion with the proton of a hydroxyl group which is

$$
\begin{aligned}
\text{Prop\_anionic(1,s):} \quad & B_s^1 + AB \xrightarrow{k_p \cdot s^\alpha} B_{s+1}^1 \\
\text{Prop\_anionic(2,s):} \quad & B_s^2 + AB \xrightarrow{k_p \cdot 2 \cdot s^\alpha} B_{s+1}^2 \\
\text{Prop\_anionic(3,s):} \quad & B_s^3 + AB \xrightarrow{k_p \cdot 3 \cdot s^\alpha} B_{s+1}^3 \\
\text{Prop\_thermal(0,s):} \quad & B_s^0 + AB \xrightarrow{k_{thr} \cdot s^\theta} B_{s+1}^0 \\
\text{Prop\_thermal(1,s):} \quad & B_s^1 + AB \xrightarrow{k_{thr} \cdot s^\theta} B_{s+1}^1 \\
\text{Prop\_thermal(2,s):} \quad & B_s^2 + AB \xrightarrow{k_{thr} \cdot s^\theta} B_{s+1}^2 \\
\text{Prop\_thermal(3,s):} \quad & B_s^3 + AB \xrightarrow{k_{thr} \cdot s^\theta} B_{s+1}^3 \\
\text{Self-Initiation:} \quad & AB + AB \xrightarrow{k_{p2} \cdot 2} B_2^0 \\
\text{TTP(1,s,0,r):} \quad & B_s^1 + B_r^0 \xrightarrow{k_t \cdot s^\gamma \cdot r^\beta} B_s^0 + B_r^1 \\
\text{TTP(1,s,1,r):} \quad & B_s^1 + B_r^1 \xrightarrow{k_t \cdot s^\gamma \cdot r^\beta} B_s^0 + B_r^2 \\
\text{TTP(1,s,2,r):} \quad & B_s^1 + B_r^2 \xrightarrow{k_t \cdot s^\gamma \cdot r^\beta} B_s^0 + B_r^3 \\
\text{TTP(2,s,0,r):} \quad & B_s^2 + B_r^0 \xrightarrow{k_t \cdot 2 \cdot s^\gamma \cdot r^\beta} B_s^1 + B_r^1 \\
\text{TTP(2,s,1,r):} \quad & B_s^2 + B_r^1 \xrightarrow{k_t \cdot 2 \cdot s^\gamma \cdot r^\beta} B_s^1 + B_r^2 \\
\text{TTP(2,s,2,r):} \quad & B_s^2 + B_r^2 \xrightarrow{k_t \cdot 2 \cdot s^\gamma \cdot r^\beta} B_s^1 + B_r^3 \\
\text{TTP(3,s,0,r):} \quad & B_s^3 + B_r^0 \xrightarrow{k_t \cdot 3 \cdot s^\gamma \cdot r^\beta} B_s^2 + B_r^1 \\
\text{TTP(3,s,1,r):} \quad & B_s^3 + B_r^1 \xrightarrow{k_t \cdot 3 \cdot s^\gamma \cdot r^\beta} B_s^2 + B_r^2 \\
\text{TTP(3,s,2,r):} \quad & B_s^3 + B_r^2 \xrightarrow{k_t \cdot 3 \cdot s^\gamma \cdot r^\beta} B_s^2 + B_r^3 \\
\text{TTM(1,s):} \quad & B_s^1 + AB \xrightarrow{k_t \cdot s^\gamma} B_s^0 + B^1 \\
\text{TTM(2,s):} \quad & B_s^2 + AB \xrightarrow{k_t \cdot 2 \cdot s^\gamma} B_s^1 + B^1 \\
\text{TTM(3,s):} \quad & B_s^3 + AB \xrightarrow{k_t \cdot 3 \cdot s^\gamma} B_s^2 + B^1 \\
\text{Mfeed:} \quad & \emptyset \xrightarrow{k_{feed}} AB
\end{aligned}
$$

Scheme 6.2. A set of reaction equations representing the first model used for the parameter estimation.

located on another molecule. This parameter may potentially become much larger than k_p and k_{thr} which can lead to performance issues for high quantities of polymers with complex polymer size distributions.

- γ defines the relationship between ion donating rate and the size of the donating polymer. This parameter is similar to α since it also defines the accessibility of the counter ion in dependence of the polymer's size. Since the elemental mechanism is different though, this parameter should be treated separately if possible.

- β defines the relationship between ion accepting rate and the size of the accepting polymer. In order to reach the equilibrium state where the number of active sites is distributed via a binomial distribution, this parameter has to be 1 because only then does every hydroxyl group have the same chance to be active. However, other values are feasible as well, since there is no guarantee such an equilibrium will be reached while the polymerization is taking place. For example, the affinity to accept a counter ion might only depend on the number of hydroxyl groups at the surface of the polymer, or it could even be independent of the polymer's size all together.

Estimating 7 parameters at once in a highly non-linear system of differential equations is a daring task and it is very unlikely to converge. Therefore, parts of the model will be treated individually at first by fixing some parameters and the results should help finding good starting values for the overall parameter estimation. It is also important to restart the iteration with differently fixed values so that a good portion of the parameter space is covered. In general, it is dangerous to fix the elemental rate coefficients k_p, k_{thr}, and k_t because their ranges are completely unknown and no reasonable boundaries can be assumed. As for the exponent coefficients, on the other hand, they can be expected to in the range of -1 to 1 and one can define critical changing points in the behavior of the system. For example, the change from positive to negative has the most crucial impact because in all cases a reaction of bigger polymers is suddenly dampened instead of being enhanced by the increase in size or vice versa. For that reason, a wide range of values for these crucial parameters is used to analyze important regions of the parameter space.

6.2.1 Estimating k_p, k_t, α and β

At first, thermal reactions were ignored by setting $k_{thr} = 0$. Furthermore, the chain-length parameter for transfer reactions was coupled to the one for the propagation reactions ($\gamma = \alpha$ always holds true).

In order to restrict the parameter space for the estimation procedure, a variation analysis was performed to assess the accuracy for the parameter combinations of k_p, $k_t \in \{10^{-8}, 10^{-6}, 10^{-4}, 10^{-2}, 10^{0}, 10^{2}, 10^{4}\}$ and α, $\beta \in \{-2/3, 0, 2/3\}$. This required performing $7 \cdot 7 \cdot 3 \cdot 3 = 441$ many simulations.

For the actual parameter estimation nine sets of starting parameters were taken, one for each combination of α and β. The initial values for k_{p1} and k_t were chosen so that the residual difference between the simulation and the experiments was lowest. Figure 6.1 illustrates the choice of stating parameters. On the left side, all residuals from the variation analysis are illustrated. The x- and y-axis show the parameters α and β, respectively, while the z-axis represent the various residuals for all parameter combinations. For clarity, the size and color of the markers were chosen according the residual as well. The blue circles show the residuals of the nine parameter combinations that were used as starting values for the parameter estimation procedure. On the right side, the starting values for all parameters are illustrated at once. The x- and y-axis again show the values for α and β, but the z-axis now shows the starting values for k_p as cyan and k_{thr} as magenta colored squares.

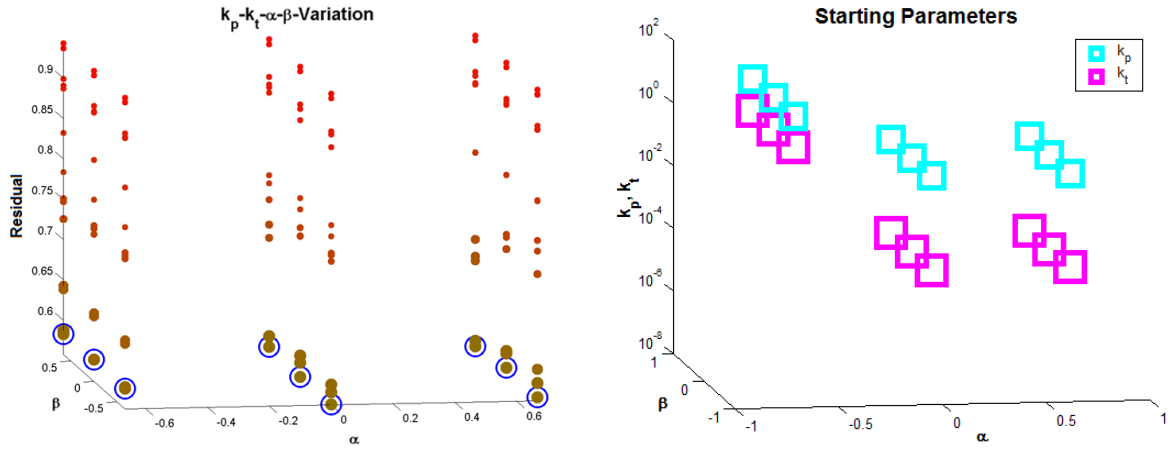

Figure 6.1. Left: visualization of the parameter variation analysis. The x- and y-axis show the crucial parameters α and β. The quality of the simulation (residual difference of $\overline{M}_n$ and $\overline{M}_w$ to the SEC measurements) is shown on the z-axis and is indicated by the color and the size of the marker for clarity. Right: illustration of the starting parameters for the following parameter estimation.

After starting the individual parameter estimation procedures, one can see a clear trend. This is illustrated in Figure 6.2. The axis are shown as described in the previous picture, but additionally to the starting residuals (left) and parameters (right), the "optimized"

parameters obtained by the parameter estimation procedure are added. Starting and final values are connected by a dotted line to illustrate the trend.

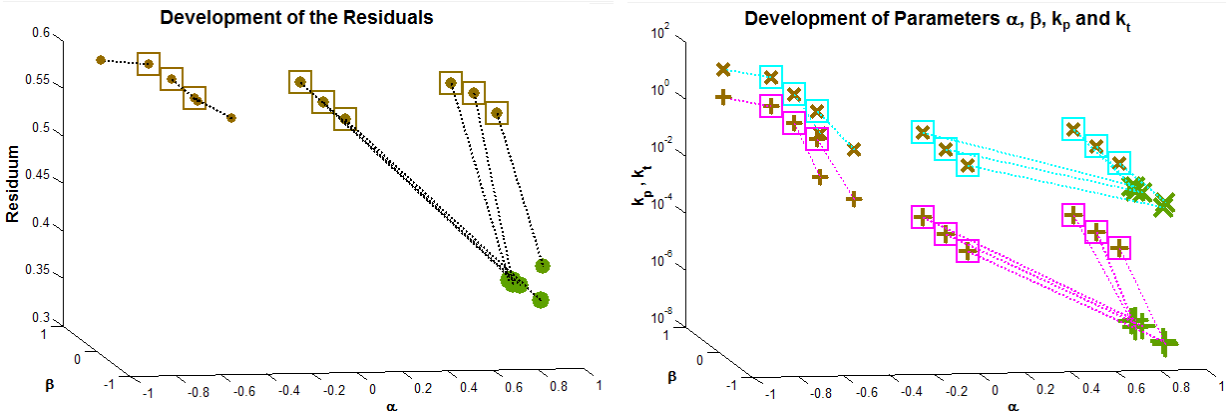

Figure 6.2. Left: residual difference of the simulation to the experimental data before and after the parameter estimation. Right: parameter values before and after the parameter estimation.

Of course the residuals became better because they were being minimized by the method and one can clearly see that the best results are clustered together with values for α of around 0.8, which means that big polymers tend to propagate faster and more frequently. However, similarly good residuals could be achieved with different values for β ($-0.7 < \beta < 0.12$), so one could conclude that this parameter had not as big of an impact on the outcome as compared to α. Table 6.3 summarizes all results of the parameter estimation.

Table 6.3. Results for the first series of parameter estimations.

ID	k_p [a]	α [b]	k_t [a]	γ [b]	β [b]	k_{thr} [a]	θ [b]	Residual [b]
1	1.85E+00	-0.611	1.82E-02	-0.611	-1.395	0	0	0.580
2	2.26E+00	-0.675	2.79E-02	-0.675	-0.813	0	0	0.583
3	1.10E+01	-0.830	1.02E-01	-0.830	1.000	0	0	0.579
4	2.80E-03	0.856	2.01E-05	0.856	-0.701	0	0	0.364
5	2.80E-03	0.856	2.00E-05	0.856	-0.092	0	0	0.364
6	2.80E-03	0.858	2.00E-05	0.858	0.125	0	0	0.364
7	1.86E-03	0.927	1.00E-05	0.927	-0.304	0	0	0.390
8	2.83E-03	0.832	1.71E-05	0.832	-0.053	0	0	0.365
9	2.87E-03	0.840	1.84E-05	0.840	0.121	0	0	0.364

[a] values in [L mol^{-1} min^{-1}]
[b] values in arbitrary units.

6.2.2 Estimating k_p, k_t α, β and γ

The restrictions to the reaction rate equations were loosened by introducing the γ parameter which was no longer coupled to the α parameter. The analysis was continued in same manner as before by firstly performing a parameter variation analysis with a broad range of values. This time, three times more simulations were required due to the new parameter ($\gamma \in \{-2/3, 0, 2/3\}$) that had to be accounted for.

The left side of figure 6.3 shows the residuals for all parameter combinations in the usual color code and the blue circles indicate the starting residuals with which the parameter estimation procedure was started. On the right side, the starting values for α, β, and γ are shown on the x-, y-, and z-axis, respectively.

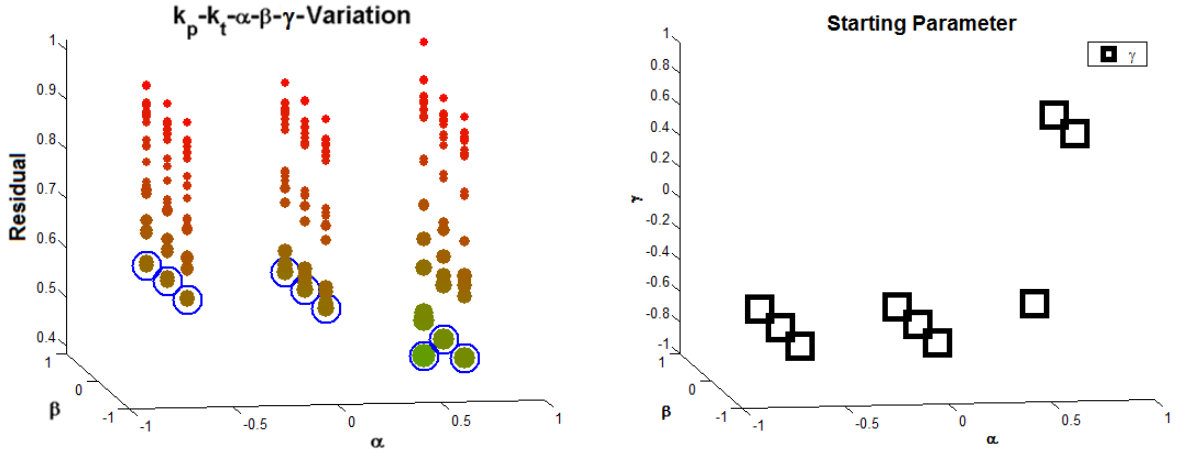

Figure 6.3. Left: visualization of the parameter variation analysis using k_p, k_t, α, β, and γ. Right: illustration of the starting parameters α, β, and γ for the following parameter estimation.

Figure 6.4 shows the starting and final values for the residual (left) and the three chain-length parameters (right).

One can see that this analysis also produces fairly acceptable residuals of around 0.36. The actual values are listed in Table 6.4. Upon inspecting the values closely, one can see that two of the three promising parameter sets (see IDs 7 and 8 in the Table) are very similar to the results from the previous parameter estimation approach. In these cases α and γ do not differ a lot. Since adding another degree of freedom, it is plausible that the old results could be reproduced. More interesting is the last result in the Table with ID 9. This result is clearly different from the ones obtained in the previous approach. A comparison of these results and a discussion of their meaning and how reasonable they are can be found at the end of this section.

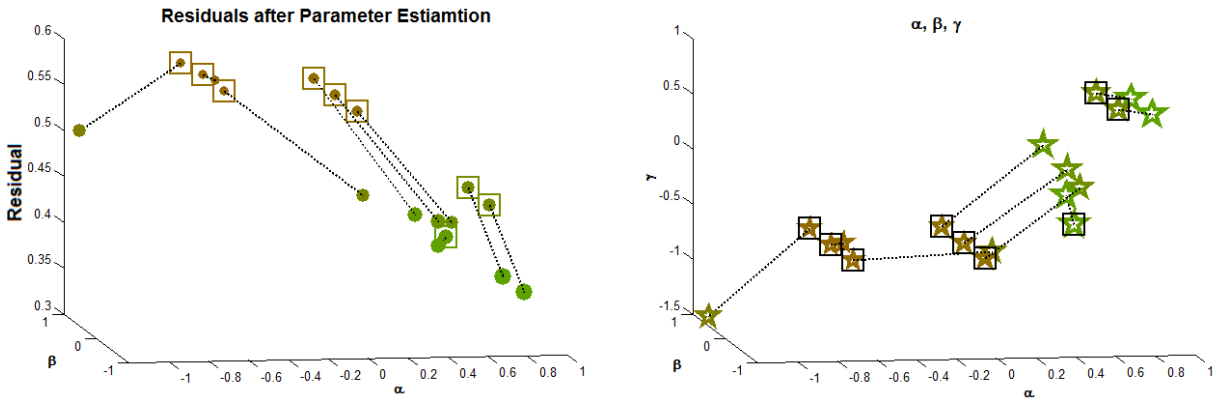

Figure 6.4. Left: illustration of the residuals before and after the parameter estimation. Right: parameter values before and after the parameter estimation

Table 6.4. Results of the second series of parameter estimations.

ID	k_p [a]	α [b]	k_t [a]	γ [b]	β [b]	k_{thr} [a]	θ [b]	Residual [b]
1	9.75E-02	-0.017	5.65E-03	-0.542	-0.960	0	0	0.477
2	8.25E-01	-0.613	9.10E-03	-0.640	-0.065	0	0	0.581
3	4.10E+01	-1.122	1.52E+00	-1.520	1.000	0	0	0.499
4	5.67E-03	0.475	2.20E-04	-0.036	-0.662	0	0	0.438
5	5.38E-03	0.519	2.38E-04	-0.018	0.000	0	0	0.420
6	4.65E-03	0.564	1.72E-04	-0.014	1.000	0	0	0.402
7	3.25E-03	0.840	6.86E-05	0.619	-0.669	0	0	0.361
8	3.26E-03	0.840	6.96E-05	0.614	-0.015	0	0	0.360
9	1.08E+00	0.681	9.32E-01	-0.481	1.000	0	0	0.368

[a] values in [L mol^{-1} min^{-1}]
[b] values in arbitrary units.

6.2.3 *Estimating k_p, k_t, α, β and k_{thr}*

For the last part of this series of parameter estimations, thermal propagation reaction were considered in addition to the ones that were analyzed before. At this point the problem becomes to complicated to be treated with all parameters. Therefore, the most reasonable assumptions were employed, i.e. $\gamma = \alpha$, $k_{thr} < k_p$ and $\theta = 1$. For the initial variation analysis $7^3 \cdot 3^2 = 3087$ many simulations had to be performed which was enough to keep four computers running for multiple days.

Figure 6.5 shows all residuals from the parameter variation as colored dot markers and the best residual for every combinations of α and β is marked by a blue circle.

The first thing that can be seen in this picture is that the values for k_{thr} are very low. This means that the thermal reaction rates have only very little influence on the outcome of

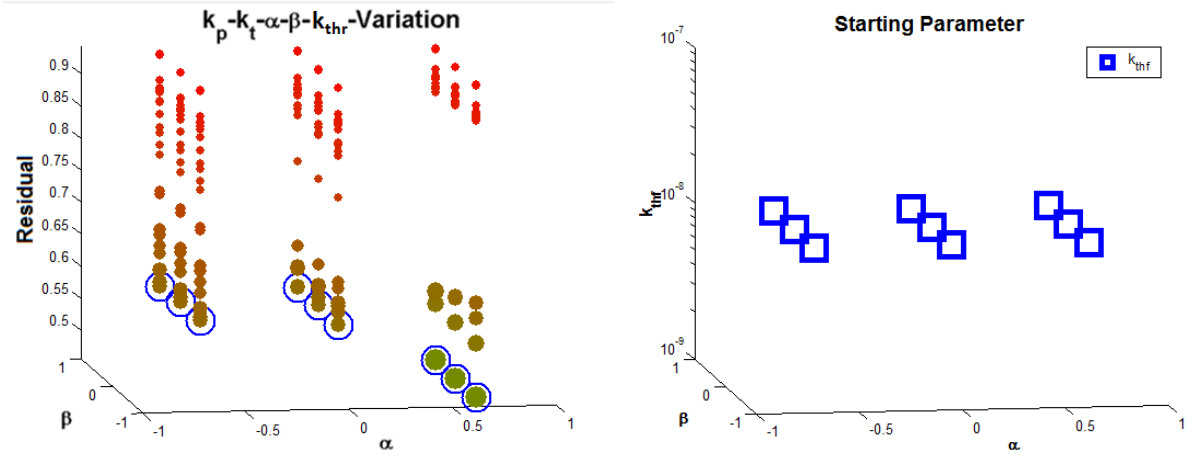

Figure 6.5. Left: visualization of the parameter variation analysis using k_p, k_t, α, β and k_{thr}. Right: illustration of the starting parameters α, β and k_{thr} for the following parameter estimation.

the simulation. Before starting the actual parameter estimation procedure, it is plausible to suspect the results not to show better agreement with the experimental data than the very first approach without thermal reactions. This suspicion is confirmed by looking at the result of the individual parameter estimations which is illustrated in Figure 6.6 and Table 6.5. First of all, one can see that the thermal reaction rate coefficient stays at very low values throughout all of the optimizations and does not differ from the original values. Secondly, after comparison of the results to the first approach in this section, one can see that the best parameters are essentially the the same. This leads to the conclusion that regarding the thermal reactions does not improve the accuracy of the model. However, due to the harsh simplification assumptions that were necessary to perform the parameter estimation procedure, one cannot rule out that thermal ring-opening reactions might have an impact after all. In the end, thermal and anionic reactions are nearly identical in their reaction schemes, i.e., they have the same species as reactants and products. The only exception is that thermal reactions can involve polymers without any active sites.

6.3 Discussion and Interpretation of the Preliminary Results

Table 6.6 summarizes all results that showed a somewhat satisfying residual difference to the experimental data. Most of the results are very similar and there is only one significantly different one. This parameter set is marked with the ID 2.9 in Table 6.5. At this point these two results from the parameter estimation procedure will be analyzed in

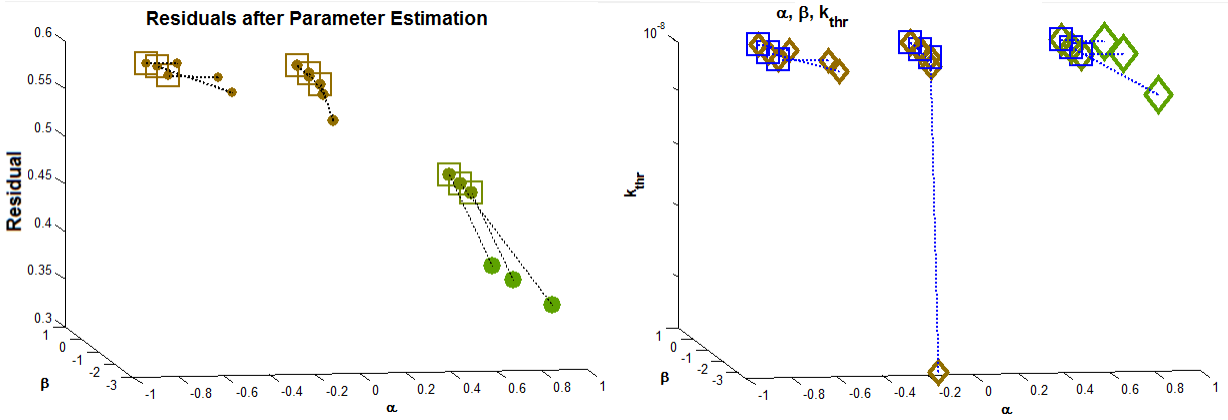

Figure 6.6. Left: residuals before and after the parameter estimation. Right: parameter values before and after the parameter estimation.

Table 6.5. Results from the third series of parameter estimations.

ID	k_p [a]	α [b]	k_t [a]	γ [b]	β [b]	k_{thr} [a]	θ [b]	Residual [b]
1	3.47E-01	-0.450	3.88E-03	-0.450	-0.696	9.97E-09	1	0.582
2	4.78E-01	-0.475	5.55E-03	-0.475	-1.837	1.00E-08	1	0.581
3	6.99E-01	-0.554	7.68E-03	-0.554	0.326	9.94E-09	1	0.583
4	4.61E-01	-0.139	4.76E-03	-0.139	-3.310	5.37E-09	1	0.569
5	2.46E-01	-0.038	3.67E-03	-0.038	-1.326	9.96E-09	1	0.570
6	3.32E-01	0.003	3.25E-03	0.003	0.007	9.99E-09	1	0.571
7	2.86E-03	0.851	1.98E-05	0.851	-0.670	1.00E-08	1	0.364
8	2.90E-03	0.860	2.32E-05	0.860	-2.831	9.65E-09	1	0.366
9	2.87E-03	0.843	1.82E-05	0.843	0.466	1.00E-08	1	0.364

[a] values in [L mol^{-1} min^{-1}]
[b] values in arbitrary units.

detail. The recurrent result will from now on be referred to as Fit 1 and the unique one (ID 2.9) as Fit 2. The residual difference between the experiments and the simulations was very similar for both cases. The achieved value of around 0.36 does not stand for a very high accuracy, but the general trend has to be captured in order to produce such a value.

To illustrate the quality of the model with the two sets of parameters, Figures 6.7 and 6.8 show the time profiles for the number- and weight-average molecular weights in the left column and the concentrations for monomers and initiators in the right one. Each row presents the results for the different experimental set-ups with targeted molecular weight of 20 kDa, 10 kDa, 5 kDa and 2.5 kDa, from top to bottom. The y-axis is plotted on a logarithmic scale in order to compare the different graphs more easily. The lines stand for the simulated and the markers for the experimental data; measurements were

Table 6.6. Summary of the best results of all parameter estimations. The parameter set with the ID 2.9 can be clearly distinguished from the rest of the sets which are very similar in all values except for β.

ID	k_p [a]	α [b]	k_t [a]	γ [b]	β [b]	k_{thr} [a]	θ [b]	Residual [b]
1.4	2.80E-03	0.860	2.01E-05	0.860	-0.700	0	0	0.3645
1.5	2.80E-03	0.860	2.00E-05	0.860	-0.090	0	0	0.3643
1.6	2.80E-03	0.860	2.00E-05	0.860	0.120	0	0	0.3642
1.7	1.86E-03	0.930	1.00E-05	0.930	-0.300	0	0	0.3895
1.8	2.83E-03	0.830	1.71E-05	0.830	-0.050	0	0	0.3646
1.9	2.87E-03	0.840	1.84E-05	0.840	0.120	0	0	0.3642
2.7	3.25E-03	0.840	6.86E-05	0.620	-0.670	0	0	0.3607
2.8	3.26E-03	0.840	6.96E-05	0.610	-0.010	0	0	0.3604
2.9	1.08E+00	0.680	9.32E-01	-0.480	1.000	0	0	0.368
3.7	2.86E-03	0.850	1.98E-05	0.850	-0.670	1.00E-08	1	0.3643
3.8	2.90E-03	0.860	2.32E-05	0.860	-2.830	9.65E-09	1	0.3656
3.9	2.87E-03	0.840	1.82E-05	0.840	0.470	1.00E-08	1	0.364

[a] values in [L mol^{-1} min^{-1}]
[b] values in arbitrary units.

only available for the average molecular weights. Comparing the number- and weight average molecular weights from fit 1 to fit 2, one can firstly see that the experimental data were similarly well reproduced, hence resulting in a similar value for the overall residual. However, there is a clear difference in the shape of the curves, especially in the early stage of the polymerization. Fit 1 with its characteristically low propagation rate and negative β exponent seems more inaccurate for the first two samples taken at early reaction times. The divergence is compensated by fitting the samples from later stages of the polymerization more accurately than fit 2. The most severe difference between the results of the two parameter sets is best illustrated in the time profiles of the monomer concentrations. Comparing the right columns of Figures 6.7 and 6.8, one can see that in the early stage of fit 1 barely any monomers react. Instead they accumulate until the concentration becomes high enough to initiate the first polymer initiation and growth steps. As the polymers become bigger, their reactivity increases (realized with a comparatively high α value of 0.84) and increased polymer growth starts to use up the accumulated monomers. At the end of the polymerization a significant concentration of free monomers are left in the system (1-4 mol per liter) and the peak of the monomer concentrations is very high with 4.5 to 8 mol/L. This effect cannot be observed for fit 2. There, the monomers also accumulate in the beginning, but polymer growth is initiated much quicker

(within the first couple of minutes), so that the monomer concentration barely reaches a maximum of 0.6 in the case where only a few initiators were added (first row).

At this point fit 1 looks very unlikely. Due to the very high reactivity of epoxides and the elevated reaction temperature, a monomer concentration as high as observed in fit 1 is very unexpected and most likely unrealistic. A couple of studies have already shown the potential of glycidol to polymerize at room temperature,[79,81,117–120] even though the experiments were set up differently in most cases and the achieved degree of polymerization was usually not very high.

One might be tempted to praise the results from fit 2 since they look reasonable and seem to reproduce the experimental results with acceptable accuracy, but this set of parameters also raises some rather baffling questions. The first aspect that does not seem to make perfect sense is the fact that the polymer size dependency parameter α seems to be positive in all cases that lead to good agreement. One would expect bigger polymers to be less mobile and have a higher fraction of secondary hydroxyl groups and that some functional groups may exhibit reduced accessibility due to steric hindrance. In fact, there is only one reason coming to mind that would explain why big polymers would show a higher tendency to undergo anionic ring-opening reactions. This is because molecules with many hydroxyl groups are more likely to contain one or more active sites and anionic reaction rates are directly dependent on the active sites of a molecule. However, in a model where the number of active sites per polymer is represented explicitly, the tendency of big polymers to have more active sites on average is supposed to be strictly decoupled from the polymer size dependency of the propagation rate, i.e., the propagation rate is multiplied by the number of active sites and not by the number of monomeric subunits. The fact that fit 2 suggests reaction rates for the ion transfers so that big polymers are (a) less likely to donate, i.e., $\gamma < 0$ and(b) more likely to accept, i.e., $\beta \approx 1$, counter ions from other molecules which they collide with, shows that it worthwhile to model this dynamic via the transfer reactions.

Based on the proceeding analysis, the effect of modeling polymers with more than one active site was tested. As discussed before, the performance of the simulation software decreases drastically when introducing these extra polymer species and a complete analysis of the parameter space is therefore, unfortunately, not possible. However, the extended model could be tested with the sets of parameters from fit 1 and 2 to see if the results are changed by this additional modeling aspect. Figures 6.9 and 6.10 show the comparison of the previous time profiles of the average molecular weights to the ones obtained with

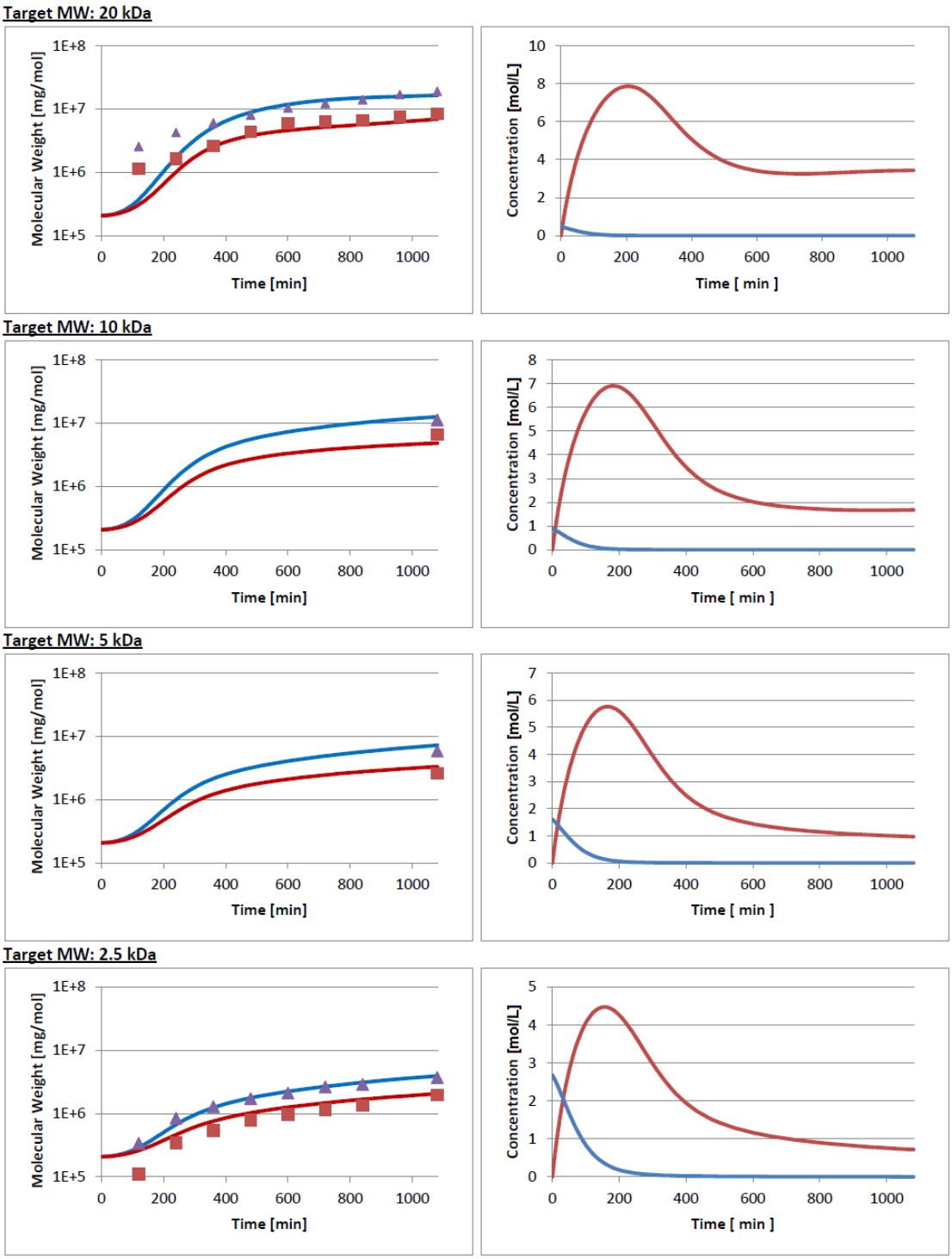

Figure 6.7. Comparison of measurements to simulations using the parameters from fit 1. In the left column, red represents the time profile for $\overline{M}_n$ and blue the one for $\overline{M}_w$. The markers show the experimental and the lines the simulated results. In the right column, red represents the time dependent monomer concentration and the initiator concentration is displayed in blue.

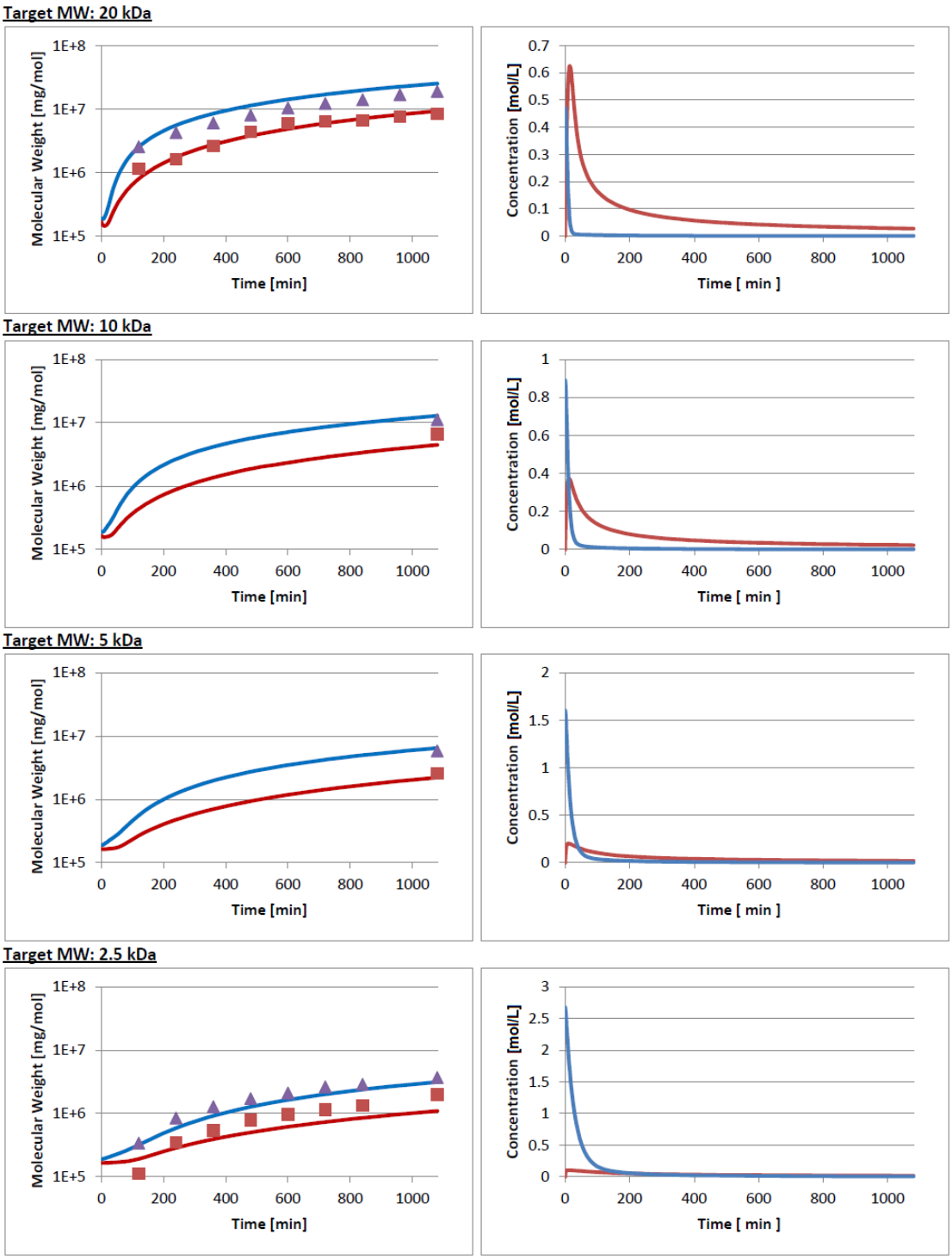

Figure 6.8. Comparison of measurements to simulations using the parameters from fit 2. In the left column, red represents the time profile for $\overline{M}_n$ and blue the one for $\overline{M}_w$. The markers show the experimental and the lines the simulated results. In the right column, red represents the time dependent monomer concentration and the initiator concentration is displayed in blue.

the extended model that incorporates double and triple activated polymer species. For less redundancy, only the results for the experiments with targeted molecular weights of 20 kDa (first row) and 2.5 kDa (second row) are presented. The left column always shows the experimental and simulated results for the model with inactive and single activated polymers, whereas the right column shows the new results from the extended model regarding additional polymer species with two and three active sites per polymer. Inspecting Figure 6.9, one can barely make out a difference between the left and the right curves. This makes sense because in this parameter set the ion transfer rate is very low and β is nearly zero, so the effect of the ion transfer reactions is minimal. On the other hand, Figure 6.10 shows a distinct difference between the simple and the extended model, especially when targeting high molecular weights. This could also be expected because of the high ion transfer rate, γ being negative and $\beta = 1$ indicating a linear dependency of the ion transfer rate on the accepting polymer's size. These results were used to attempt estimating the parameters in the extended model, but without success. From this starting point, the parameter estimation procedure failed to improve the residual and also guessing lower ion transfer rate coefficients while limiting α and γ to negative and β to positive values did not result in a new set of parameters that could predict the experimental outcome better than before.

The situation is unsatisfying because the parameter estimation seems to work although the results are highly doubtful. Changing the definition of the average molecular weight to include the monomer's weight did not solve the problem either. The results from fit 2 that could be reproduced by no parameter set with negative values for α were found to represent the experimental data accurately.

There is one more possible explanation for the positive values of α. Due to the similarity of thermal and anionic propagation schemes and the obvious assumption that polymers with many hydroxyl groups are more likely to undergo thermal ring-opening reactions, i.e., $\theta \approx 1$, thermal reaction might help to explain the estimated parameters. This is not a trivial task because, even though the reaction schemes are very similar, thermal reactions can involve inactive polymers, whereas anionic ones cannot. This is especially important if the number of free monomers, which are also considered to be inactive molecules, is large in comparison to the number of polymers. Thermally combined monomers induce a dynamic much different from that of transfer to monomer reactions because they can happen directly and do not involve a complicated transition where an active molecule is donating its counter ion to a free monomer which then again combines with another

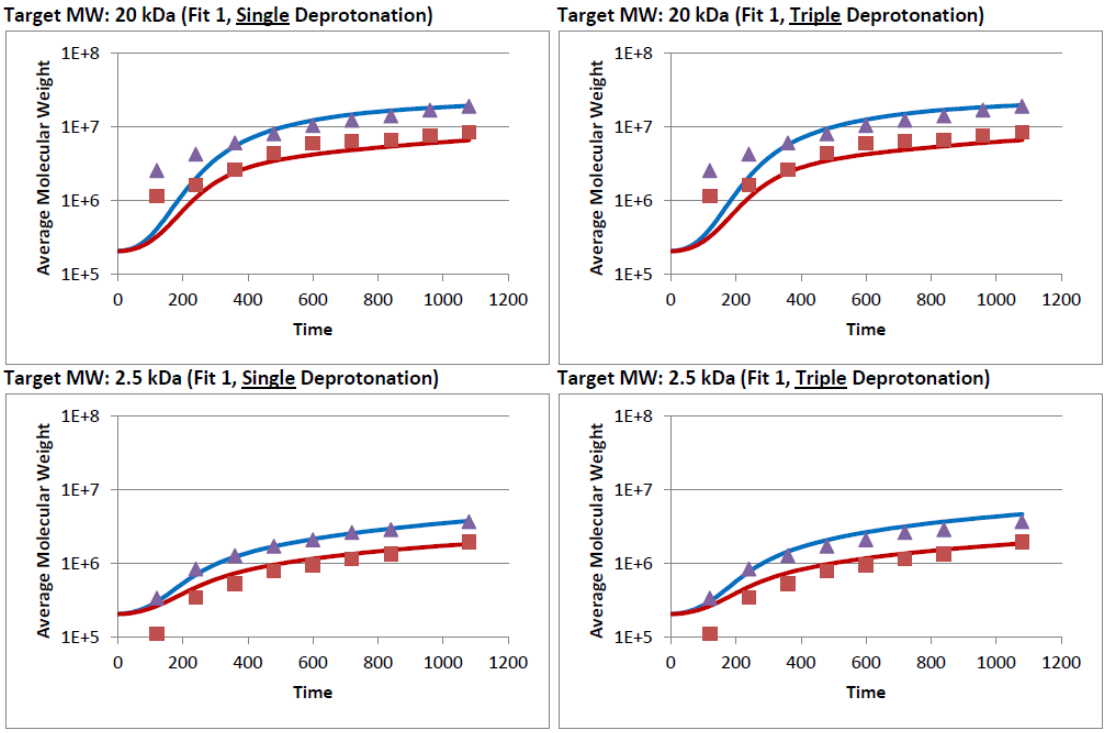

Figure 6.9. Analyzing the effect of multiple activation based on the parameters from fit 1.

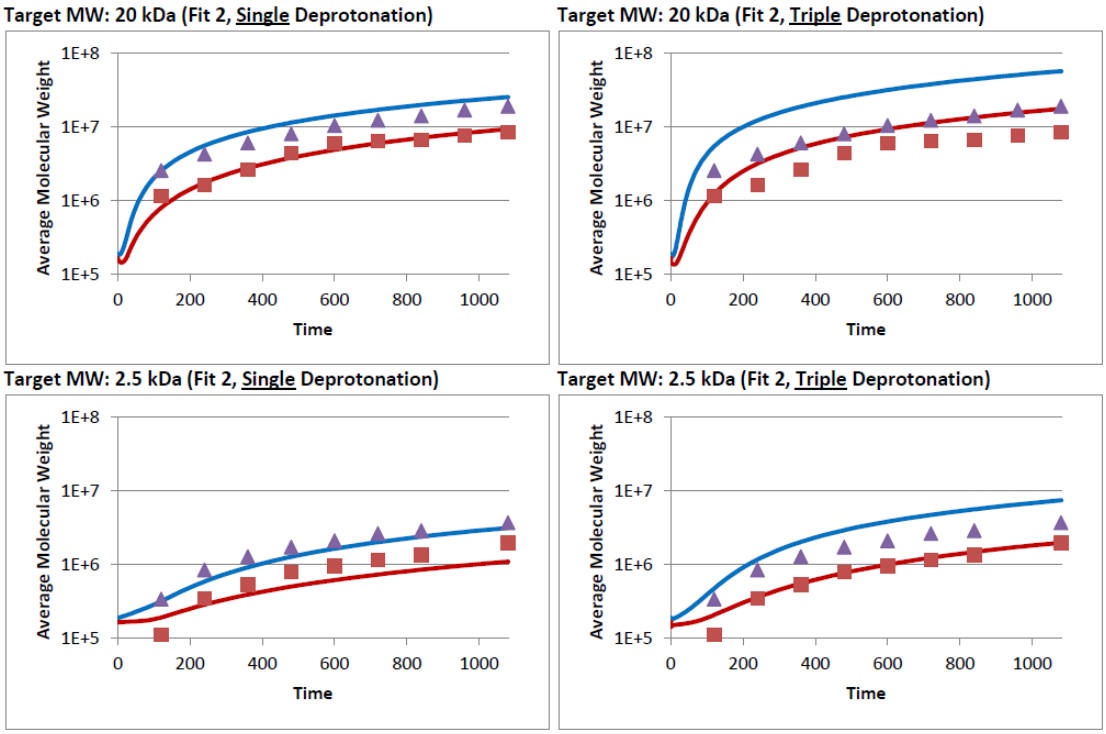

Figure 6.10. Analyzing the effect of multiple activation based on the parameters from fit 2.

monomer rather than binding to an existing polymer in a standard propagation reaction.

An attempt was made to adjust the more promising parameter set from fit 2 to account for thermal ring-opening reaction rates. In order to keep the computation time reasonably low and to ensure the stability of the parameter estimation, fixed values were used ($\alpha = \gamma = 0$, $\beta = 1$) and the thermal ring-opening reaction rates were limited by the anionic reaction rates ($k_{thr} \leq k_p$). To quickly cover a broad spectrum of parameters the simulated annealing procedure was used rather than the tedious iteration of boxsearch and parameter estimation and covering as many parts of the parameter space. The decision for this method stems from the fact that the crucial parameters α and β were fixed. Doing so resulted in a parameter set that looks somewhat similar to that from Fit 1. The final residual was worse with 0.432 and the optimal parameters were $k_{thr} = k_p = 5.77E-02$, $k_t = 9.97E-03$ and $\theta = 0.795$. Figure 6.11 shows the time profiles for the number- and weight-average molecular weights in the left column and the monomer concentration on the right. The rows account for the simulated and experimental results for the experiment with different targeted molecular weight of 20 kDa, 10 kDa, 5 kDa and 2.5 kDa (from top to bottom). The model with these specific parameters appears to reproduce the average molecular weight quite well while keeping the monomer concentration low. Upon close inspection of the result at 2.5 kDa, one can see distinct deviations which cause the total residual to be lower than in the previous parameter estimations.

Also the last attempt to explain the experimental data with the current model is not very likely because the estimated coefficients for the thermal and the anionic ring-opening reactions were the same. Considering that the thermal coefficient is multiplied by the polymers' size and the anionic one is not, the thermal reaction would be much faster for big polymers. This is an unreasonable result, but it gave us a hint on how to proceed in this study. It showed that thermal reaction may very well have big influence on the whole system.

Based on all the results presented so far, it was decided to analyze the thermal ring-opening reaction rates in more detail. For this, the experiments without initiators were analyzed in detail.

6.4 Estimating Thermal Ring-opening Reaction Rates

After evaluating a broad variety of models by optimizing the kinetic parameters, very interesting but also somewhat unsatisfying results were obtained. Because of this, the

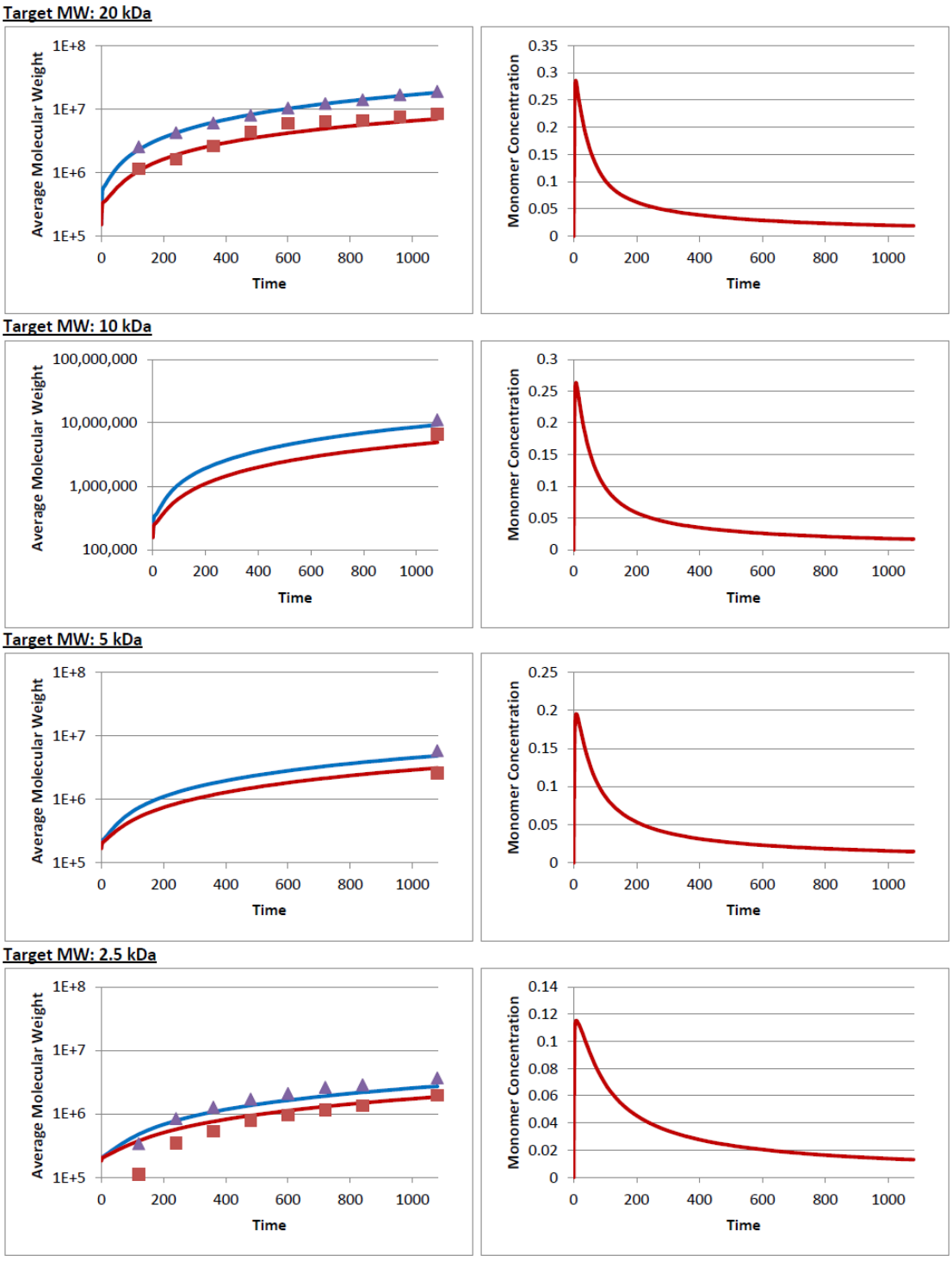

Figure 6.11. Time profiles for $\overline{M}_n$ (red line in left column), $\overline{M}_w$ (blue line in left column) and the monomer concentration (red line in right column). The simulations are compared to the experimental data indicated by the markers.

analyzing strategy was drastically changed and the problem was reduced in order to analyze the dynamics in parts. This was done in a way that the results could be used to analyze the anionic polymerization process. Therefore, the following results were engineered to be incorporated into the bigger model, which could then be analyzed with a reduced number of parameters. The thermal ring-opening reactions were isolated by not adding any initiators and no counter ions. This ensured that any observed reaction could only occur thermally and were not mediated by a catalyst. For the early stages of the polymerization, this meant that monomers could only react with each other to form self-initiated polymers which in turn could propagate or combine via the thermal ring-opening mechanism. Such systems have been known for a long time and many studies were carried out already.[3,105,106,115] However, nobody has analyzed a process that is identical to the one at hand. Flory, for instance, has disregarded intramolecular reactions completely due to technical difficulties, whereas others were analyzing only reversible combination and cyclization reactions. The importance of cyclization reactions was illustrated nicely by Dusek et al.,[113] but for the system studied here, reversibility of the cyclization reaction can be ruled out because an uncatalyzed formation of an epoxide is highly unlikely. However, the system being regarded here can be reduced to fit previously derived models if assumptions are made accordingly.

The results described in this section were partially published in 2012.[121]

Modeling the thermal ring-opening reactions raises the following questions.

- How does the reaction rate depend on the number and the type of hydroxyl groups on the reacting molecule?
- How can one calculate the cyclization rate per polymer?
- How are the reactions effected by the reactor's temperature?

As discussed earlier the values for $\overline{M}_n$ and $\overline{M}_w$ measured with SEC were used to test different modeling concepts and to estimate kinetic parameters.

As a starting point, a simplistic model without polymer size dependencies was tested. Furthermore, it was assumed that a dimer is undergoing cycle formation instantaneously, so that the following system can be modeled as illustrated in Scheme 6.3.

$$\begin{aligned} \text{Init:} \quad AB + AB &\xrightarrow{k_p \cdot 2} B_2 \\ \text{Prop(x):} \quad B_x + AB &\xrightarrow{k_p} B_{x+1} \\ \text{Mfeed:} \quad \emptyset &\xrightarrow{k_{feed}} AB \end{aligned}$$

Scheme 6.3. Recapitulation of the simplistic model.

This model was easily tested by performing a parameter variation analysis.

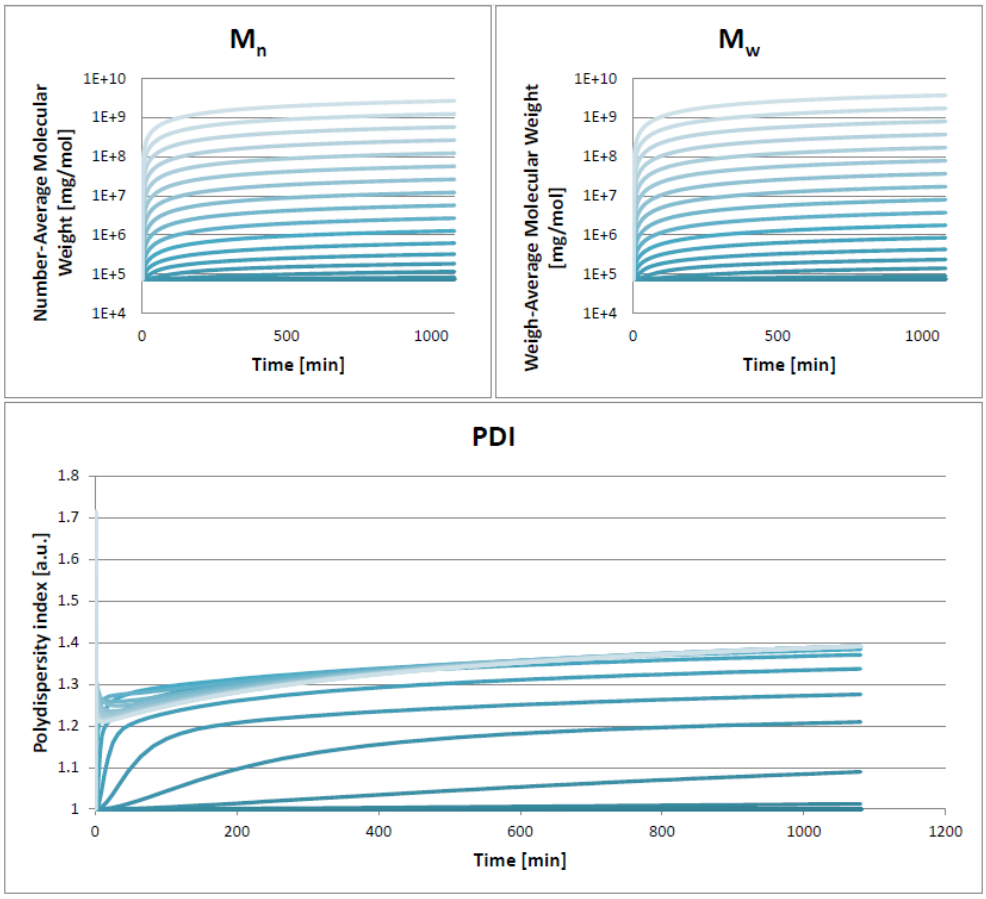

Figure 6.12. Time profiles for $\overline{M}_n$ (top, left), $\overline{M}_w$ (top, right) and PDI (bottom) using the simplistic model. Results for different parameters are displayed in different shades of blue.

Figure 6.12 shows the time profiles for $\overline{M}_n$ (a), $\overline{M}_w$ (b), and PDI (c). One can see that the average molecular weight can reach a broad range of values, but the crucial point was that the polydispersity index never took values higher than 2. This was a contradiction to the high values ($PDI \approx 7$) observed in the experiments.

The next idea to improve the model was to incorporate the reaction rate's dependency on the number of hydroxyl groups. Modeling a rate proportional to the polymer size (by

replacing k_p with $k_p \cdot x$ for the propagation reaction) yielded the following time profiles for the average molecular weights and the PDI.

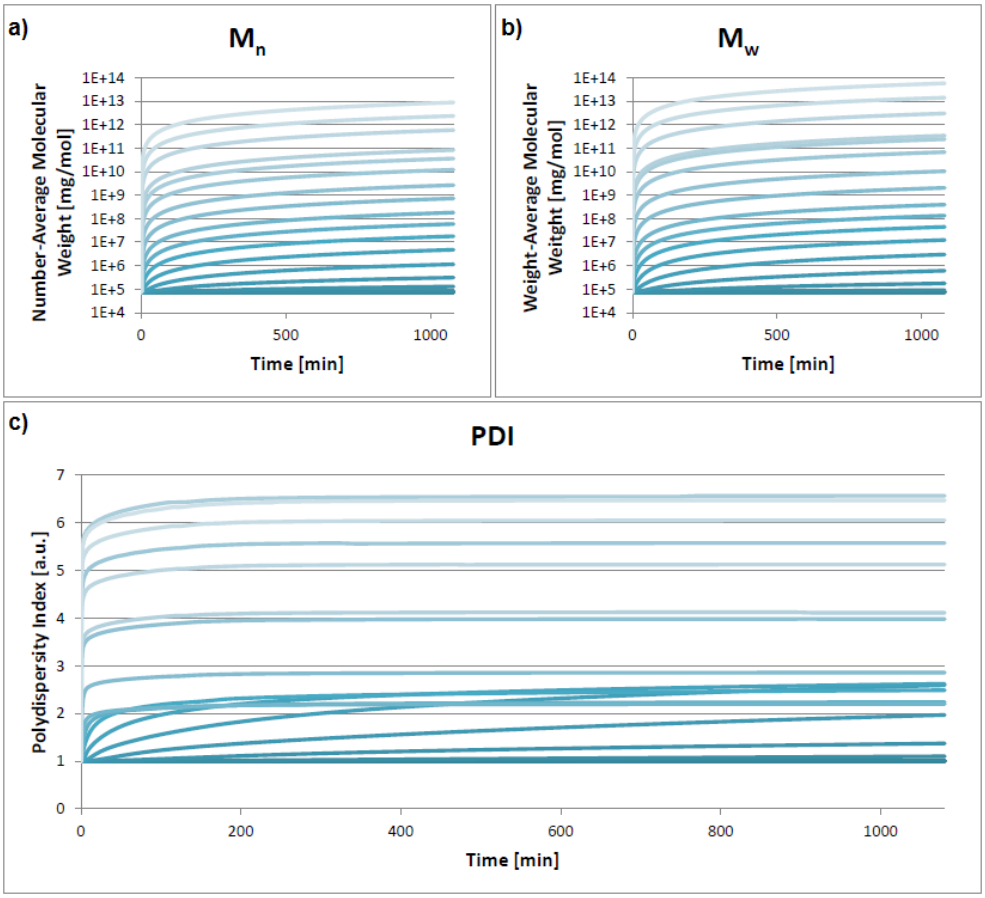

Figure 6.13. Time profiles for $\overline{M}_n$ (top, left), $\overline{M}_w$ (top, right) and PDI (bottom) using propagation rates proportional to the polymer's size. Results for different parameters are displayed in different shades of blue.

Figure 6.13 shows the time profiles for $\overline{M}_n$ (a), $\overline{M}_w$ (b), and PDI (c). In contrast to the previous model, this one can be used to produce polydispersities in the desired range. Therefore, this model was analyzed further and optimal parameters were estimated by executing the simulated annealing method that is provided by the PREDICI software. The results were verified by a combination of a boxsearch with a subsequent parameter optimization. Both methods found similar optima for the reaction coefficient and the time profiles are depicted in Figure 6.14.

Even though this model is capable of producing very broad MMDs (indicated by a high value for the PDI), the samples with a feasible average molecular weight are much less disperse than the experiments suggest. Therefore, this model cannot be to reproduce the

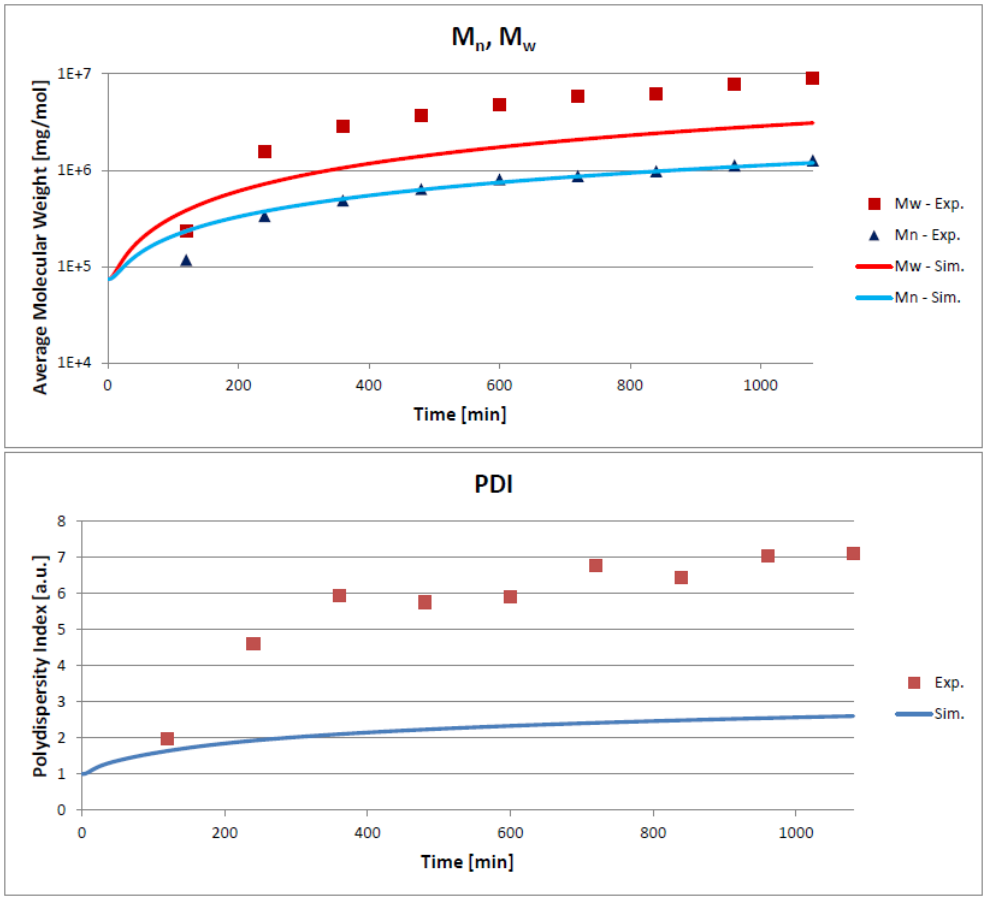

Figure 6.14. Time profiles for $\overline{M}_n$ (top row, blue line), $\overline{M}_w$ (top row, red line) and PDI (bottom) for the optimized parameters using the simplistic model with polymer size dependent propagation rates. The markers indicate the experimental data for comparison.

experimental data and a more complex version has to be tested.

The next model to be tested incorporates the overall ratio of primary to secondary hydroxyl groups. A model was constructed according to the model extension M4. This is easy cyclization and combination reactions are not accounted for. However, a quick variation analysis with subsequent simulated annealing shows that this method as well cannot reproduce the experimental data.

Figure 6.15 shows the time profiles for $\overline{M}_n$ (red) and $\overline{M}_w$(blue) for various values of k_p and a. For clarity, b was set to zero, but varying b as well does not change the range of the output that can be achieved. The graphs indicate that the simulated $\overline{M}_n$ exceeds the experimental values for $k_p > 10^{-2}$. At that point, the simulated $\overline{M}_w$ is much lower than the experimental one.

Figure 6.16 shows the results after estimation of parameters k_p, a and b via simulated

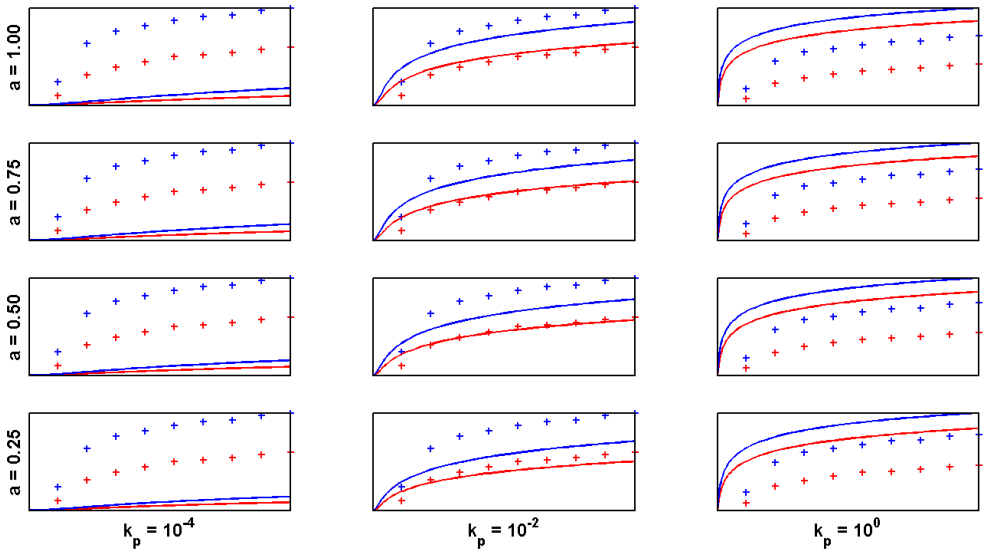

Figure 6.15. Time profiles for $\overline{M}_n$ are shown in red and for $\overline{M}_w$ in blue. The markers represent the experiments and the lines were created by simulation. In all cases, the y-axis shows the reaction time. Different columns correspond to different values of k_p and different rows correspond to different values of a

annealing. Interestingly, the optimal value for a was very close to 1 and the value for b was nearly 0. Therefore, this model is nearly identical to the previous one with propagation rates proportional to the total number of hydroxyl groups. It can be explained why this model is not able to reproduce the polydispersities of experiments better than the previous one, even though it has more degrees of freedom. Considering different reactivities will only decrease the overall reaction rate for later stages of the polymerization where the number of primary and secondary hydroxyl groups have balanced according to their reactivities. Since the structure of the polymers is not effected by this, similarly shaped MMDs are produced. If one could model different ratios for polymers of different sizes, one would observe that bigger polymers contain more secondary hydroxyl groups than primary ones which means that the reactivity increases less than proportionally to the number of hydroxyl groups. This compensates the tailing and broadening effect of a proportional reaction rate.

The next will be a more general model which accounts for propagation rates that increase non-linearly to the polymer's size. The reaction rates are formulated as follows.

$$R(B_s) = k_p \cdot s^{\alpha}$$

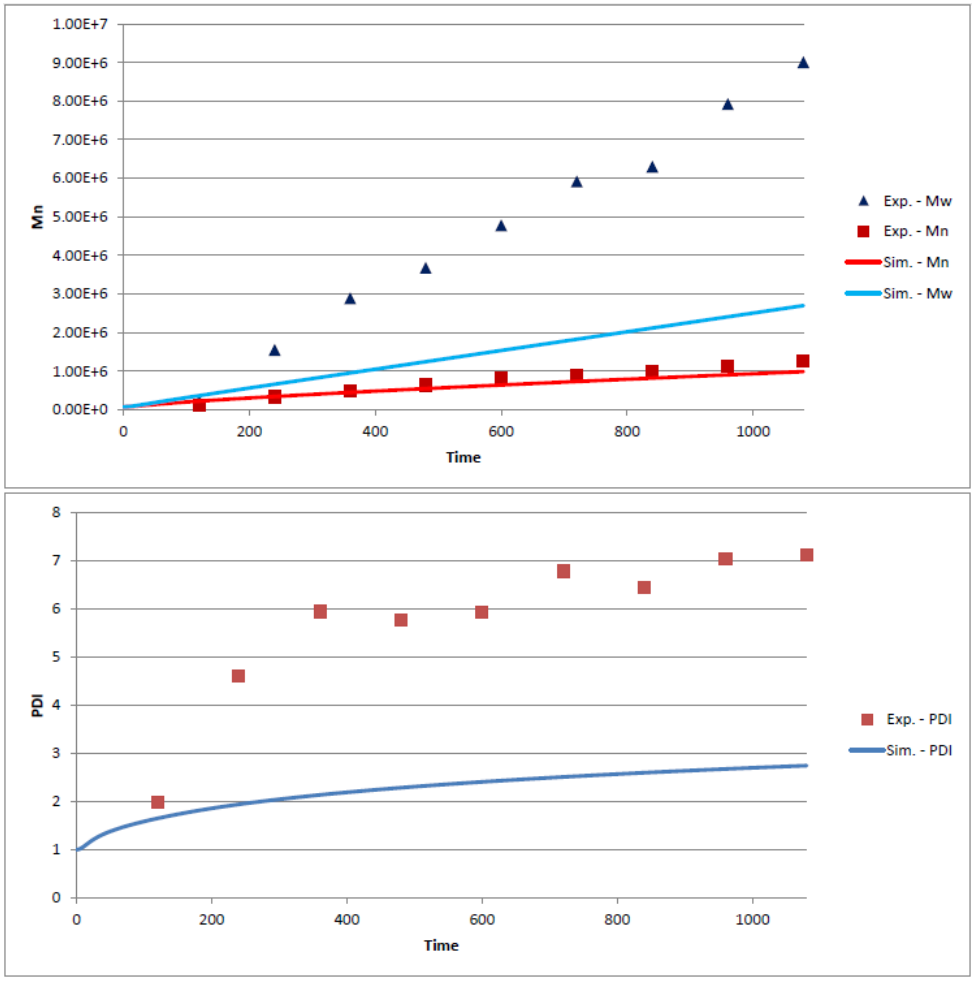

Figure 6.16. Time profiles for $\overline{M}_n$ (top row, blue line), $\overline{M}_w$ (top row, red line) and PDI (bottom row, blue line) for the optimized parameters considering different reactivities for primary and secondary hydroxyl groups. The markers indicate the experimental data for comparison.

With this model a big variety of polymer size dependent effects can be tested. If $\alpha = 0$ then the rate is independent of the reacting polymer's size, and if $\alpha = 1$ a linear dependency is modeled. Values between 0 and 1 could arise from the fact that some of the hydroxyl groups are less reactive, e.g., because big polymers have a bigger fraction of secondary hydroxyl groups or reactions occur only on the outer shell of a polymer. Values for α below 0 were also tested. This accounted for the fact that big molecules are less mobile and therefore less likely to meet reaction partners in space. Combined effects were also included by allowing any value for α between -1 and 1. Values below -1 could also be feasible, but were not tested in this approach as they do not indicate improvement of the simulation.

Similar to the earlier findings, the highest polydispersity index can be reached with $\alpha = 1$ and this value is still far below the measured value. Figure 6.17 shows the time profiles of $\overline{M}_n$ and $\overline{M}_w$ from simulations where k_p and α were varied. The y-axis was drawn in logarithmic scale. The labels of the axes were omitted because only the comparison to the experimental data is important. Results for simulations with low values of α were discarded for clarity. The figure shows that high or low values for k_p are not viable and the best agreement between simulations and experiments is obtained with $k_p = 10^{-2}$ and $\alpha = 1$.

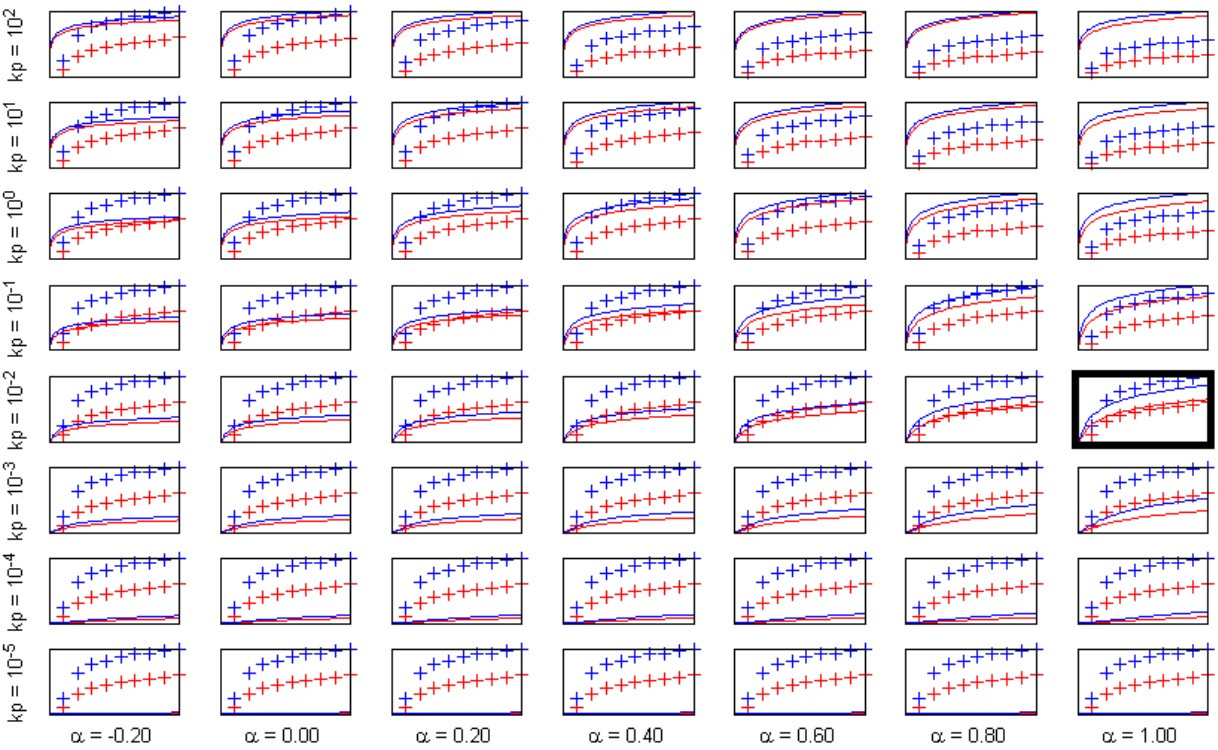

Figure 6.17. An illustration of the results simulated with different values of k_p (rows) and α (columns). The solid lines show the simulated and the markers the experimental data. Red color indicates the values for $\overline{M}_n$ and blue for $\overline{M}_w$. Best agreement between simulations and experiments was highlighted ($\alpha = 1$ and $k_p = 10^{-2}$ $L/mol/min$).

So far, neither cyclization nor combination reactions were regarded. Previous studies have shown that combination reactions of growing polymers lead to a step-growth polymerization with a characteristically broad MMDs.[15] This knowledge was an indication that these schemes might be better suited to fit the experimental data.

Adding combination reactions made every simulation far more complicated and some parameter combinations were not processable at all. In cases where the cyclization rate was

very small and the propagation rate much higher, almost all polymers in the system could combine with each other. In the extreme case, this would lead to the formation of a single molecule that incorporated the whole mass that was introduced into the system. This concept is called gel formation and modeling this effect is one of the persisting challenges in polymer science. However, such cases can basically be ignored because the formation of a gel could have been easily observed in the experiments. Nonetheless, these cases still posed a problem for the parameter estimation since it was not clear how to restrict the parameter space in order to avoid these special cases. There are a couple of modeling concepts that can be introduced in order to avoid the extreme broadening of the MMD that causes heavy numerical issues for the simulation software. One of these concepts is called the fractionation method, where the life span of a polymer is divided into different generations and the polymer's properties could vary for different generations. In the case of gel formation, one could regard polymers as usual until they reached a certain size and after which the number of incorporated monomers became irrelevant. In other words, a reaction was introduced that transformed a polymer into a low molecular species that is only characterized by its total mass. However, this is a very crude way to model the gel because it is no longer possible to accurately predict further reactions of this gel. This would not be problematic in this study because we know that there should no gel be formed we can just use it for the parameter estimation by punishing simulations proportional to the amount of gel that is produced. There is a second way to overcome this problem which is more specific to the process at hand. Because any self-initiated polymer is assumed to undergo cyclization reaction at some point, there is a theoretical limit to how big these polymers may become. We can exploit this by introducing a cut-off value for the size of acyclic polymers by excluding any reaction that would create a self-initiated polymer of that size or bigger. In order to realize this modification of the model, 11 new low molecular species were introduced that represented self-initiated polymers of sizes 2 to 12. This allows one control which reactions these molecules may participate in. The error introduced by this modification can be analyzed by examining the number of polymers of size 12. If the cyclization rate is too low, these polymers will accumulate in the system. The system can be further extended with more low molecular species, but at some point it will become inefficient because the software's chain length discretization scheme is bypassed. The software also provides a feature to assign a maximum for the chain length property of different polymers, but this induces the loss of mass throughout the polymerization which can lead to more severe errors. Additionally, by declaring the individual oligomer species

one can control the reaction rate of every combination of the molecular species separately. After all, both ways work and have their individual advantages and disadvantages, but the more straightforward approach was chosen and extra low molecular species were introduced.

Using the boxsearch feature provided by the software to quickly compare experimental results to the simulations with a big variety of parameter combination produced the following Figure 6.18.

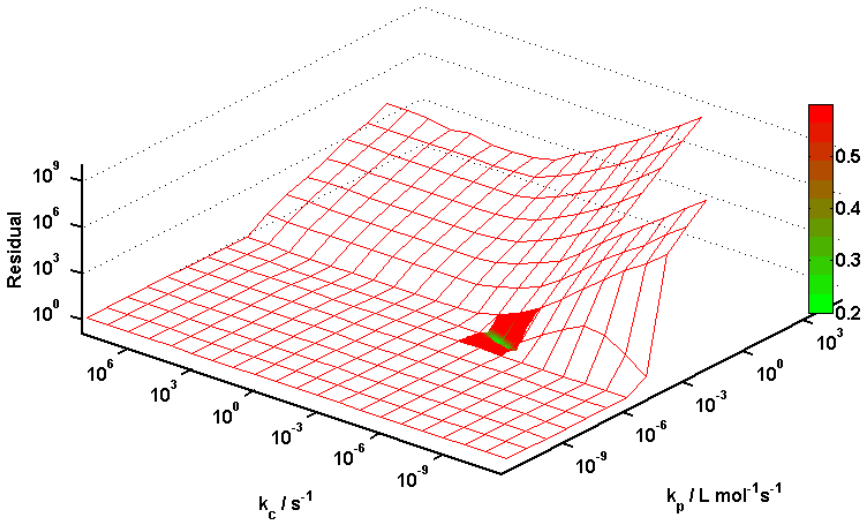

Figure 6.18. Visualization of the residual landscape after the variation analysis of k_p and k_c. The y-axis as well as th color indicate the residual. The colored surface in the middle represents the promising region which shows very low residuals.

One can see that the residuals are very bad for most parameter combinations, but one can observe very promising values in a small region ($L < k_p, k_c < U$). The residuals of the modified model may be regarded as a lower boundary for the residuals of the original one, because the simulated values for M_n and M_w are always higher for the unprocessable parameter combinations than the measured ones. This can also be seen in the mesh diagram above where very high residuals were achieved. The values become so high because the software uses a residuals weighted by the measured data:

$$R_{rel} = \sqrt{\frac{1}{N}\sum_{i=1}^{N}\frac{(m_i - s_i)^2}{m_i^2}}$$

Here, m_i stands for the measured data and s_i for the simulated output consisting a total of

N data points. As indicated by the formula, simulated output lower than the measurements result in a residual below 1 whereas output greater than the experimental data can result in very high residuals.

After identifying the promising region in parameter space, the original model was tested with the same parameters and it could be shown that the algorithm was stable for this region. It could also be seen that both models produced nearly the same output for these parameter values. Therefore, subsequent simulations were performed only with the original model and the modification was not applied anymore.

Since the boxsearch already found parameters that produced results very close to the experimental ones, it is not surprising that the subsequent parameter estimation would produce also very good results. A further analysis of the model in comparison to the experimental data that were obtained at different temperatures (90, 105, and 120 °C) was performed. Since these reactions were assumed to be highly sensitive to reaction temperature, it would be beneficial to assess this dependencies by formulating the Arrhenius expressions for the involved rate coefficients. The Arrhenius relationship reads as follows.

$$k = A(k) \cdot \exp\left(\frac{-E_a(k)}{R \cdot T}\right)$$

For every parameter p one needs to determine the prefactor A and the activation energy E_a. R is the universal gas constant and T the operating temperature.

PREDICI allows one to formulate the coefficients as Arrhenius expressions and one can even use the built-in optimization methodology to estimate prefactors and activation energies directly. Unfortunately, such an optimization problem is a highly non-linear one and does not converge in most cases where the initial values have not been chosen very well.

There is an alternative way to estimate Arrhenius parameters by determining optimal parameters for every experiment at different temperatures individually and than calculate the thermal dependency via linear regression of an Arrhenius plot.

Figure 6.19 shows the residual landscapes for the above-mentioned region in parameter space. The analysis was performed for all three experiments without initiators, so that 3 different graphs can be generated.

It can be seen that very good agreement can be found for each of the experiments and that the regions may vary in size and shape. The question remains whether these values will fit to a specific Arrhenius expression. Figure 6.20 shows the Arrhenius plot generated with the best parameters obtained so far.

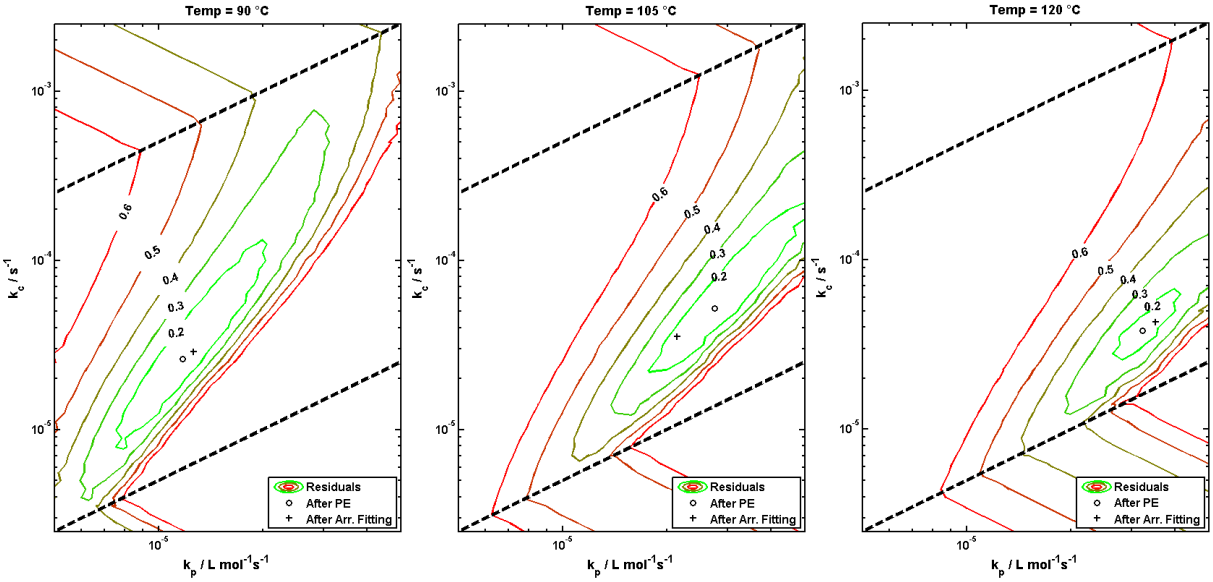

Figure 6.19. Visualization of the residual landscape for experiments at various temperatures. The innermost region indicated by the contour plot indicates very good agreement between simulated and experimental results. The markers indicate the results of the individual parameter estimations (as circles) and after estimating the Arrhenius parameters directly (as crosses).

Figure 6.20 also shows the linear regression of the Arrhenius plot. It works reasonable well for k_p, but the fit for k_c is not convincing. To analyze the subject further the best parameters for each trial were regarded. As a cut-off value for the residual we used 0.2, a value that is commonly accepted to represent very good agreement.

The top part of Figure 6.21 shows the chosen parameter values for all three experiments in one plot. The two plots below show the Arrhenius plots including all parameters from the top. Upper and lower boundaries (green and blue lines) were added as well as the optimal parameters (red markers) for clarity. This should illustrate that a regression line can be found that lies completely within the boundaries, so that simulations with such Arrhenius parameters will produce results that are very close (with a residual of lower than 0.2) to all experiments regardless of the temperature that was used. This can be verified by running the parameter optimization tool with the regressed parameters as starting values. This means that one model with parameters given as Arrhenius expression is used to fit all three experiments at the same time. The final residual was 0.12 which is extremely good in comparison to other parameter optimization studies. The quality of the parameter estimation can also be seen in Figure 6.22 which shows a comparison of the simulated and measured time profiles for all three temperatures.

One can see very good agreement of the time dependent average molecular weights.

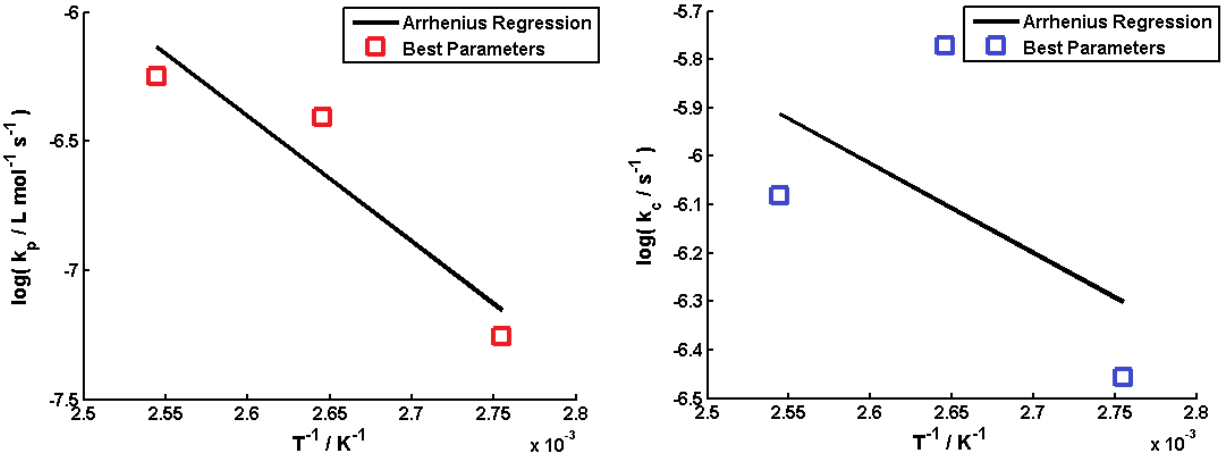

Figure 6.20. Arrhenius plots for the parameters k_p (left) and k_c (right). The markers show the best values after individually estimation at different temperatures. The solid line is the result of the regression of the individually optimized parameter values.

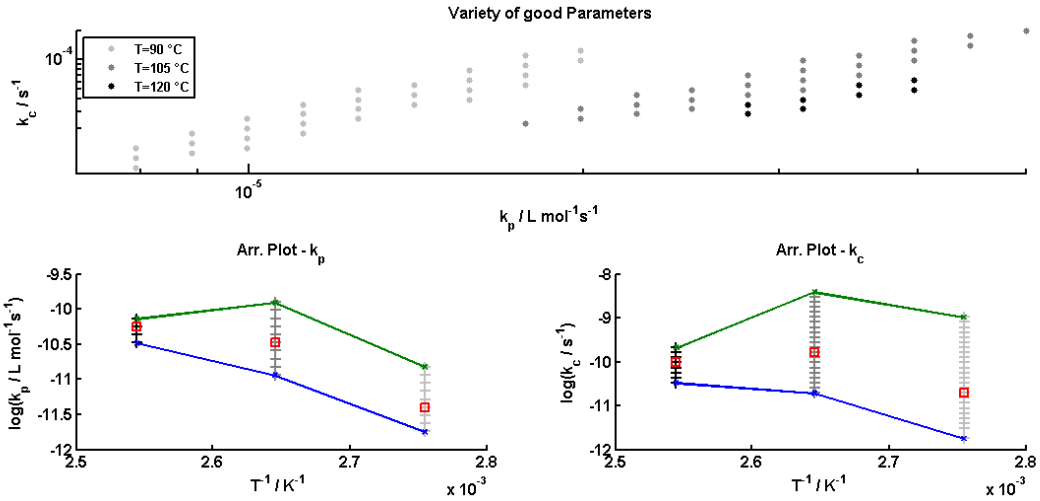

Figure 6.21. Another representation of the Arrhenius analysis. In the top part, all "good" parameter values (producing residuals below 0.2) are drawn in a single plot with different color coding. The bottom row shows the same Arrhenius plots as in the previous Figure 6.20, but this time, all "good" parameter values are displayed.

The only noteworthy difference is for early samples of the experiment at 90 °C. However, the behavior at this point seems unpredictable and the most likely explanation for this are measurement inaccuracies. These have been elaborated in detail in an earlier section and cannot be avoided. In order to ensure that these values do not disturb the parameter estimation procedure, they were not included in the calculation of the residuals. Therefore,

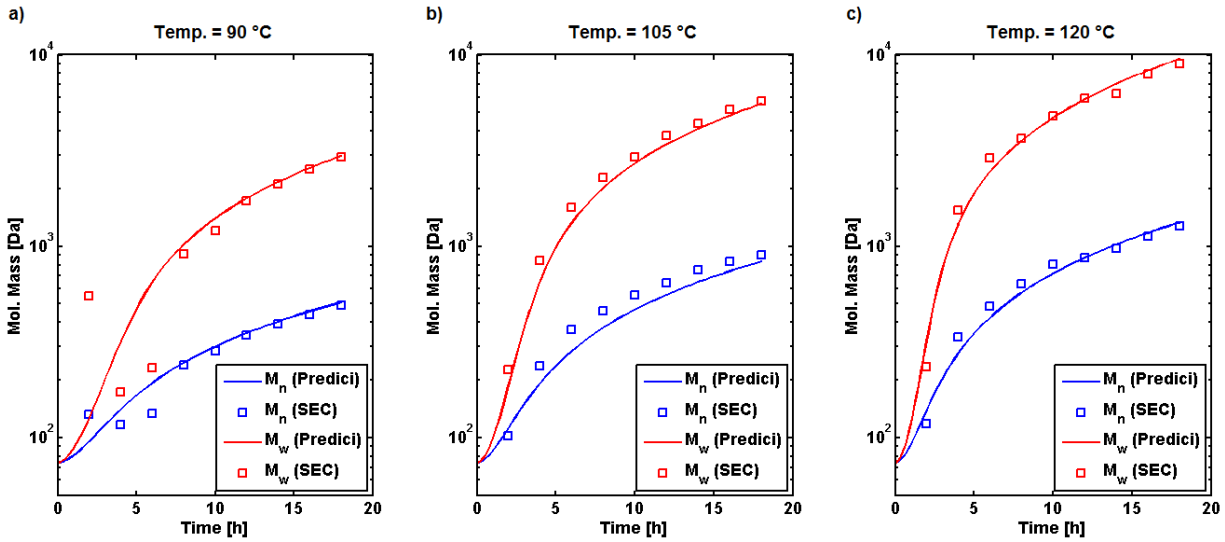

Figure 6.22. Time profiles of $\overline{M}_n$ (blue) and $\overline{M}_w$ (red) at different temperatures. The solid lines show the simulated and the markers the experimental results. For better comparison of the different experiments, the y-axis is plotted on a log scale.

Table 6.7. Summary of all estimated parameters based on the experiments without initiators at different reaction temperatures.

Parameter	I	II	III	IV
$A(k_p)^{a}$	n/a	n/a	8.26	8.26
$E_a(k_p)^{b}$	n/a	n/a	4.04×10^4	4.04×10^4
$A(k_c)^{c}$	n/a	n/a	4.93×10^{-3}	4.92×10
$E_a(k_c)^{b}$	n/a	n/a	1.54×10^4	1.55×10^4
k_p $(120\ °C)^{a}$	3.54×10^{-5}	3.23×10^{-5}	3.61×10^{-5}	3.50×10^{-5}
k_p $(105\ °C)^{a}$	2.81×10^{-5}	2.75×10^{-5}	2.21×10^{-5}	2.14×10^{-5}
k_p $(90\ °C)^{a}$	1.12×10^{-5}	1.17×10^{-5}	1.30×10^{-5}	1.26×10^{-5}
k_c $(120\ °C)^{c}$	4.45×10^{-5}	3.80×10^{-5}	4.51×10^{-5}	4.28×10^{-5}
k_c $(105\ °C)^{c}$	5.60×10^{-5}	5.19×10^{-5}	3.74×10^{-5}	3.55×10^{-5}
k_c $(90\ °C)^{c}$	2.23×10^{-5}	2.62×10^{-5}	3.06×10^{-5}	2.89×10^{-5}

[a] values in [L mol^{-1} s^{-1}]
[b] values in [J mol^{-1}]
[c] values in [L s^{-1}]

it must be noted that including these values will yield worse residuals.

Table 6.7 summarizes the whole parameter estimation procedure. Columns **I** and **II** show the best parameter combinations after boxsearch and parameter optimization, respectively. These tools were used for each of the three experimental data sets individually. Therefore the resulting parameters cannot be related via an Arrhenius expression. The last

two columns (**III** and **IV**) show the Arrhenius parameters calculated via linear regression of the Arrhenius plot and by using the build-in parameter estimation procedure for further optimization.

6.5 Estimating Anionic Ring-opening Reaction Rates

Knowing the thermal ring-opening reaction rates allows us to analyze the more complex system where a part of the hydroxyl groups is activated by abstraction of a proton to form alcoxides.

Unfortunately, since it was mandatory to use a very complex model for the thermal ring-opening reactions (2 polymer species with combination reactions for every self-initiated polymer), the complexity of the model which incorporates active sites is limited. As a consequence, it is not possible to explicitly model the number of active site so that the expectation value based on binomially distributed counter ions is used instead. As a result, the system of reaction equations can be represented as illustrated in Scheme 6.4.

$$
\begin{aligned}
&\text{Comb11(s,r):} && B_s + AB_r && \xrightarrow{k_p \cdot s \cdot p} && B_{s+r} \\
&\text{Comb21(s,r):} && cB_s + AB_r && \xrightarrow{k_p \cdot s \cdot p} && cB_{s+r} \\
&\text{Comb31(s,r):} && AB_s + AB_r && \xrightarrow{k_p \cdot s \cdot p} && AB_{s+r} \\
&\text{Comb12(s,r):} && B_s + AB_r && \xrightarrow{k_{thr} \cdot s \cdot (1-p)} && B_{s+r} \\
&\text{Comb22(s,r):} && cB_s + A_r && \xrightarrow{k_{thr} \cdot s \cdot (1-p)} && cB_{s+r} \\
&\text{Comb32(s,r):} && AB_s + AB_r && \xrightarrow{k_{thr} \cdot s \cdot (1-p)} && AB_{s+r} \\
&\text{Cyc1(s):} && AB_s && \xrightarrow{k_{cyc1} \cdot s^{\beta} \cdot p} && B_s \\
&\text{Cyc2(s):} && AB_s && \xrightarrow{k_{cyc2} \cdot s^{\beta} \cdot (1-p)} && B_s \\
&\text{Mfeed:} && \emptyset && \xrightarrow{k_{feed}} && AB
\end{aligned}
$$

Scheme 6.4. A set of reaction equations that can be used to model the anionic ring-opening polymerization of glycidol under consideration of thermal side reactions. The number of active sites per polymer is approximated by the expected number of counter ions binomially distributed onto all hydroxyl groups in the system.

In the case without initiators and active sites, $p = 0$ holds true throughout the simulation. This way, the only reaction coefficients that have an impact are k_{thr} and k_{cyc2}. Obviously, this model is capable of reproducing the results from the previous section if the parameters remain unchanged. In this model the β exponent for the cyclization rate was

fixed, although very good agreement could be achieved with various values between 0 and 1. When adjusting β one also has to adjust k_{thr} accordingly, so the most computationally stable version with $\beta = 1$ and the other coefficients as they were reported in the previous section was used for the following parameter estimation.

After performing the parameter estimation procedure, one could detect differences between experimental and simulated data of around 0.28 in terms of the total weighted residual. However, the quality of the simulation can be illustrated better with the time profiles of $\overline{M}_n$, $\overline{M}_w$, and PDI.

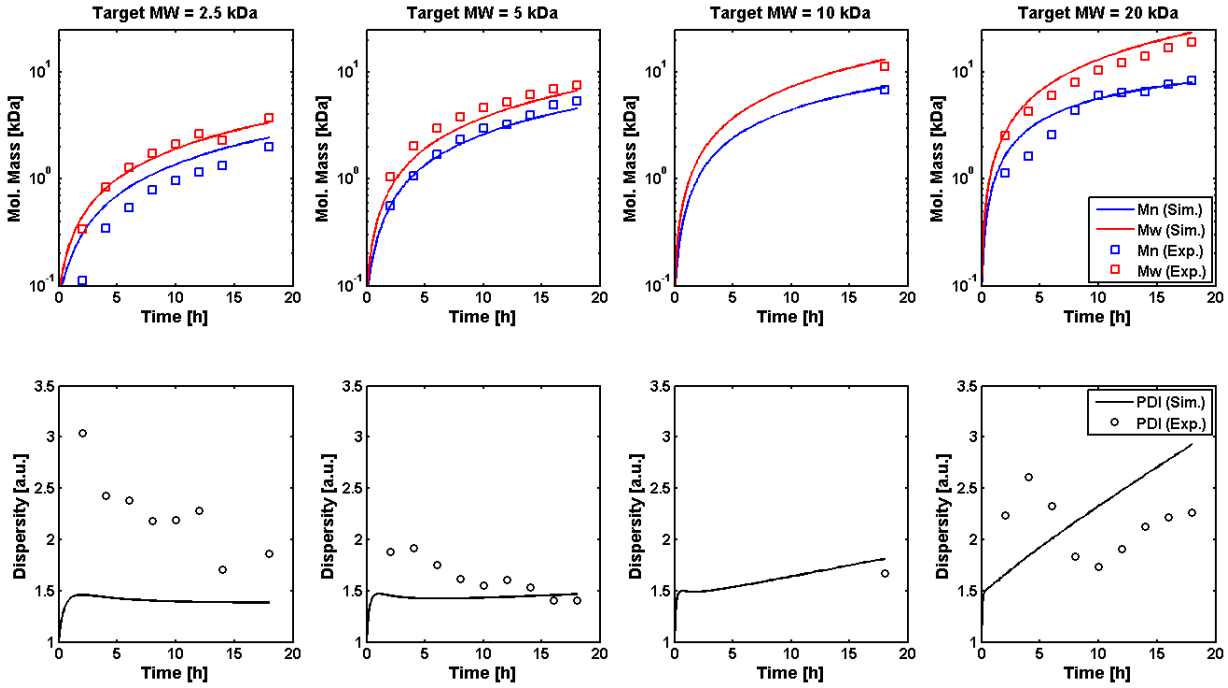

Figure 6.23. Time profiles for $\overline{M}_n$ (blue line/marker in top row), $\overline{M}_w$ (red line/marker in top row) and PDI (black line/marker in bottom row) for experiments with different target molecular weights. Solid lines display the simulated and markers the experimental data.

Figure 6.23 illustrated how the PDI is underestimated when using many initiators (left), whereas the PDI is overestimated in the case with only a few initiators (right). In any case, the agreement is well within the expected measurement error.

The final parameters that were determined are the following:

$$k_p = 1.04 \text{ L mol}^{-1} \text{ s}^{-1}$$
$$k_{thr} = 2.48 \times 10^{-5} \text{ L mol}^{-1} \text{ s}^{-1}$$
$$k_{cyc1} = 2.69 \times 10^{-1} \text{ s}^{-1}$$
$$k_{cyc2} = 2.48 \times 10^{-5} \text{ s}^{-1}$$

Finally, the model was also tested against the experiments with varying monomer addition techniques. Without changing the parameters the agreement with the results of the altered process were not very convincing. Figure 6.24 shows the time profiles of $\overline{M}_n$, $\overline{M}_w$, and PDI for the experiments where monomers are added at an increasing (left) or decreasing (right) rate.

The differences between experimental and simulated data were quite significant and performing a new parameter estimation only with data of the experiments targeting at a molecular weight of 20 kDa (with linear, logarithmic or exponential monomer addition) did not improve the accuracy of the prediction. One can see that that divergence of simulated and experimental data is highest when the monomer addition rate is the highest as well. Therefore, the PDI is drastically overestimated for the last samples of the experiment with increasing monomer addition rate and for the first samples of the experiment with decreasing monomer addition rate. This was disappointing, but the error may very well lie in the experimental set-up since the monomer addition rate gets very high at certain points. This might have introduced inhomogeneities in the reaction mixture which cannot be modeled without simulating the 3-dimensional coordinates of every molecule.

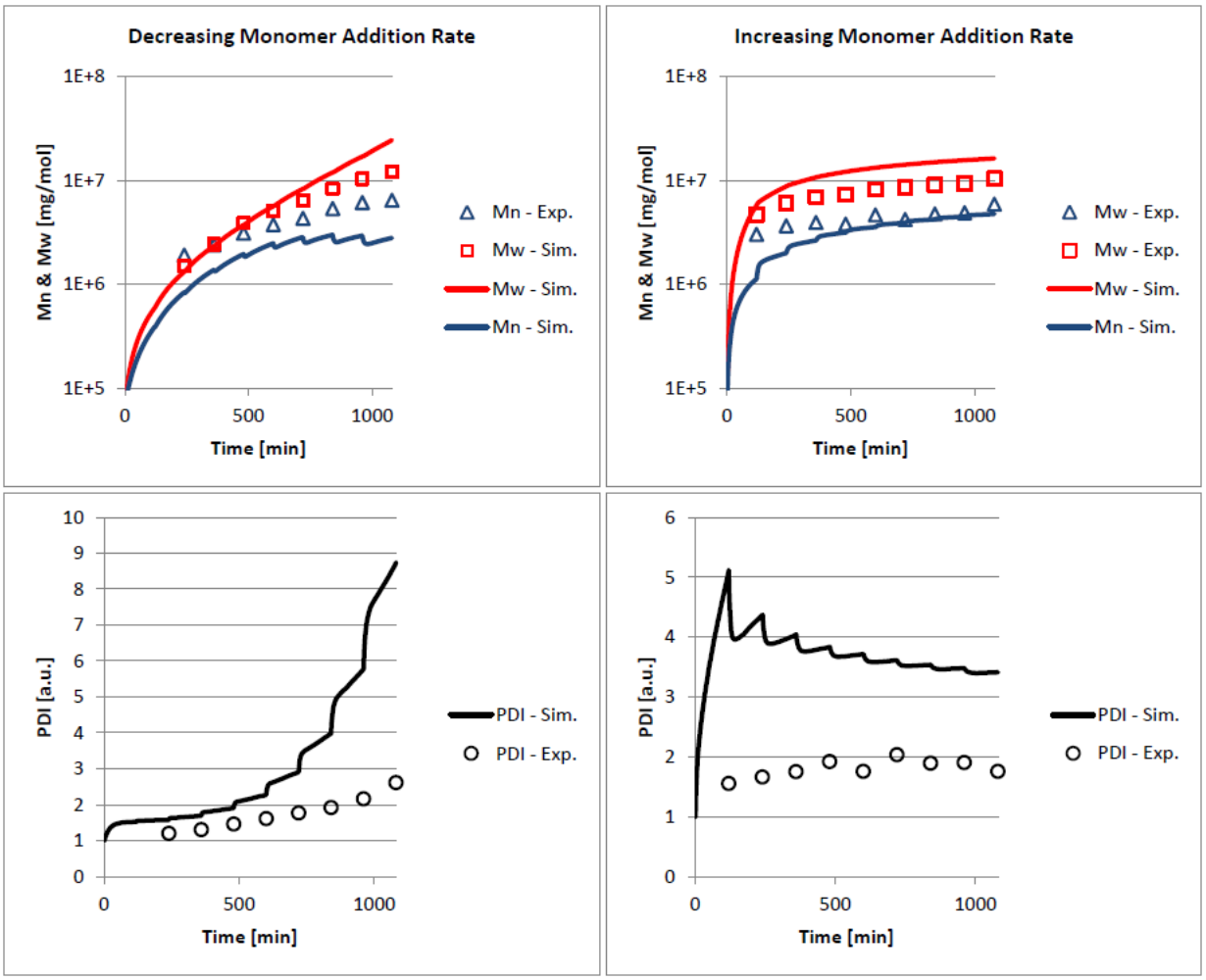

Figure 6.24. Time profiles for $\overline{M}_n$ (blue line/marker in top row), $\overline{M}_w$ (red line/marker in top row) and PDI (black line/marker in bottom row) for experiments with different monomer addition technique. Solid lines display the simulated and markers the experimental data.

7. CONCLUSIONS

This work provides an in-depth analysis of the reaction kinetics of the ring-opening polymerization of glycidol in combination with anionic core-forming molecules, slow addition of highly diluted monomers and elevated temperatures. The described process shows a very high degree of complexity and many different side reactions have to be considered and evaluated.

After analysis of the proceeding work of Flory, Vandenberg, Sander, Müller, Frey, Haag, and others, the existing theory was extended by the side reactions that were suspected to lower the quality of the final product. Various ways to model these effects were discussed with a special focus on the applicability to the simulation software PREDICI. The advantages as well as the limitations of the software framework were discussed in the context of the given polymerization process and some alternative approaches were proposed.

The derived models were tested by comparing the simulations to experiments where key parameters of the process were altered. The first trial led to a model that was able to describe the different average molecular weights achieved by varying the monomer-to-initiator ratio. The conclusion was that the propagation rate of a molecule had to be proportional or at least nearly proportional to the number of hydroxyl groups it contains. Otherwise it was not possible to obtain polydispersity indexes as high as the SEC measurements suggested. Two questions remained though. Firstly, it was not clear why the propagation rates should be proportional without consideration of polymers with multiple active sites and, secondly, whether thermal ring-opening reaction rates have an effect on the product. In order to answer these questions, new experiments were designed without the addition of any initiator, i.e., the theoretical monomer-to-initiator ratio is infinity. Without initiators there would also not be any active sites in the system and any polymer growth observed must consequently result from the reaction of inactive functional groups. Indeed, the new experiments indicated that polymers were formed with a notable average degree of polymerization of up to 16 monomeric subunits and a polydispersity index of more than 7. These experiments were instrumental in understanding the dynamics induced by

the thermal combination of free monomers. Not only did this reveal the importance of thermal ring-opening reactions, one could also calculate the cyclization and combination rates that were essential for producing a polydispersity index as high as the experiments suggested. The newly gained insight was used to develop a simplified model for the anionic polymerization for which the parameter estimation procedure was conclusive.

Upon estimating the anionic reaction parameters, it became clear that the anionic ring-opening reaction rate could not be modeled as a constant. The experimental data could only be reproduced with a model where big polymers were growing faster than small ones. This effect had to be incorporated in the anionic reaction rate and could not arise solely from the thermal reaction rates. The reason for that is that the thermal rates are too low to produce molecular weights as high as the experiments suggest. Because the anionic reactions could only be effected by the number of active sites and not the number of hydroxyl groups, it was concluded that big polymers must be more likely to accept a counter ion than small ones. This way the probability for big molecules to contain one or more active sites is much higher and thus, they grow faster. An attempt to model the proton-ion exchange reactions explicitly was undertaken, but it became far too demanding in terms of computation time and resources to model the fast transfer reactions between the polymers. It was only possible to model polymers with 3 or less active sites at the same time and even then some simulations were not able to complete. This motivated a detailed analysis of the dynamical distribution of counter ions over the hydroxyl groups in the system. It was easy to prove that the average number of active sites was below one throughout the polymerization, but on average big polymers were more often activated and also showed some multiple activation whereas small molecule remained inactive most of the time. In general, this would be a positive finding, but because some polymers will always get deactivated while growing and it may take some time for them to get reactivated. This way, the inactive polymers form a plateau in the PSD which results in an increased polydispersity index. Furthermore, when only few initiators were used monomers were accumulating before they could undergo an anionic reaction. This provokes ion transfer to monomer and thermal self-initiation reactions which again induce a broadening of the PSD. To avoid the calculation of the fast ion transfer reaction rates, the anionic reaction rates were modified to incorporate an approximation for the expected number of active sites. Under the assumption that ion transfers occurred much faster than every other reaction, the elemental probability of every hydroxyl group to be deprotonated becomes uniform. Finally, the anionic reaction rate of any polymer was modeled proportionally to

its size times the ratio of counter ions to hydroxyl groups in the system. This was shown to be the key factor that allows one to reproduce the measured data. Another interesting observation was that the individual probability for every hydroxyl group decreased in time since the number of counter ions was fixed and the number of hydroxyl groups increased with every monomer that was added into the system. It would be interesting to know how the dynamics would change if additional counter ions were introduced into the system over the course of the reaction. Doing so should accelerate the polymer propagation reactions and the thermal ring-opening reactions would play only a minor role at any time. One has to keep in mind though that ion transfers to monomers will be prompted as well and more low molecular polymers could arise. However, testing these hypotheses was not in the scope of this work because it requires a new reactor to be set up which would introduce many other issues.

The polymerization process without initiators was simple enough to incorporate temperature dependencies in the model by formulating the kinetic rate coefficients as Arrhenius expressions. The software package PREDICI provided the possibility to do so and even allowed a direct estimation of these parameters, i.e., activation energy and prefactor. Because of the non-linear nature of the Arrhenius equation, the corresponding optimization problem could not be guaranteed to converge and a solution might not be found. It was shown in the results section how this problem was overcome and that it was possible to find Arrhenius parameters for results which were in excellent agreement with the experiments. In theory, this approach could be applied to the anionic reaction as well, but the experiments will have to be repeated first at various temperatures. While this is a tempting thought, it would consume a lot of time and effort since a decent number of different temperatures (at least 3) and monomer-to-initiator ratios would have to be considered. For the following parameter estimation procedure this means a tremendous increase in complexity as well and it is not guaranteed that a satisfying solution can be found. Therefore, it was mandatory to first find good parameters for a fixed temperature. The kinetic parameters of this study can be used to further analyze the temperature dependencies of the anionic ring-opening reaction rates. Knowing the temperature dependencies for the thermal and anionic reactions makes it possible to find the optimal reaction temperature so that the difference in thermal and anionic reaction rates is maximized.

In conclusion, self-initiation reactions are the biggest concern for the synthesis. It does not matter whether they were catalyzed by a proceeding ion transfer to monomer

reaction or simply resulted as a result of the elevated reaction temperature. Through these reactions, small molecules are created throughout the polymerization and the average molecular weight is drastically lowered. The other factor that induces a drastic broadening of the polymer size distribution arises from the fact that big polymers grow faster than smaller ones. This conclusion is solely based on the parameter estimation procedure which is highly sensitive to the experimental results and their quality. It was shown that using anionic initiators and slowly adding monomers to the system allows control of the molecular weight, but only to a certain degree. Self-initiations can still occur and the polymer growth is not uniform for all polymers. Although, these techniques are very beneficial to the synthesis, there is still potential for further improvement, especially when targeting high molecular weights.

The only way to prevent self-initiation reactions is to keep the monomer concentration minimal at all time. The slow monomer addition technique helps tremendously in this respect and a non-linear addition did not result in a better quality of the final product. In theory, the monomer addition should be adjusted according to the overall reactivity of the system, i.e., the sum of all ring-opening reaction rates. With the derived model, the overall reactivity is dictated by the amounts of counter ions and hydroxyl groups. The number of active sites stays always the same and the number of hydroxyl groups rises proportionally to the amount of monomers added. This suggests an exponentially increasing monomer addition rate. However, it was shown that a faster monomer addition rate will inevitably lead to an increased amount of self-initiated polymers. This effect is likely to be the result of inhomogeneities at the location where the monomers are added. Since the presented model employs the indispensable assumption that reactivities for molecules are independent of their location in three-dimensional space, such an effect cannot be captured by the model. Solely on the basis of the experiments, one can conclude that a constant monomer addition rate seems to be the best choice because this is the only way to keep a minimal rate at all time. Therefore, changing the monomer addition technique does not promise improvement of the process. A better option might be to increase the number of counter ions steadily over time without adding more hydroxyl groups or byproducts. This could lead to a constant ratio of counter ions to hydroxyl groups and thermal ring-opening reactions might not have as big of an impact. This way, products of higher molecular weight could be targeted, but how this can be achieved cannot be decided from a theoretical point of view.

After all, it is very difficult to postulate clear changes that could yield an improved synthesis. However, the insight about the reaction kinetics will prove very valuable for

further studies. The conclusion that thermal ring-opening reactions cannot be ignored and that they are the limiting factor to achieving products of higher molecular weight is essential to the ongoing research. In the same context it is important to know that self-initiated polymers do not undergo cyclization instantly and instead possess the tendency to combine with other polymers for a limited period of time. Similarly to the random polycondensation of AB_2-type monomers very broad molecular weight distributions are produced, if the number of counter ions is small in comparison to the number of hydroxyl groups. Lastly, the experimental data suggest that the counter ions are indeed close to binomially distributed over all hydroxyl groups in the system. This has been assumed many times, but nobody has attempted to prove this hypothesis up to now.

The conclusions of this work and the mathematical model as a powerful simulation tool present an invaluable contribution to the research field concerning the synthesis of dendritic polymers.

8. SUMMARY

Dendritic polymers belong to the least investigated class of molecules with complex structure. They exhibit unique properties, such as compactness, multivalency, and solubility, which makes them very appealing for many chemical and biomedical applications. Most of the existing synthesizing strategies are very cumbersome, expensive, and time-consuming; therefore, great effort is invested to improve these processes. The chemical mechanisms are not well understood so far and most previous studies relied heavily on assumptions. Due to constant improvement in computational chemistry and the development of efficient modeling concepts the polymers' nano-architecture can now be analyzed in detail. Being able to accurately estimate the molecules' structure permits simulating the elemental mechanisms which was not possible before. Furthermore, by creating a mathematically sound model, the synthesis can be improved with well-known optimization methodologies that were developed in other fields.

The goal of this study was to derive a kinetic model that could be used to simulate the outcome of the "anionic ring-opening polymerization of glycidol". After a thorough investigation of the existing literature, the important mechanisms were identified, analyzed, and translated into the framework of the simulation software PREDICI. For many of the relevant reactions the kinetic parameters were unknown and often too complex to be considered explicitly. Therefore, a variety of different modeling strategies was developed at different levels of detail. The derived models were evaluated on the basis of experiments that were designed to assess the importance of key parameters, such as the initiator amount, reaction temperature, and monomer addition rate.

The greatest challenge in this study was to simplify the model, so that elaborate parameter estimation methods could be applied. At the same time, enough detail to realistically capture the essential mechanisms of the process had to be included. The problem was solved by designing new experiments to isolate the thermal side reactions which allowed accurate estimation of their kinetic parameters. After the calculation of the thermal rate coefficients, the remaining parameters for the anionic ring-opening reactions could be estimated as well. By dividing the problem into two easier ones, the final model

could be obtained with which all experiments could be reproduced accurately.

The evaluation of the different modeling concepts provided valuable insight into the underlying dynamics of the anionic ring-opening polymerization of glycidol. It could be shown that utilizing anionic initiators and the slow monomer addition technique could not completely prevent the spontaneous combination reactions between free monomers. These self-initiation reactions were mostly induced by the thermal ring-opening mechanism which dominates the system's dynamic if the hydroxyl groups drastically outnumber the counter ions in the system. Furthermore, it could be shown that polymers could contain more than one active sites and that this effect had to be incorporated in the model.

This was the first study in which the limitations to the synthesis of dendritic polyglycerol were quantified with mathematical methods and future investigations will strongly benefit from these findings. Additionally, the developed mathematical model provides a powerful tool to evaluate the impact of key parameters on the final product through simulations. This way, elaborate experiments can be avoided and the procedure can be improved in a quick and efficient manner.

9. ZUSAMMENFASSUNG

Dendritische Polymere stellen sich als die bisher am wenigsten untersuchte Klasse von Makromolekülen dar. Aufgrund ihrer außergewöhnlichen Eigenschaften, wie zum Beispiel Kompaktheit, Multivalenz und Lösbarkeit, sind diese Materialien sehr nutzbringend für eine Vielzahl biomedizinischer Anwendungen. Die bisherigen Syntheseverfahren zur Herstellung von dendritischen Polymeren erweisen sich zumeist als sehr kompliziert, kostspielig und zeitaufwendig, was das große Interesse an der Verbesserung der bestehenden und an der Erforschung neuer Verfahren erklärt. Die chemischen Mechanismen, die diese Polymerisationsprozesse beeinflussen, sind weitgehend nur unzureichend untersucht, so dass in vorangegangenen Studien viele der Nebenreaktionen bislang nicht explizit Berücksichtigung fanden. Es ist dem stetigen Fortschritt in den Bereichen der Informationstechnologie und der Entwicklung effizienter Modellierungskonzepte zu verdanken, dass solche Nebeneffekte nunmehr simuliert werden können und eine deutlich bessere Vorhersage des Prozesses möglich ist. Desweiteren können mathematisch wohldefinierte Modelle mittels erprobter Optimierungsmethoden analysiert werden, wodurch sich viele Alternativen zur Verbesserung des Syntheseprozesses eröffnen.

Das Ziel dieser Arbeit bestand darin, ein umfangreiches mathematisches Modell zu entwickeln, das die "anionische Ringöffnungspolymerisation von Glycidol" beschreiben und simulieren kann. Nach gründlicher Aufbereitung der bestehenden Literatur wurden die wichtigsten Mechanismen identifiziert, ausgewertet und in die Simulationssoftware PREDICI übertragen. Um den Prozess möglichst genau zu modellieren, wurde eine Vielzahl verschiedener Modellierungskonzepte getestet und anhand experimenteller Daten evaluiert. Die Experimente wurden entworfen, um den Einfluss spezieller Prozessparameter auf das Endprodukt zu untersuchen, wobei die Initiatormenge, die Reaktortemperatur und die Monomerzugabetechnik zahlreiche genau untersucht wurden.

Die größte Herausforderung bestand darin, das Modell soweit zu vereinfachen, so dass sich aufwendige mathematische Optimierungsmethoden anwenden ließen, um die kinetischen Reaktionsparameter zu schätzen. Zugleich musste das Modell aber auch detailliert genug sein, so dass alle essentiellen Mechanismen erfassbar und die experimentellen

Daten reproduzierbar waren. Um die Komplexität des Problems zu reduzieren, wurden Experimente ohne Zugabe von anionischen Initiatoren entworfen, um den Einfluss der thermischen Nebenreaktionen separat zu analysieren. Mit den dadurch gewonnenen Erkenntnissen konnte die Anzahl der unbekannten Parameter der anionischen Polymerisation gesenkt werden, was die akkurate Schätzung der restlichen Parameter ermöglichte. Nach der Optimierung des endgültigen Modells ließen sich alle Experimente mit zufriedenstellender Genauigkeit darstellen.

Die Bewertung der verschiedenen Modellierungskonzepte führte zu wertvollen und aussagekräftigen Schlussfolgerungen über die beteiligten Mechanismen. Es zeigte sich, dass durch die Verwendung von anionischen Initiatoren sowie die langsame Monomerzugabe sich das Syntheseprodukt zwar deutlich verbessern, aber die spontane Selbstinitiation freier Monomere sich nicht komplett verhindern ließ. Spezielle Experimente erbrachten den Nachweis thermischer Ringöffnungsreaktionen, deren kinetische Parameter genau bestimmt werden konnten. Desweiteren konnte belegt werden, dass sich große Polymere mehrfach aktivieren ließen, was in dem Modell explizit oder implizit berücksichtigt wurde.

In dieser Studie wurden die Grenzen des Syntheseverfahrens erstmals mit gesicherten Methoden untersucht, was als Grundlage für zukünftige Untersuchungen gilt. Das entwickelte Modell bietet ein verlässliches Hilfsmittel, um den Einfluss verschiedener Prozessparameter auf das Endprodukt der Synthese vorherzusehen. Durch Simulationen lassen sich aufwendige und langwierige Experimente vermeiden und das Syntheseverfahren kann schnell und effizient verbessert werden.

LIST OF TABLES

LIST OF FIGURES

LIST OF SCHEMES

BIBLIOGRAPHY

[1] C. A. Harper, *Handbook of Plastics, Elastomers, and Composites*. New York: McGraw-Hill, 4th ed., 2002.

[2] T. Meyer and J. Keurentjes, *Handbook of Polymer Reaction Engineering*. Weinheim, Germany: Wiley VCH, 2005.

[3] J. M. J. Fréchet and D. A. Tomalia, *Dendrimers and Other Dendritic Polymers*. New York: Wiley VCH, 2001.

[4] J. M. J. Fréchet, "Functional polymers and dendrimers: Reactivity, molecular architecture, and interfacial energy," *Science*, vol. 263, no. 5154, pp. 1710–5, 1994.

[5] Y. H. Kim, "Hyperbranched polymers 10 years after," *Journal of Polymer Science Part A: Polymer Chemistry*, vol. 36, no. 11, pp. 1685–1698, 1998.

[6] B. I. Voit, "New developments in hyperbranched polymers," *Journal of Polymer Science Part A: Polymer Chemistry*, vol. 38, no. 14, pp. 2505–2525, 2000.

[7] C. Gao and D. Yan, "Hyperbranched polymers: From synthesis to applications," *Progress in Polymer Science*, vol. 29, no. 3, pp. 183–275, 2004.

[8] R. Haag and F. Kratz, "Polymer therapeutics: Concepts and applications," *Angewandte Chemie International Edition*, vol. 45, no. 8, pp. 1198–215, 2006.

[9] A. Sunder, R. Mülhaupt, R. Haag, and H. Frey, "Hyperbranched polyether polyols: A modular approach to complex polymer architectures," *Advanced Materials*, vol. 12, no. 3, pp. 235–239, 2000.

[10] P. Deuflhard, *Newton Methods for Nonlinear Problems - Affine Invariance and Adaptive Alforithms*. Berlin Heidelberg: Springer, 2004.

[11] R. Mülhaupt, "Hermann Staudinger and the origin of macromolecular chemistry," *Angewandte Chemie International Edition*, vol. 43, no. 9, pp. 1054–63, 2004.

[12] E. J. Corey and X.-M. Cheng, *The Logic of Chemical Synthesis*. New York: Wiley, 1989.

[13] E. Heilbronner and J. D. Dunitz, *Reflections on Symmetry*. New York: VCH Publishers, Inc., 1993.

[14] H. Staudinger, *From Organic Chemistry to Macromolecules*. New York: Wiley-interscience, 1970.

[15] P. J. Flory, *Principles of Polymer Chemistry*. Ithaca, New York: Cornell University Press, 1953.

[16] E. Buhleier, W. Wehner, and F. Vögtle, "Cascade- and nonskid-chain-like syntheses of molecular cavity topologies," *Synthesis*, vol. 1978, no. 02, pp. 155–158, 1978.

[17] D. A. Tomalia, H. Baker, J. Dewald, M. Hall, G. Kallos, S. Martin, J. Roeck, J. Ryder, and P. Smith, "A new class of polymers: Starburst-dendritic macromolecules," *Polymer Journal*, vol. 17, no. 1, pp. 117–132, 1985.

[18] D. A. Tomalia, "Birth of a new macromolecular architecture: Dendrimers as quantized building blocks for nanoscale synthetic polymer chemistry," *Progress in Polymer Science*, vol. 30, no. 3-4, pp. 294–324, 2005.

[19] D. A. Tomalia and D. Hedstrand, "Comb-burst dendrimer topology: New macromolecular architecture derived from dendritic grafting," *Macromolecules*, vol. 24, pp. 1435–1438, 1991.

[20] D. A. Tomalia, A. M. Naylor, and W. A. Goddard, "Starburst dendrimers: Molecular-level control of size, shape, surface chemistry, topology, and flexibility from atoms to macroscopic matter," *Angewandte Chemie International Edition*, vol. 29, no. 2, pp. 138–175, 1990.

[21] P. Lang, H. J. Spinelli, L. Page, M. S. Wolfe, and W. Burchard, "Structure of PMMA/EGDMA star-branched microgels," *Macromolecules*, vol. 24, no. 6, pp. 1306–1314, 1991.

[22] C. Siegers, M. Biesalski, and R. Haag, "Self-assembled monolayers of dendritic polyglycerol derivatives on gold that resist the adsorption of proteins," *Chemistry - A European Journal*, vol. 10, no. 11, pp. 2831–8, 2004.

[23] S. C. Zimmerman, J. R. Quinn, E. Burakowska, and R. Haag, "Cross-linked glycerol dendrimers and hyperbranched polymers as ionophoric, organic nanoparticles soluble in water and organic solvents," *Angewandte Chemie International Edition*, vol. 46, no. 43, pp. 8164–7, 2007.

[24] E. Burakowska and R. Haag, "Dendritic Polyglycerol Core-Double-Shell Architectures: Synthesis and Transport Properties," *Macromolecules*, vol. 42, no. 15, pp. 5545–5550, 2009.

[25] E. Burakowska, S. C. Zimmerman, and R. Haag, "Photoresponsive crosslinked hyperbranched polyglycerols as smart nanocarriers for guest binding and controlled release," *Small*, vol. 5, no. 19, pp. 2199–204, 2009.

[26] R. F. Barth, D. M. Adams, a. H. Soloway, F. Alam, and M. V. Darby, "Boronated starburst dendrimer-monoclonal antibody immunoconjugates: Evaluation as a potential delivery system for neutron capture therapy," *Bioconjugate Chemistry*, vol. 5, no. 1, pp. 58–66, 1994.

[27] J. F. G. A. Jansen and E. W. Meijer, "The dendritic box: Shape-selective liberation of encapsulated guests," *Journal of the American Chemical Society*, vol. 117, pp. 4417–4418, 1995.

[28] S. Stevelmans, J. C. M. van Hest, J. F. G. A. Jansen, D. A. F. J. van Boxtel, E. M. M. de Brabander-van den Berg, and E. W. Meijer, "Synthesis, characterization, and guest-host properties of inverted unimoleculat dendritic micelles," *Journal of the American Chemical Society*, vol. 118, pp. 7398–7399, 1996.

[29] A. I. Cooper, J. D. Londono, G. Wignall, J. B. McClain, E. T. Samulski, J. S. Lin, A. Dobrynin, M. Rubinstein, A. L. C. Burke, J. M. J. Fréchet, and J. M. DeSimone, "Extraction of a hydrophilic compound from water into liquid CO_2 using dendritic surfactants," *Nature*, vol. 389, pp. 368–371, 1997.

[30] A. Schmitzer, E. Perez, I. Rico-Lattes, A. Lattes, and S. Rosca, "First example of supramolecular assemblies in water of new amphiphilic glucose-persubstituted poly(amidoamine) dendrimers," *Langmuir*, vol. 15, no. 13, pp. 4397–4403, 1999.

[31] C. Z. Chen, N. C. Beck-Tan, P. Dhurjati, T. K. van Dyk, R. a. LaRossa, and S. L. Cooper, "Quaternary ammonium functionalized poly(propylene imine) dendrimers

as effective antimicrobials: Structure-activity studies," *Biomacromolecules*, vol. 1, no. 3, pp. 473–80, 2000.

[32] N. Malik, R. Wiwattanapatapee, R. Klopsch, K. Lorenz, H. Frey, J. W. Weener, E. W. Meijer, W. Paulus, and R. Duncan, "Dendrimers: Relationship between structure and biocompatibility in vitro, and preliminary studies on the biodistribution of 125I-labelled polyamidoamine dendrimers in vivo," *Journal of Controlled Release*, vol. 65, no. 1-2, pp. 133–48, 2000.

[33] C. Kojima, K. Kono, K. Maruyama, and T. Takagishi, "Synthesis of polyamidoamine dendrimers having poly(ethylene glycol) grafts and their ability to encapsulate anticancer drugs," *Bioconjugate Chemistry*, vol. 11, no. 6, pp. 910–7, 2000.

[34] D. Astruc and F. Chardac, "Dendritic catalysts and dendrimers in catalysis," *Chemical Reviews*, vol. 101, no. 9, pp. 2991–3024, 2001.

[35] R. van Heerbeek, P. C. J. Kamer, P. W. N. M. van Leeuwen, and J. N. H. Reek, "Dendrimers as support for recoverable catalysts and reagents," *Chemical Reviews*, vol. 102, no. 10, pp. 3717–56, 2002.

[36] S. K. Ghosh, S. Kawaguchi, Y. Jinbo, Y. Izumi, K. Yamaguchi, T. Taniguchi, K. Nagai, and K. Koyama, "Nanoscale solution structure and transfer capacity of amphiphilic poly(amidoamine) dendrimers having water and polar guest molecules inside," *Macromolecules*, vol. 36, no. 24, pp. 9162–9169, 2003.

[37] N. Nishiyama, H. R. Stapert, G.-D. Zhang, D. Takasu, D.-L. Jiang, T. Nagano, T. Aida, and K. Kataoka, "Light-harvesting ionic dendrimer porphyrins as new photosensitizers for photodynamic therapy," *Bioconjugate Chemistry*, vol. 14, no. 1, pp. 58–66, 2003.

[38] M. Adeli and R. Haag, "Multiarm star nanocarriers containing a poly(ethylene imine) core and polylactide arms," *Journal of Polymer Science Part A: Polymer Chemistry*, vol. 44, pp. 5740–5749, 2006.

[39] M. R. Radowski, A. Shukla, H. von Berlepsch, C. Böttcher, G. Pickaert, H. Rehage, and R. Haag, "Supramolecular aggregates of dendritic multishell architectures as universal nanocarriers," *Angewandte Chemie International Edition*, vol. 46, no. 8, pp. 1265–9, 2007.

[40] Y. H. Kim and O. W. Webster, "Hyperbranched polyphenylenes," *Macromolecules*, vol. 25, no. 21, pp. 5561–5572, 1992.

[41] K. E. Uhrich, C. J. Hawker, J. M. J. Fréchet, and S. R. Turner, "One-pot synthesis of hyperbranched polyethers," *Macromolecules*, vol. 25, no. 18, pp. 4583–4587, 1992.

[42] V. Percec, P. Chu, and M. Kawasumi, "Toward willowlike thermotropic dendrimers," *Macromolecules*, vol. 27, no. 16, pp. 4441–4453, 1994.

[43] C. J. Hawker, R. Lee, and J. M. J. Fréchet, "One-step synthesis of hyperbranched dendritic polyesters," *Journal of the American Chemical Society*, vol. 113, no. 12, pp. 4583–4588, 1991.

[44] S. R. Turner, B. I. Voit, and T. H. Mourey, "All-aromatic hyperbranched polyesters with phenol and acetate end groups: Synthesis and characterization," *Macromolecules*, vol. 26, no. 17, pp. 4617–4623, 1993.

[45] E. Malmström, M. Johansson, and A. Hult, "Hyperbranched Aliphatic Polyesters," *Macromolecules*, vol. 28, no. 5, pp. 1698–1703, 1995.

[46] H. R. Kricheldorf, O. Stoeber, and D. Luebbers, "New Polymer Syntheses. 78. Star-shaped and hyperbranched polyesters by polycondensation of trimethylsilyl 3,5-diacetoxybenzoate," *Macromolecules*, vol. 28, no. 7, pp. 2118–2123, 1995.

[47] Y. H. Kim, "Lyotropic liquid crystalline hyperbranched aromatic polyamides," *Journal of the American Chemical Society*, vol. 114, no. 12, pp. 4947–4948, 1992.

[48] G. Yang, M. Jikei, and M.-a. Kakimoto, "Synthesis and properties of hyperbranched aromatic polyamide," *Macromolecules*, vol. 32, no. 7, pp. 2215–2220, 1999.

[49] D. H. Bolton and K. L. Wooley, "Synthesis and characterization of hyperbranched polycarbonates," *Macromolecules*, vol. 30, no. 7, pp. 1890–1896, 1997.

[50] C. J. Hawker and F. Chu, "Hyperbranched poly(ether ketones): Manipulation of structure and physical properties," *Macromolecules*, vol. 29, no. 12, pp. 4370–4380, 1996.

[51] A. Morikawa, "Preparation and properties of hyperbranched poly(ether ketones) with a various number of phenylene units," *Macromolecules*, vol. 31, no. 18, pp. 5999–6009, 1998.

[52] C.-f. Shu and C.-m. Leu, "Hyperbranched poly(ether ketone) with carboxylic acid terminal groups: Synthesis, characterization, and derivatization," *Macromolecules*, vol. 32, no. 1, pp. 100–105, 1999.

[53] R. Spindler and J. M. J. Fréchet, "Synthesis and characterization of hyperbranched polyurethanes prepared from blocked isocyanate monomers by step-growth polymerization," *Macromolecules*, vol. 26, no. 18, pp. 4809–4813, 1993.

[54] L. J. Mathias and T. W. Carothers, "Hyperbranched poly(siloxysilanes)," *Journal of the American Chemical Society*, vol. 113, no. 10, pp. 4043–4044, 1991.

[55] C. Lach and H. Frey, "Enhancing the degree of branching of hyperbranched polymers by postsynthetic modification," *Macromolecules*, vol. 31, no. 7, pp. 2381–2383, 1998.

[56] L. J. Hobson and W. J. Feast, "Poly(amidoamine) hyperbranched systems: Synthesis, structure and characterization," *Polymer*, vol. 40, no. 5, pp. 1279–1297, 1999.

[57] T. M. Londergan, Y. You, M. E. Thompson, and W. P. Weber, "Ruthenium catalyzed synthesis of cross-conjugated polymers and related hyperbranched materials. Copoly(arylene/1,1-vinylene)s," *Macromolecules*, vol. 31, no. 9, pp. 2784–2788, 1998.

[58] J. M. J. Fréchet, M. Henmi, I. Gitsov, S. Aoshima, M. R. Leduc, and R. B. Grubbs, "Self-condensing vinyl polymerization: An approach to dendritic materials.," *Science*, vol. 269, no. 5227, pp. 1080–3, 1995.

[59] P. F. W. Simon, W. Radke, and A. H. E. Müller, "Hyperbranched methacrylates by self-condensing group transfer polymerization," *Macromolecular Rapid Communications*, vol. 18, pp. 865–873, 1997.

[60] P. F. W. Simon and A. H. E. Müller, "Synthesis of hyperbranched and highly branched methacrylates by self-condensing group transfer copolymerization," *Macromolecules*, vol. 34, no. 18, pp. 6206–6213, 2001.

[61] T. E. Patten and K. Matyjaszewski, "Atom transfer radical polymerization and the synthesis of polymeric materials," *Advanced Materials*, vol. 10, no. 12, pp. 901–915, 1998.

[62] V. Coessens, T. Pintauer, and K. Matyjaszewski, "Functional polymers by atom transfer radical polymerization," *Progress in Polymer Science*, vol. 26, pp. 337–377, 2001.

[63] M. Suzuki, S. Yoshida, K. Shiraga, and T. Saegusa, "New ring-opening polymerization via a π-allylpalladium complex. 5. Multibranching polymerization of cyclic carbamate to produce hyperbranched dendritic polyamine," *Macromolecules*, vol. 31, no. 6, pp. 1716–1719, 1998.

[64] H. Magnusson, E. Malmström, and A. Hult, "Synthesis of hyperbranched aliphatic polyethers via cationic ring-opening polymerization of 3-ethyl-3-(hydroxymethyl) oxetane," *Macromolecular Rapid Communications*, vol. 20, pp. 453–457, 1999.

[65] Y. Chen, M. Bednarek, P. Kubisa, and S. Penczek, "Synthesis of multihydroxyl branched polyethers by cationic copolymerization of 3,3-bis(hydroxymethyl)oxetane and 3-ethyl-3-(hydroxymethyl)oxetane," *Journal of Polymer Science Part A: Polymer Chemistry*, vol. 40, no. 12, pp. 1991–2002, 2002.

[66] E. J. Vandenberg, "Polymerization of glycidol and its derivatives: A new rearrangement polymerization," *Journal of Polymer Science Part A: Polymer Chemistry*, vol. 23, no. 4, pp. 915–949, 1985.

[67] R. Tokar, P. Kubisa, S. Penczek, and A. Dworak, "Cationic polymerization of glycidol: Coexistence of the activated monomer and active chain end mechanism," *Macromolecules*, vol. 27, no. 2, pp. 320–322, 1994.

[68] A. Sunder, R. Hanselmann, H. Frey, and R. Mülhaupt, "Controlled synthesis of hyperbranched polyglycerols by ring-opening multibranching polymerization," *Macromolecules*, vol. 32, no. 13, pp. 4240–4246, 1999.

[69] M. Liu, N. Vladimirov, and J. M. J. Fréchet, "A new approach to hyperbranched polymers by ring-opening polymerization of an AB monomer: 4-(2-hydroxyethyl)-ϵ-caprolactone," *Macromolecules*, vol. 32, no. 20, pp. 6881–6884, 1999.

[70] C. Gong and J. M. J. Fréchet, "Proton transfer polymerization in the preparation of hyperbranched polyesters with epoxide chain-ends and internal hydroxyl functionalities," *Macromolecules*, vol. 33, no. 14, pp. 4997–4999, 2000.

[71] J. K. Paulasaari and W. P. Weber, "Synthesis of hyperbranched polysiloxanes by base-catalyzed proton-transfer polymerization. Comparison of hyperbranched polymer microstructure and properties to those of linear analogues prepared by cationic or anionic ring-opening polymerization," *Macromolecules*, vol. 33, no. 6, pp. 2005–2010, 2000.

[72] J. M. J. Fréchet, C. J. Hawker, I. Gitsov, and J. Leon, "Dendrimers and hyperbranched polymers: Two families of three-dimensional macromolecules with similar but clearly distinct properties," *Journal of Macromolecular Science, Part A: Pure and Applied Chemistry*, vol. 33, no. 10, pp. 1399–1425, 1996.

[73] L. J. Hobson and R. Harrison, "Dendritic and hyperbranched polymers: Advances in synthesis and applications," *Current Opinion in Solid State and Materials Science*, vol. 2, no. 6, pp. 683–692, 1997.

[74] E. Malmström and A. Hult, "Hyperbranched polymers: A review," *Polymer Reviews*, vol. 37, no. 3, pp. 555–579, 1997.

[75] C. J. Hawker, "Dendritic and hyperbranched macromolecules - Precisely controlled macromolecular architectures," *Advances in Polymer Science*, vol. 147, pp. 113–160, 1999.

[76] A. Hult, M. Johansson, and E. Malmström, "Hyperbranched polymers," *Advances in Polymer Science*, vol. 143, pp. 1–34, 1999.

[77] M. Jikei, S.-H. Chon, M.-a. Kakimoto, S. Kawauchi, T. Imase, and J. Watanebe, "Synthesis of hyperbranched aromatic polyamide from aromatic diamines and trimesic acid," *Macromolecules*, vol. 32, no. 6, pp. 2061–2064, 1999.

[78] T. Emrick, H.-t. Chang, and J. M. J. Fréchet, "An A_2+B_3 approach to hyperbranched aliphatic polyethers containing chain end epoxy substituents," *Macromolecules*, vol. 32, no. 19, pp. 6380–6382, 1999.

[79] T. H. Rider and A. J. Hill, "Studies of glycidol. I. Preparation from glycerol monochlorohydrin," *Journal of the American Chemical Society*, vol. 52, no. 4, pp. 1521–1527, 1930.

[80] E. J. Goethals, R. R. De Clercq, H. C. De Clercq, and P. J. Hartmann, "Synthesis and reactions of telechelic polyacetals," *Macromolecular Symposia*, vol. 47, no. 1, pp. 151–162, 1991.

[81] S. R. Sandler and F. R. Berg, "Room temperature polymerization of glycidol," *Journal of Polymer Science Part A: Polymer Chemistry*, vol. 4, no. 5, pp. 1253–1259, 1966.

[82] W. H. Ray, "On the mathematical modeling of polymerization reactors," *Polymer Reviews*, vol. 8, no. 1, pp. 1–56, 1972.

[83] M. Wulkow, "The simulation of molecular weight distributions in polyreaction kinetics by discrete Galerkin methods," *Macromolecular Theory and Simulations*, vol. 5, no. 3, pp. 393–416, 1996.

[84] A. H. E. Müller, D. Yan, and M. Wulkow, "Molecular parameters of hyperbranched polymers made by self-condensing vinyl polymerization. 1. Molecular weight distribution," *Macromolecules*, vol. 30, no. 23, pp. 7015–7023, 1997.

[85] D. Hölter, A. Burgath, and H. Frey, "Degree of branching in hyperbranched polymers," *Acta Polymerica*, vol. 48, no. 1-2, pp. 30–35, 1997.

[86] D. Yan, A. H. E. Müller, and K. Matyjaszewski, "Molecular parameters of hyperbranched polymers made by self-condensing vinyl polymerization. 2. Degree of branching," *Macromolecules*, vol. 30, no. 23, pp. 7024–7033, 1997.

[87] D. C. Rapaport, *The art of molecular dynamics simulation*. New York: Cambridge University Press, 2nd ed., 2004.

[88] B. J. Alder and T. E. Wainwright, "Studies in molecular dynamics. I. General method," *The Journal of Chemical Physics*, vol. 31, no. 2, p. 459, 1959.

[89] F. Horn and R. Jackson, "General mass action kinetics," *Archive for Rational Mechanics and Analysis*, vol. 47, no. 2, pp. 81–116, 1972.

[90] D. T. Gillespie, "A general method for numerically simulating the stochastic time evolution of coupled chemical reactions," *Journal of Computational Physics*, vol. 22, no. 4, pp. 403–434, 1976.

[91] D. T. Gillespie, "A rigorous derivation of the chemical master equation," *Physica A: Statistical Mechanics and its Applications*, vol. 188, no. 1-3, pp. 404–425, 1992.

[92] O. Y. Ababneh and R. Ahmad, "Design of new diagonally implicit Runge-Kutta methods for stiff problems," *Applied Mathematical Sciences*, vol. 3, no. 45, pp. 2241–2253, 2009.

[93] R. Weiss, "The application of implicit Runge-Kutta and collocation methods to boundary-value problems," *Mathematics of Computation*, vol. 28, no. 126, p. 449, 1974.

[94] M. Wulkow, "Adaptive treatment of polyreactions in weighted sequence spaces," *IMPACT of Computing in Science and Engineering*, vol. 4, no. 2, pp. 153–193, 1992.

[95] A. Gil, J. Segura, and N. M. Temme, *Numerical Methods for Special Functions*. Philadelphia: Society for Industrial and Applied Mathematics, 2007.

[96] M. Wulkow, "Computer aided modeling of polymer reaction engineering - The status of Predici, 1 - simulation," *Macromolecular Reaction Engineering*, vol. 2, no. 6, pp. 461–494, 2008.

[97] W. Schiesser, *The Numerical Method of Lines: Integration of Partial Differential Equations*. Academic Press, 1991.

[98] F. A. Bornemann, "An adaptive multilevel approach to parabolic equations I. General theory and 1D implementation," *IMPACT of Computing in Science and Engineering*, vol. 2, no. 4, pp. 279–317, 1990.

[99] J. Lang and A. Walter, "An adaptive Rothe method for nonlinear reaction-diffusion systems," *Applied Numerical Mathematics*, vol. 13, no. 1-3, pp. 135–146, 1993.

[100] C. Schütte and M. Wulkow, "A hybrid Galerkin-Monte-Carlo approach to higher-dimensional population balances in polymerization kinetics," *Macromolecular Reaction Engineering*, vol. 4, no. 9-10, pp. 562–577, 2010.

[101] P. J. Flory, "Molecular size distribution in three dimensional polymers. I. Gelation," *Journal of the American Chemical Society*, vol. 63, no. 11, pp. 3083–3090, 1941.

[102] P. J. Flory, "Molecular size distribution in three dimensional polymers. II. Trifunctional branching units," *Journal of the American Chemical Society*, vol. 63, no. 11, pp. 3091–3096, 1941.

[103] P. J. Flory, "Molecular size distribution in three dimensional polymers. III. Tetrafunctional branching units," *Journal of the American Chemical Society*, vol. 63, no. 11, pp. 3096–3100, 1941.

[104] P. J. Flory, "Molecular size distribution in three dimensional polymers. V. Post-gelation relationships," *Journal of the American Chemical Society*, vol. 69, no. 1, pp. 30–35, 1947.

[105] P. J. Flory, "Molecular size distribution in three dimensional polymers. VI. branched polymers containing A-R-B(f-1) type units," *Journal of the American Chemical Society*, vol. 74, no. 11, pp. 2718–2723, 1952.

[106] W. Radke, G. Litvinenko, and A. H. E. Müller, "Effect of core-forming molecules on molecular weight distribution and degree of branching in the synthesis of hyperbranched polymers," *Macromolecules*, vol. 31, no. 2, pp. 239–248, 1998.

[107] M. B. Smith and J. March, *March's Advanced Organic Chemistry: Reactions, Mechanisms, and Structure*. New York: Wiley-Interscience, 5th ed., 2001.

[108] D. T. Gillespie, "Stochastic simulation of chemical kinetics," *Annual Review of Physical Chemistry*, vol. 58, pp. 35–55, 2007.

[109] P. R. Dvornić and M. S. Jaćović, "The viscosity effect on autoacceleration of the rate of free radical polymerization," *Polymer Engineering and Science*, vol. 21, no. 12, pp. 792–796, 1981.

[110] A. P. Minton, "Implications of macromolecular crowding for protein assembly," *Current Opinion in Structural Biology*, vol. 10, no. 1, pp. 34–39, 2000.

[111] E. K. Lin, R. Kolb, S. K. Satija, and W.-l. Wu, "Reduced polymer mobility near the polymer/solid interface as measured by neutron reflectivity," *Macromolecules*, vol. 32, no. 11, pp. 3753–3757, 1999.

[112] H. Jacobson and W. H. Stockmayer, "Intramolecular reaction in polycondensations. I. The theory of linear systems," *The Journal of Chemical Physics*, vol. 18, no. 12, pp. 1600–1606, 1950.

[113] K. Dušek, J. Šomvársky, M. Smrčková, W. J. Simonsick Jr., and L. Wilczek, "Role of cyclization in the degree-of-polymerization distribution of hyperbranched polymers," *Polymer Bulletin*, vol. 42, no. 4, pp. 489–496, 1999.

[114] H. Frey and R. Haag, "Dendritic polyglycerol: A new versatile biocompatible material," *Reviews in Molecular Biotechnology*, vol. 90, no. 3-4, pp. 257–267, 2002.

[115] R. Hanselmann, D. Hölter, and H. Frey, "Hyperbranched polymers prepared via the core-dilution/slow addition technique: Computer simulation of molecular weight distribution and degree of branching," *Macromolecules*, vol. 31, no. 12, pp. 3790–3801, 1998.

[116] M. Sturm, A. Bertsch, C. Gröpl, A. Hildebrandt, R. Hussong, E. Lange, N. Pfeifer, O. Schulz-Trieglaff, A. Zerck, K. Reinert, and O. Kohlbacher, "OpenMS - an open-source software framework for mass spectrometry," *BMC Bioinformatics*, vol. 9, p. 163, 2008.

[117] D. Taton, A. Le Borgne, M. Sepulchre, and N. Spassky, "Synthesis of chiral and racemic functional polymers from glycidol and thioglycidol," *Macromolecular Chemistry and Physics*, vol. 195, no. 1, pp. 139–148, 1994.

[118] A. Dworak, W. Walach, and B. Trzebicka, "Cationic polymerization of glycidol. Polymer structure and polymerization mechanism," *Macromolecular Chemistry and Physics*, vol. 196, no. 6, pp. 1963–1970, 1995.

[119] E. J. Vandenberg, J. C. Mullis, and R. S. Juvet Jr, "Poly [3, 3-bis (hydroxymethyl) oxetane]-an analog of cellulose: Synthesis, characterization, and properties," *Journal of Polymer Science Part A: Polymer Chemistry*, vol. 27, pp. 3083–3112, 1989.

[120] B. Vazquez, L. Fomina, R. Salazar, and S. Fomine, "Theoretical study of glycidol hyperbranching polymerisation," *Macromolecular Theory and Simulations*, vol. 10, no. 8, p. 762, 2001.

[121] M. E. R. Weiss, F. Paulus, D. Steinhilber, A. N. Nikitin, R. Haag, and C. Schütte, "Estimating kinetic parameters for the spontaneous polymerization of glycidol at elevated temperatures," *Macromolecular Theory and Simulations*, 2012, DOI:10.1002/mats.201200003.